

---

Electronic Theses and Dissertations, 2004-2019

---

2008

## The Effects Of Phosphate And Silicate Inhibitors On Surface Roughness And Copper Release In Water Distribution Systems

David MacNevin  
*University of Central Florida*

 Part of the [Environmental Engineering Commons](#)  
Find similar works at: <https://stars.library.ucf.edu/etd>  
University of Central Florida Libraries <http://library.ucf.edu>

This Doctoral Dissertation (Open Access) is brought to you for free and open access by STARS. It has been accepted for inclusion in Electronic Theses and Dissertations, 2004-2019 by an authorized administrator of STARS. For more information, please contact [STARS@ucf.edu](mailto:STARS@ucf.edu).

---

### STARS Citation

MacNevin, David, "The Effects Of Phosphate And Silicate Inhibitors On Surface Roughness And Copper Release In Water Distribution Systems" (2008). *Electronic Theses and Dissertations, 2004-2019*. 3607. <https://stars.library.ucf.edu/etd/3607>

THE EFFECTS OF PHOSPHATE AND SILICATE INHIBITORS ON SURFACE  
ROUGHNESS AND COPPER RELEASE IN WATER DISTRIBUTION  
SYSTEMS

by  
DAVID EARL MACNEVIN  
B.S., University of Central Florida, 2005.

A dissertation submitted in partial fulfillment of the requirements  
for the degree of Doctor of Philosophy  
in the Department of Civil and Environmental Engineering  
in the College of Engineering and Computer Science  
at the University of Central Florida  
Orlando, Florida

Fall Term  
2007

Major Professor: James S. Taylor

© 2007 David E. MacNevin

## ABSTRACT

The effects of corrosion inhibitors on water quality and the distribution system were studied. This dissertation investigates the effect of inhibitors on iron surface roughness, copper surface roughness, and copper release.

Corrosion inhibitors included blended poly/ortho phosphate, sodium orthophosphate, zinc orthophosphate, and sodium silicate. These inhibitors were added to a blend of surface water, groundwater, and desalinated brackish water.

Surface roughness of galvanized iron, unlined cast iron, lined cast iron, and polyvinyl chloride was measured using pipe coupons exposed for three months. Roughness of each pipe coupon was measured with an optical surface profiler before and after exposure to inhibitors. For most materials, inhibitor did not have a significant effect on surface roughness; instead, the most significant factor determining the final surface roughness was the initial surface roughness. Coupons with low initial surface roughness tended to have an increase in surface roughness during exposure, and vice versa, implying that surface roughness tended to regress towards an average or equilibrium value. For unlined cast iron, increased alkalinity and increased temperature tended to correspond with increases in surface roughness. Unlined cast iron coupons receiving phosphate inhibitors were more likely to have a significant change in surface roughness, suggesting that phosphate inhibitors affect stability of iron pipe scales.

Similar roughness data collected with new copper coupons showed that elevated orthophosphate, alkalinity, and temperature were all factors associated with increased copper surface roughness. The greatest increases in surface roughness were observed with copper coupons receiving phosphate inhibitors. Smaller increases were observed with copper coupons receiving silicate inhibitor or no inhibitor. With phosphate inhibitors, elevated temperature and

alkalinity were associated with larger increases in surface roughness and blue-green copper (II) scales. Otherwise a compact, dull red copper (I) scale was observed. These data suggest that phosphate inhibitor addition corresponds with changes in surface morphology, and surface composition, including the oxidation state of copper solids.

The effects of corrosion inhibitors on copper surface chemistry and cuprosolvency were investigated. Most copper scales had X-ray photoelectron spectroscopy binding energies consistent with a mixture of  $\text{Cu}_2\text{O}$ ,  $\text{CuO}$ ,  $\text{Cu}(\text{OH})_2$ , and other copper (II) salts. Orthophosphate and silica were detected on copper surfaces exposed to each inhibitor.

All phosphate and silicate inhibitors reduced copper release relative to the no inhibitor treatments, keeping total copper below the 1.3 mg/L MCLG for all water quality blends. All three kinds of phosphate inhibitors, when added at 1 mg/L as P, corresponded with a 60% reduction in copper release relative to the no inhibitor control. On average, this percent reduction was consistent across varying water quality conditions in all four phases. Similarly when silicate inhibitor was added at 6 mg/L as  $\text{SiO}_2$ , this corresponded with a 25-40% reduction in copper release relative to the no inhibitor control. Hence, on average, for the given inhibitors and doses, phosphate inhibitors provided more predictable control of copper release across changing water quality conditions. A plot of cupric ion concentration versus orthophosphate concentration showed a decrease in copper release consistent with mechanistic control by either cupric phosphate solubility or a diffusion limiting phosphate film.

Thermodynamic models were developed to identify feasible controlling solids. For the no inhibitor treatment,  $\text{Cu}(\text{OH})_2$  provided the closest prediction of copper release. With phosphate inhibitors both  $\text{Cu}(\text{OH})_2$  and  $\text{Cu}(\text{PO}_4)\cdot 2\text{H}_2\text{O}$  models provided plausible predictions. Similarly, with silicate inhibitor, the  $\text{Cu}(\text{OH})_2$  and  $\text{CuSiO}_3\cdot \text{H}_2\text{O}$  models provided plausible predictions.

## **ACKNOWLEDGMENTS**

This dissertation would not have been possible without the contributions of my coworkers in the Environmental Systems Engineering Institute. Staff members included Dr. Charles Norris, Dr. John Dietz, and Maria Pia Real Robert. Fellow students who were essential to this research include Abdul Alshehri, Tony Kwan, Philip Lintereur, Erica Stone, Raj Vaidya, , Bingjie Zhao, Avinash Shekhar, and Stephen Glatthorn. Raj provided many helpful comments which have improved this manuscript. Committee members Dr. C. Clausen, Dr. S.J. Duranceau, Dr. L. An, and Dr. A.A Randall, provided helpful technical feedback and guidance. I would especially like to acknowledge the support of Dr. Taylor. I am confident that all I have learned in these past four years will benefit me for years to come.

I would also like to acknowledge Tampa Bay Water (TBW); Hillsborough County, Fla.; Pasco County, Fla.; Pinellas County, Fla.; City of New Port Richey, Fla.; City of St. Petersburg, Fla.; and City of Tampa, Fla. which are the Member Governments of TBW and the American Water Works Association Research Foundation (AwwaRF) for their support and funding of this project.

Finally, I would like to acknowledge my family for their support throughout my education. Thank you.

## TABLE OF CONTENTS

CHAPTER 1 INTRODUCTION .....	1
Organization.....	1
Problem Statement.....	1
CHAPTER 2 SURFACE ROUGHNESS .....	3
Definition .....	3
Measurement.....	3
Profilometry .....	4
Flow Testing .....	5
Significance.....	5
Pipe Pressure Losses .....	5
Biofilm Density.....	6
Chlorine Decay .....	7
Polyphosphate Reversion.....	9
Control .....	9
Chemical Control.....	9
Physical Control.....	10
CHAPTER 3 COPPER CORROSION .....	12
Introduction.....	12
Corrosion Products.....	13
Inhibition.....	14
Inhibition by Copper Oxides.....	14
Inhibition by Orthophosphates.....	15
Transient Release .....	16
Thermodynamic Modeling.....	17
Dissolved Copper Speciation.....	19
CHAPTER 4 MATERIALS AND METHODS .....	22
Pilot Testing.....	22
Source Waters .....	22
Corrosion Inhibitors.....	24
Pilot Distribution Systems .....	25
Pipe Coupons .....	25
Corrosion Shed.....	26
Corrosion Coupons .....	26
Surface Characterization.....	29
Surface Structure.....	29
Surface Composition.....	32
Thermodynamic Modeling.....	34
Copper Solubility .....	34

CHAPTER 5 SURFACE ROUGHNESS OF COMMON WATER DISTRIBUTION SYSTEM MATERIALS.....	37
Abstract.....	37
Introduction.....	38
Distribution System Water Quality.....	38
Effects of Surface Roughness.....	39
Measurement of Surface Roughness.....	43
Materials and Methods.....	46
Pilot Testing.....	46
Surface Characterization.....	49
Results and Discussion.....	51
Galvanized Iron.....	52
Lined Cast Iron.....	54
Polyvinyl Chloride.....	54
Unlined Cast Iron.....	55
Conclusions.....	59
Recommendations.....	59
CHAPTER 6 SURFACE CHARACTERIZATION AND SOLUBILITY MODELING OF COPPER LOOPS RECEIVING PHOSPHATE INHIBITORS.....	61
Abstract.....	61
Introduction.....	62
Copper Corrosion.....	62
Materials and Methods.....	65
Pilot Testing.....	65
X-Ray Photoelectron Spectroscopy.....	68
Thermodynamic Modeling.....	69
Mechanistic Investigation of Copper Release.....	72
Results and Discussion.....	75
Effect of Phosphate Inhibitor on Copper Release.....	75
XPS Identification of Copper Corrosion Products.....	78
Thermodynamic Modeling.....	85
Mechanistic Investigation of Copper Release.....	89
Conclusions.....	91

CHAPTER 7 SURFACE CHARACTERIZATION AND SOLUBILITY MODELING OF COPPER IN WATER DISTRIBUTION SYSTEMS RECEIVING SILICATE INHIBITORS ..	93
Abstract .....	93
Introduction .....	94
Copper Corrosion .....	94
Silicate Inhibitors .....	95
Pilot Testing .....	97
X-Ray Photoelectron Spectroscopy .....	100
Thermodynamic Modeling .....	101
Results and Discussion .....	104
Effect of Silicate Inhibitor on Copper Release .....	104
XPS Identification of Copper Corrosion Products .....	106
Thermodynamic Modeling .....	108
Conclusions .....	110
CHAPTER 8 EFFECTS OF PHOSPHATE AND SILICATE CORROSION INHIBITORS ON THE SURFACE MORPHOLOGY OF COPPER .....	111
Abstract .....	111
Introduction .....	113
Color of Copper Corrosion Products .....	113
Surface Roughness .....	114
Materials and Methods .....	117
Pilot Testing .....	117
Surface Characterization .....	121
Results and Discussion .....	123
Surface Roughness of Copper .....	123
Scanning Electron Microscopy .....	130
Conclusions .....	135
REFERENCES .....	136

## LIST OF FIGURES

Figure 3.1 Essentials components of corrosion .....	12
Figure 3.2 pC-pH diagram depicting effect of alkalinity on cuprosolvency with a $\text{Cu}(\text{OH})_2$ controlling solid without consideration of inhibitors.....	20
Figure 3.3 Speciation of copper (II) at pH 8.0 under $\text{Cu}(\text{OH})_2$ control without alkalinity.....	21
Figure 3.4 Speciation of copper (II) at pH 8.0 under $\text{Cu}(\text{OH})_2$ control with alkalinity 30 mg/L as $\text{CaCO}_3$ .....	21
Figure 4.1 Truck and stainless steel trailer used to haul raw surface water.....	27
Figure 4.2 Raw surface water storage.....	27
Figure 4.3 Covered tanks for process treatment .....	27
Figure 4.4 Field trailers.....	27
Figure 4.5 Influent standpipes.....	27
Figure 4.6 Inhibitor tanks and feed pumps .....	27
Figure 4.7 Pilot distribution systems .....	28
Figure 4.8 Cradles for housing coupons .....	28
Figure 4.9 Mounted coupons .....	28
Figure 4.10 Corrosion shed.....	28
Figure 4.11 Copper lines with lead coupons.....	28
Figure 4.12 Electrochemical Noise Trailer.....	28
Figure 4.13 WYKO NT 3300 optical profiler .....	29
Figure 4.14 SEM JEOL 6400F .....	32
Figure 4.15 Physical Electronics 5400 ESCA XPS .....	33
Figure 5.1 Sample OIP Scan of UCI pipe surface with $R_a$ of 83.2 $\mu\text{m}$ .....	45
Figure 5.2 Covered tanks for process treatment .....	48
Figure 5.3 Pilot distribution systems .....	48
Figure 5.4 Cradles for housing coupons .....	48
Figure 5.5 Mounted coupons .....	48
Figure 5.6 WYKO NT 3300 optical profiler .....	49
Figure 5.7 Change of initial roughness, $\Delta R$ , versus initial roughness, $R_i$ , for galvanized iron coupons by phase .....	53
Figure 6.1 Covered tanks for process treatment .....	67
Figure 6.2 Pilot distribution systems .....	67
Figure 6.3 Corrosion shed.....	67
Figure 6.4 Copper lines.....	67
Figure 6.5 PhysicalElectronics 5400 ESCA XPS.....	69
Figure 6.6 Time series plot of copper release with BOP inhibitor addition .....	76
Figure 6.7 Time series plot of copper release with OP inhibitor addition.....	76
Figure 6.8 Time series plot of copper release with ZOP inhibitor addition .....	77
Figure 6.9 Time series plot of copper release by pH without inhibitor addition .....	77
Figure 6.10 Survey spectrum of a copper coupon from 1.0 ZOP, Phase III.....	78
Figure 6.11 Deconvolution of copper for the coupon exposed to BOP during Phase IV.....	79
Figure 6.12 Distribution of copper compounds for all phases.....	81
Figure 6.13 Comparison of diffusion model and solubility model as mechanisms for the effect of orthophosphate on copper Release.....	90
Figure 7.1 Covered tanks for process treatment .....	99

Figure 7.2 Pilot distribution systems .....	99
Figure 7.3 Corrosion shed.....	99
Figure 7.4 Copper lines.....	99
Figure 7.5 Time series plot of copper release with Si inhibitor addition.....	105
Figure 7.6 Time series plot of copper release by pH without inhibitor addition .....	105
Figure 8.1 Sample optical profiler scan of copper surface with $R_a$ of 2.96 $\mu\text{m}$ .....	116
Figure 8.2 Covered tanks for process treatment .....	120
Figure 8.3 Pilot distribution systems .....	120
Figure 8.4 Electrochemical noise trailer .....	120
Figure 8.5 Corrosion shed.....	120
Figure 8.6 Copper lines.....	121
Figure 8.7 Photographs of typical copper coupons before exposure to inhibitors.....	123
Figure 8.8 $\Delta$ roughness of copper coupons by inhibitor and phase .....	128
Figure 8.9 Visual comparison of surface scales on Phase III copper coupons .....	128
Figure 8.10 Visual comparison of surface scales on Phase IV copper coupons.....	128
Figure 8.11 Paired replicate surface roughness data for copper coupons from Phase III.....	129
Figure 8.12 Paired replicate surface roughness data for copper coupons from Phase IV .....	129
Figure 8.13 Copper surface exposed to zinc orthophosphate dose of 1.0 mg/L as $\text{PO}_4^{3-}$ for three months.....	132
Figure 8.14 Copper surface exposed to silicate inhibitor 6.0 mg/L as $\text{SiO}_2$ for three months ...	133
Figure 8.15 Copper surface receiving no inhibitor for three months.....	134

## LIST OF TABLES

Table 4.1 Blend ratios and water quality by phase .....	23
Table 4.2 Water Quality Profile.....	24
Table 4.3 Number of surface roughness coupons by material and phase.....	30
Table 4.4 Number of measurements per coupon by material and phase .....	30
Table 5.1 Blend ratios and water quality by phase .....	47
Table 5.2 Number of surface roughness coupons by material and phase.....	50
Table 5.3 Number of measurements per coupon by material and phase .....	50
Table 5.4 Roughness summary by material.....	51
Table 5.5 Statistical comparison of UCI initial and final surface roughness.....	57
Table 5.6 Statistical comparison of UCI initial and final surface roughness.....	58
Table 6.1 Blend ratios and water quality by phase .....	66
Table 6.2 Comparison of observed copper release from inhibitor PDSs to pH <sub>s</sub> +0.3 .....	75
Table 6.3 Compounds identified in scale on copper coupons in the presence of OP inhibitor ....	82
Table 6.4 Compounds identified in scale on copper coupons in the presence of pH <sub>s</sub> +0.3 treated waters .....	84
Table 6.5 Copper thermodynamic modeling of pH <sub>s</sub> +0.3 .....	86
Table 6.6 Copper thermodynamic modeling of OP .....	89
Table 7.1 Blend ratios and water quality by phase .....	98
Table 7.2 Comparison of observed copper release from inhibitor PDSs to pH <sub>s</sub> +0.3 .....	106
Table 7.3 Compounds identified in scale on copper coupons in the presence of Si inhibitor ....	107
Table 7.4 Copper thermodynamic modeling of Si.....	109
Table 8.1 Blend ratios and water quality by phase .....	117
Table 8.2 Statistical comparison of Cu initial and final surface roughness.....	125

## **CHAPTER 1 INTRODUCTION**

### **Organization**

This dissertation examines the effects of corrosion inhibitors on iron surface roughness , copper release from copper tubing, and copper surface roughness. It begins with introductory chapters on Surface Roughness and Copper Corrosion, with a Materials and Methods chapter following. Subsequently, the results are presented in four individual chapters on Inhibitors and Iron Roughness, Phosphate Inhibitors and Copper Corrosion, Silicate Inhibitors and Copper Corrosion, and Inhibitors and Copper Roughness. Each of these four chapters was prepared as an article and may be read independently.

### **Problem Statement**

Maintenance of drinking water distribution systems is important to control pumping costs and protect drinking water quality up to the point of delivery to consumers. Hence, water suppliers are interested in methods to improve or maintain the hydraulic efficiency of pipes while preventing unwanted metal release into the waters.

Corrosion inhibitors have been proposed as agents for the control of distribution system surface roughness and metal release. To the author's knowledge there are no published peer-reviewed studies quantifying an effect of corrosion inhibitors in reducing or controlling pipe surface roughness. The technique for measuring surface roughness is suitable for small pilot studies where it is not feasible to perform pressure loss tests.

In contrast, corrosion inhibitors are widely reported as effective agents for the control of copper release in distribution systems. This dissertation presents results on the effectiveness of phosphate and silicate inhibitors under changing water quality conditions. Results of surface

characterization and thermodynamic modeling are also presented in an effort to explain how inhibitors reduce copper release.

## CHAPTER 2 SURFACE ROUGHNESS

### Definition

Surface roughness may be defined as the small-scale morphology or “shape” of a surface. A three-dimensional surface profile will contain many features including peaks, valleys, ridges, and grooves. A non-smooth surface is usually quite complex, and difficult to describe. Consequently, there are several statistics (Lippold and Podlesny, 1998) describing either the height or the spacing of peaks and valleys in the profile.

$R_a$  is the roughness average. It is the arithmetic mean of the surface deviations from the mean plane. For an array of M by N elevation points, it can be written as in Equation 2.1.

$$R_a = \frac{1}{MN} \sum_{j=1}^M \sum_{i=1}^N |Z_{ij}| \quad \text{Equation 2.1}$$

Where  $|Z_{ij}|$  is the absolute difference at point (i,j) of the surface from the mean plane.  $R_a$  is not sensitive to differences in the spacing of roughness peaks and valleys. Unless stated otherwise, all surface roughness measurements in this dissertation are all based on  $R_a$ .

### Measurement

There are two common methods for the measurement of pipe surface roughness. Profilometry is a direct technique that measures the actual shape of the pipe surface; whereas, flow testing is an indirect technique that measures the reduction in flow due to pipe surface roughness.

## *Profilometry*

There are two common kinds of surface profilers available for measurement of pipe surface roughness. Results from either kind of profiler can be used to calculate surface roughness parameters, such as  $R_a$ . The working principle of the stylus profiler and the optical profiler are presented and the advantages and disadvantages of each are noted.

With a stylus profiler, a stylus is traced in a line across the surface, and the displacement of the stylus is recorded along the trace line. In contrast, an optical profiler uses the interference of light to measure surface roughness over a scanning area. A monochromatic beam of light is split and directed towards a flat reference surface and the measurement surface. The light is reflected from each surface and recombined within the profiler. When the beams of light recombine, interference fringes form because the phase of the light reflected from the measurement surface depends on the distance of the optical path, which depends on the height of the surface.

Stylus profilometry measures the surface profile by direct physical contact. However, it is only capable of measuring the surface profile along one line at a time. It is not well suited for soft materials, such as plastics, which give way to the force of the stylus. Also, stylus profilometry is not well suited for very rough materials which may damage the stylus.

Optical profilometry is a more recent technique for the measurement of surface roughness. It measures the surface profile over an area without physical contact. This makes it possible to construct a three dimensional picture of the surface. Being a non-contact technique optical profilometry is appropriate for measuring soft materials and very rough materials. Optical profilometry works best with uniformly reflective materials. In the author's experience

measurement of dull or non-uniformly reflective materials is possible; however, the scan quality will be poorer.

### *Flow Testing*

Flow tests may also be used to quantify pipe surface roughness. Increased surface roughness in pipes tends to reduce the flow of water under a given pressure gradient. Hence, by measuring the flow of water through a pipe under a known pressure gradient it is possible to deduce the surface roughness of that pipe using empirical relationships of fluid mechanics. These tests can be conducted in a laboratory or in the field. The following section on pipe pressure losses provides more information on flow tests for surface roughness.

### **Significance**

Surface roughness causes pressure loss in flowing pipes. It is also a suspected factor in water quality phenomena at the pipe wall including biofilm density, chlorine decay, and polyphosphate reversion.

### *Pipe Pressure Losses*

The hydraulic capacity of a pipe describes the flow rate a pipe may carry under a reasonable pressure gradient. Pipes with low hydraulic capacity carry less water under the same pressure gradient than pipes with higher hydraulic capacity. Surface roughness has been linked to hydraulic capacity (Nikuradse 1950) and is measured indirectly in a distribution system by a flow test (Walski et al. 2003).

In the literature on hydraulic capacity in distribution systems, the most common formula used to relate hydraulic capacity and head loss is the empirical Hazen-Williams equation, which is presented in Equation 2.2.

$$V = 1.318 C_{HW} R_h^{0.63} S^{0.54} \quad \text{Equation 2.2}$$

where  $V$  = average velocity (ft/s)  
 $C_{HW}$  = Hazen-Williams Coefficient  
 $R_h$  = hydraulic radius (ft)  
 $S$  = slope of the energy grade line (ft/ft)

The hydraulic radius,  $R_h$ , is the ratio of the cross-section area to the cross-section wetted perimeter. The energy grade line slope,  $S$ , is the ratio of the hydraulic head loss to the length of pipe over which that loss occurred. The Hazen-Williams coefficient ( $C_{HW}$ ) is the measure of pipe hydraulic capacity. Higher  $C_{HW}$  correspond with a higher hydraulic capacity, like that found in new pipe. Lower  $C_{HW}$  corresponds with a lower hydraulic capacity, like that found in old, highly-tuberculated unlined iron pipe. Thus, the  $C_{HW}$  is inversely proportional to pipe surface roughness. The  $C_{HW}$  is also a function of fluid velocity, fluid kinematic viscosity, and pipe diameter (Sharp and Walski 1988).

### *Biofilm Density*

Historically, surface roughness in the distribution system has been considered for its effect on flow capacity. However, surface roughness may also be a factor influencing various water quality phenomena occurring at the pipe wall, such as biofilms and chlorine dissipation. Fletcher and Marshall (1982) found the rate of biofilm formation to be dependent on the surface chemistry, surface roughness, and the organism.

LePuil et al. (2005) measured biofilm density using the protein exoproteolytic activity (PEPA) assay by Laurent and Servais (1995) and found that PEPA was greatest for UCI pipe followed by LCI and G pipe, which had similar PEPA and the least biofilm density was observed for the PVC pipe. Visual observations of the roughness of these materials lead to the conclusion that differences in biofilm density by material may be related to differences in material surface roughness.

### *Chlorine Decay*

Surface roughness has been proposed as a factor affecting chlorine decay at the pipe wall; however, published studies seem to suggest that material is more important than surface roughness in determining wall rate constants. The following paragraphs discuss how roughness would be included in a chlorine decay model. After this, evidence is presented against roughness being a significant factor in chlorine decay.

Rossman, Clark, and Grayman (1994) developed a mass-transfer based model for chlorine decay, assuming first order kinetics in the bulk flow and at the pipe wall. The overall first order decay constant,  $K_i$ , is given in Equation 2.3.

$$K_i = k_b + \frac{k_w k_f}{r_h (k_w + k_f)} \quad \text{Equation 2.3}$$

where  $k_b$  = decay rate constant in the bulk flow,  $\text{time}^{-1}$

$k_w$  = decay rate constant at the wall,  $L \cdot \text{time}^{-1}$

$k_f$  = mass transfer coefficient,  $L \cdot \text{time}^{-1}$

Surface roughness changes the pipe surface area and the thickness of the boundary layer present at the pipe wall under turbulent flow. Therefore, any influence of surface roughness on chlorine decay would appear in the second additive term of Equation 2.3. Disinfection residual decay at the pipe wall must consider the reactions at the wall, the mass transfer limitations and the available surface area to volume geometry (Frateur et al. 1999; Vikesland, Ozekin, and Valentine 2001; Vikesland and Valentine 2002; Hallam et al. 2002). Arevalo (2003) and Kiéné, Lu, and Lévi (1998) found that old cast iron and steel pipes had a higher chlorine demand than pipes of synthetic materials. The difference on decay rates between iron-based and synthetic materials could be due to oxidation of iron and iron corrosion by-products or higher surface area in the corroded pipes.

Doshi, Grayman, and Guastella (2003) conducted a series of simultaneous chlorine loss and head loss tests within the water distribution system of Detroit, Mich. Most of the pipes were unlined cast iron, from 70 to 135 years old. Using a first-order mass-transfer model, they reported that the wall decay coefficient of chlorine,  $k_w$  ( $L/time^{-1}$ ), did not appear to be related to the Hazen-Williams coefficient (i.e. pipe roughness), but rather  $k_w$  increased directly with increasing flow.

Vasconcelos et al. (1997) developed a distribution system chlorine decay model for unlined cast iron pipe that took both bulk and wall chlorine decay into account. The both zero order and first order wall rate constants were determined assuming that the wall rate constant for each pipe varied inversely with the Hazen-Williams coefficient on record for that pipe. However, inclusion of the roughness term in the model provided only a minimal improvement in the predictive power of the chlorine decay model.

Furthermore, there is evidence suggesting that pipe material is the most important factor affecting wall rate constants. Arevalo (2003) and Kiéné, Lu, and Lévi (1998) have all found that old cast iron and steel pipes had a higher chlorine demand than plastic pipes, suggesting that oxidation of ferrous iron to ferric iron is a key factor responsible for decay of chlorine residual at the pipe wall.

### *Polyphosphate Reversion*

Polyphosphates have been used as corrosion inhibitors in water distribution systems. Over time, polyphosphates tend to revert via acid hydrolysis to orthophosphate (Snoeyink and Jenkins, 1980). Hence if localized regions of low pH form on corroding pipe surfaces, it is possible that a rougher surface would provide more sites for polyphosphate reversion to occur.

## **Control**

The effects of surface roughness on hydraulic efficiency and water quality provide an incentive for utilities to proactively manage and control surface roughness within the distribution system. Surface roughness may be controlled by chemical and physical techniques.

### *Chemical Control*

Surface roughness is influenced by both water quality and inhibitor addition. Hudson (1966) examined the decline in carrying capacity of water distribution systems in seven cities. The decline in Hazen-Williams coefficient varied by each city, suggesting that roughness growth rates,  $\alpha$ , may vary with water quality.

Larson and Sollo (1967) examined the relationship between water quality and corrosion rate of unlined cast iron. They recommended that the pH be adjusted to maintain a zero saturation index in order to avoid losses in pipe carrying capacity, as indicated by declines in the Hazen-Williams coefficient,  $C_{HW}$ .

Sharp and Walski (1988) developed a model for predicting the increase in roughness of unlined metal pipes and water quality. The model assumed that roughness increased linearly with time, and the rate of roughness increase was dependent on Langelier index (LI), with more negative LIs corresponding with greater rates of roughness increase. By incorporating the LI into the roughness growth model, Sharp and Walski, demonstrated that calcium hardness and alkalinity, in addition to pH, are factors affecting the roughness growth rate. These studies suggest roughness growth rate is largely influenced by water quality.

There is limited evidence that phosphate inhibitors interact with preexisting iron scales. In a laboratory scale study, Shull (1980) showed that iron pipe treated with bimetallic zinc phosphate had a lower head loss than a pH control. He et al. (1996) showed that phosphate inhibitors influence the aggregation behavior of ferric hydroxide. Swayze (1983) found that phosphate inhibitor tended to promote the removal of preexisting tuberculation and deposits in iron pipe in the distribution system.

### *Physical Control*

Surface roughness of unlined iron pipe may also be controlled by flushing of the pipes with water or scraping the insides of the pipe walls with an abrasive “pig.” After cleaning, the surface may be kept smooth by spraying a smooth nonmetal coating on the inside of the pipe, or

inserting a slip-lining inside the old pipe; however, both of these options are costly. The final physical option, pipe excavation and replacement, is typically the most costly option.

## CHAPTER 3 COPPER CORROSION

### Introduction

Copper tubing corrodes from its metallic form of  $\text{Cu}^0$  to the, cuprous,  $\text{Cu(I)}$  and cupric,  $\text{Cu(II)}$  ions. Excessive dissolved copper can cause acute gastrointestinal distress, and/or renal damage (Barceloux and Barceloux, 1999), while also causing “blue water.” The maximum contaminant level goal (MCLG) and action level for LCR compliance for copper in potable water systems is 1.3 mg/L. Copper release occurs in both dissolved and particulate forms, with dissolved copper usually being the predominant form.

An understanding of copper corrosion is beneficial because it allows one to find ways to inhibit the release of copper. Corrosion is an electron transfer reaction where the oxidizing and reducing species are react indirectly at a surface via an electrolyte. The four essentials of the corrosion reaction (Figure 3.1) are the anode, cathode, electrical connection, and electrolyte.

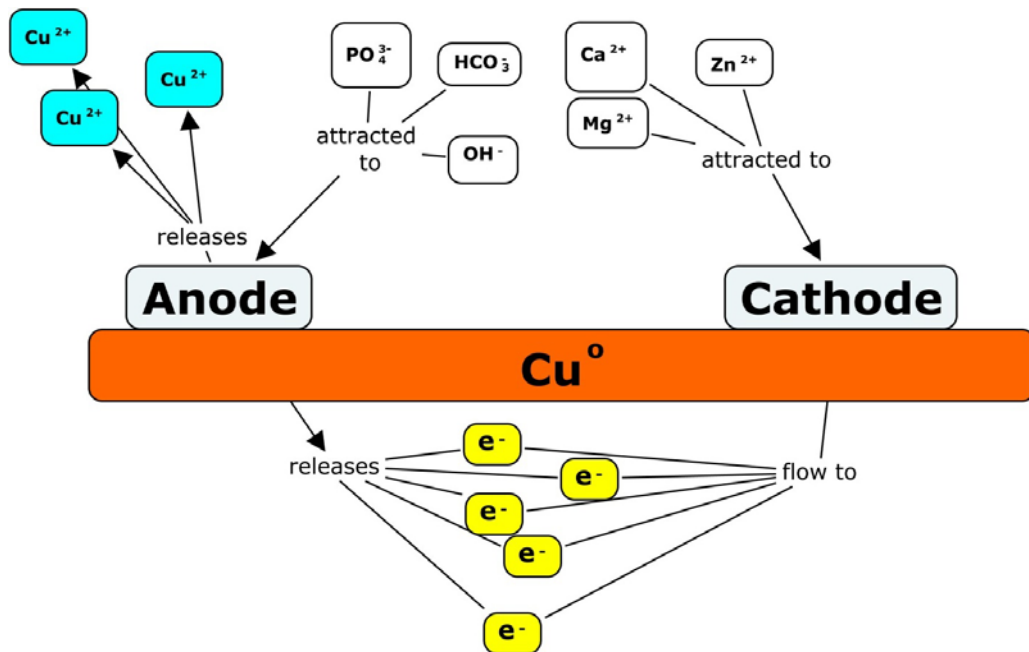


Figure 3.1 Essentials components of corrosion

The anode is the surface where metal oxidation occurs. After oxidation, the metal may form an insoluble corrosion product on the surface, or be dissolved into solution. Rapid formation of an insoluble corrosion product on the anode can slow the corrosion reaction by increasing the activity of the metal ion at the anode, and shifting the corrosion equilibrium. The electrolyte contains anionic species such as,  $\text{CO}_3^{2-}$ ,  $\text{OH}^-$ , and  $\text{PO}_4^{3-}$  which are attracted to the anode surface where they often interact with the dissolved metal, sometimes forming deposits (Figure 3.1).

Electrons from the anode flow through the metal and semiconducting metal oxides to the cathodes where they react with electron acceptors such as  $\text{O}_2$ ,  $\text{HOCl}$ , or  $\text{H}^+$  (Figure 3.1). Cathode based control strategies include the formation of an insoluble insulating film that can limit electron transfer and dissolution of electron acceptors to the underlying cathode. Also, control of electron acceptor activity during post-treatment can slow the corrosion reaction. The electrolyte contains cationic species such as  $\text{Ca}^{2+}$  and  $\text{Zn}^{2+}$  which may form surface films on the cathode.

### **Corrosion Products**

Upon exposure to natural waters, fresh copper tubing tends to oxidize rapidly, forming an adherent cuprite ( $\text{Cu}_2\text{O}$ ) film. Over time, a less adherent, more porous layer of copper (II) oxides and salts builds up on this cuprite layer (Ives and Rawson 1962).

In new piping generally up to 5 years of use, copper (II) concentrations are controlled by  $\text{Cu}(\text{OH})_2$  solid phases, which can age with time to form less soluble tenorite,  $\text{CuO}$ , or malachite,  $\text{Cu}_2(\text{OH})_2\text{CO}_3$  scales (Schock, Lytle, and Clement; 1995). Although copper (I) can exist in solution, for the pH and ORP associated with drinking water systems, it is usually oxidized to copper (II).

In 2003, a similar study was conducted using the same pilot facility described in this dissertation which investigated treatment process impacts on water quality without use of inhibitors. Cuprite ( $\text{Cu}_2\text{O}$ ) was the only crystalline structure found in the corrosion layer using XRD (Taylor et al., 2005). Cupric hydroxide ( $\text{Cu}(\text{OH})_2$ ), tenorite ( $\text{CuO}$ ), and cuprite ( $\text{Cu}_2\text{O}$ ), made up the bulk surface composition on copper coupons identified by XPS.

Thermodynamic modeling indicated that copper release was well described by equilibrium with  $\text{Cu}(\text{OH})_2$  acting as the controlling solid (Xiao; 2004). Alkalinity increased copper release; whereas pH elevation above  $\text{pH}_s$  and silica reduced copper release. Long term exposure to limited alkalinity can promote the formation of malachite,  $\text{Cu}_2(\text{OH})_2\text{CO}_3$  which is highly insoluble.

Looking at the complexation chemistry of copper, conditions favoring the formation of the charged complex  $\text{Cu}(\text{CO}_3)_2^{2-}$  might help promote malachite growth by producing an anionic complex which would be attracted to the anode to form a scale. In contrast, the uncharged complex  $\text{CuCO}_3^0$  would not tend to aggregate around the anode, and would not be expected to promote malachite formation. Hence, complexation chemistry might help to explain the paradoxical benefit of alkalinity at the right levels over the long term. Although this idea is presently a conjecture, further studies may find a relationship between water quality, copper complexes, and the formation of malachite.

## **Inhibition**

### *Inhibition by Copper Oxides*

The formation of a passivating copper oxide film, such as  $\text{Cu}_2\text{O}$ , is an important first step in passivation of copper corrosion (Uhlig 1985) (Eldredge and Warner 1948). The primary

benefit of the metal oxide layer is its role as a diffusion barrier, especially to O<sub>2</sub>. (Kruger 1959) (Shanley, Hummel, and Verink 1980). This film is thought to form first on the anodes from which it can spread to cover the cathodes as well (Ryder and Wagner 1985) After the oxide layers reach sufficient thickness a change in the controlling solid for copper release can occur. Chlorides can penetrate oxide films, causing internal charged repulsion, and increased permeability (Uhlig 1985).

### *Inhibition by Orthophosphates*

Some have suggested that orthophosphate inhibitors function by forming a cupric phosphate scale (Edwards, McNeill, and Holm 2001); however, data on cupric phosphate solids is scarce making it difficult to demonstrate conclusively (Schock, Lytle, and Clement 1995). Orthophosphate is also thought by some to be most effective in controlling copper release in the pH range of 6.5 to 7.5 (Schock, Lytle, and Clement 1995).

Another proposed mechanism is the “adsorbed layer” mechanism whereby orthophosphate ions adsorb to the metal surface displacing H<sub>2</sub>O atoms, slowing the rate of anodic dissolution (Uhlig 1985), and changing the surface potential (Cartledge 1962) (Eldredge and Warner 1948)(Hackerman 1962). It is difficult to distinguish between the two mechanisms because the corrosion product film which forms over the anode is thin (Uhlig 1985).

However, when considering inhibition by phosphoric acid, one must keep in mind the change in phosphate species with pH.. Orthophosphate ion, PO<sub>4</sub><sup>3-</sup> is only present in minute quantities at pH<10. Hence, more attention should be given to the role of the biphosphate ion, HPO<sub>4</sub><sup>2-</sup>, as the “working species” in corrosion inhibition because biphosphate is the predominant species of phosphoric acid over the pH range 7.2 to 12.3.

When inhibitors are not added, other methods for controlling copper release include raising the pH, and or reducing the alkalinity. CO<sub>2</sub> stripping has been recommended as one way to increase the pH without increasing alkalinity (Edwards, Hidmi, and Gladwell; 2003). However, decreasing the alkalinity can increase lead solubility (Taylor et al. 2005). Inhibitors may overcome the apparent tradeoff between control of copper or lead release concentration.

### **Transient Release**

After a copper tube is flushed, copper will dissolve into solution to replace the dissolved copper which was carried away during the flush. Simultaneously, some of this dissolved copper will begin to precipitate slowly on the surface. If the initial rate of dissolution is high enough, the concentration of copper will peak, and then slowly decrease toward an equilibrium concentration with continued precipitation of solids. It can take 48 to 72 hours to reach equilibrium copper levels in a disinfected copper loop (Schock, Lytle, and Clement 1995). The essential factors governing the shape of the concentration profile are the relative kinetics of copper dissolution and copper solids precipitation. A comprehensive mathematical model describing the concentration profile of transient copper release is given by Merkel et al. (2002).

Comparison of results between different studies of copper release is often complicated by variability in stagnation times before copper sampling. Usually samples are taken before the copper has reached equilibrium. Although this can complicate thermodynamic modeling, which assumes equilibrium conditions, such “early” sampling is more representative of actual usage in domestic systems.

## Thermodynamic Modeling

A thermodynamic model of copper release can be developed to provide insight into various water quality effects on cuprosolvency. Thermodynamic modeling is based on the assumption of equilibrium conditions. Hence, although, sometimes a reaction may be thermodynamically favored, it may proceed so slowly as to be insignificant. A notable example of this phenomenon is  $\text{Cu}(\text{OH})_2$  which only exists as a metastable corrosion product of copper. Over time, this compound is thought to age to a less soluble  $\text{CuO}$ .

Cuprosolvency is controlled by two-step equilibrium process of dissolution and complexation. Copper dissolution is modeled by selection of a copper controlling solid. Usually, this solid is the copper compound which is thermodynamically favored (least soluble) for the general water quality conditions under study. A solubility product equilibrium equation is written for the solid and solved for the dissolved copper concentration, which is a function of the solubility product constant, and activity of anions in the copper solid. For example, the concentration of dissolved copper under  $\text{Cu}(\text{OH})_2$  control (Equation 3.1), is essentially a function of the hydroxide ion activity (i.e. a function of pH).

$$[\text{Cu}^{2+}] = \frac{K_{sp}}{[\text{OH}^-]^2} \quad \text{Equation 3.1}$$

Thermodynamically, other species such as  $\text{CO}_3^{2-}$  which are not in the controlling solid do not change the equilibrium concentration of free dissolved copper. Apart from kinetic effects, other water quality parameters increase cuprosolvency by complexation.

Species in solution may form complexes or “coordination compounds” with the free copper (I) or copper (II) ion. In fact, the “free” copper ions are complexed with water molecules; however, they are referred to as the “free copper” or “uncomplexed copper” forms for convenience. Complexation occurs when a species with a free electron pair, the ligand, complexes or “coordinates with” copper (II) which is the central metal ion, accepting the electron pair. In sufficient concentration, these ligands may form complexes with copper that exceed the original concentration of the free copper ion. An essential point to understand in this process is that the equilibrium free copper ion concentration does not change with complexation, since any free copper which is lost to complexation is replaced by further dissolution from the copper solid.

The sensitivity of copper release to alkalinity can be readily explained using complexation chemistry. The carbonate ion,  $\text{CO}_3^{2-}$ , has a strong affinity for Cu (II), with which it forms the complexes  $\text{CuCO}_3^0$ , and  $\text{Cu}(\text{CO}_3)_2^{2-}$ . Because  $\text{CuCO}_3^0$  is uncharged, it would not be expected to accumulate through surface polarization as other charged complexes, like  $\text{Cu}(\text{CO}_3)_2^{2-}$  may. Hence, it can dissolve away freely from the copper surface. This may be a factor in the kinetics of cuprosolvency. Research investigating the role of water quality in copper complexes as possible seeds for malachite formation would be beneficial. An example complexation equilibrium equation (Equation 3.2) is given below. Further information on writing copper complexation equilibria is given by Schock (1999). In practice, all possible copper complexes would be calculated individually and summed together with the free copper ion to obtain the estimated total solubility of copper as shown in Equation 3.3 .



$$\begin{aligned}
\text{Cu}_T = & [\text{Cu}^{2+}] + [\text{CuOH}^+] + [\text{Cu}(\text{OH})_2^{\circ}] + [\text{Cu}(\text{OH})_3^-] + [\text{CuHCO}_3^+] + [\text{CuCO}_3^{\circ}] \\
& + [\text{Cu}(\text{CO}_3)^{2-}] + [\text{Cu}(\text{OH})\text{CO}_3^-] + [\text{Cu}(\text{OH})_2\text{CO}_3^{2-}] + [\text{CuH}_2\text{PO}_4^+] \\
& + [\text{CuHPO}_4^{\circ}] + [\text{CuSO}_4^{\circ}] + [\text{Cu}(\text{NH}_3)^{2+}] + [\text{Cu}(\text{NH}_3)_2^{2+}] + [\text{Cu}(\text{NH}_3)_3^{2+}] \\
& + [\text{Cu}(\text{NH}_3)_4^{2+}] + [\text{Cu}(\text{NH}_3)_5^{2+}] + [\text{CuCl}^+] + [\text{CuCl}^{\circ}]
\end{aligned}
\tag{Equation 3.3}$$

### Dissolved Copper Speciation

A thermodynamic model assuming  $\text{Cu}(\text{OH})_2$  as the controlling solid was used to generate Figure 3.2, which shows the effect of increasing alkalinity on cuprosolvency. Cuprosolvency is represented by  $\text{pTDCu}^{2+}$ , which represents the negative base 10 logarithm of total dissolved copper (II). Consequently, lower numbers indicate increased solubility whereas, higher number indicate less solubility. In all cases, the copper concentration decreases with increasing pH. With no alkalinity, the copper concentration decreases until about pH 9.5, at which point  $\text{Cu}(\text{OH})_2^{\circ}$  accounts for 88% of the dissolved copper (II). At higher pH's hydroxocopper (II) complexes predominate. With increasing alkalinity, the solubility shifts upward with  $\text{Cu}(\text{CO}_3)^{\circ}$  and  $\text{Cu}(\text{CO}_3)^{2-}$  emerging as the primary forms of dissolved copper. The 1.3 ppm Cu regulatory MCLG for copper is indicated at  $\text{pCu}=4.7$

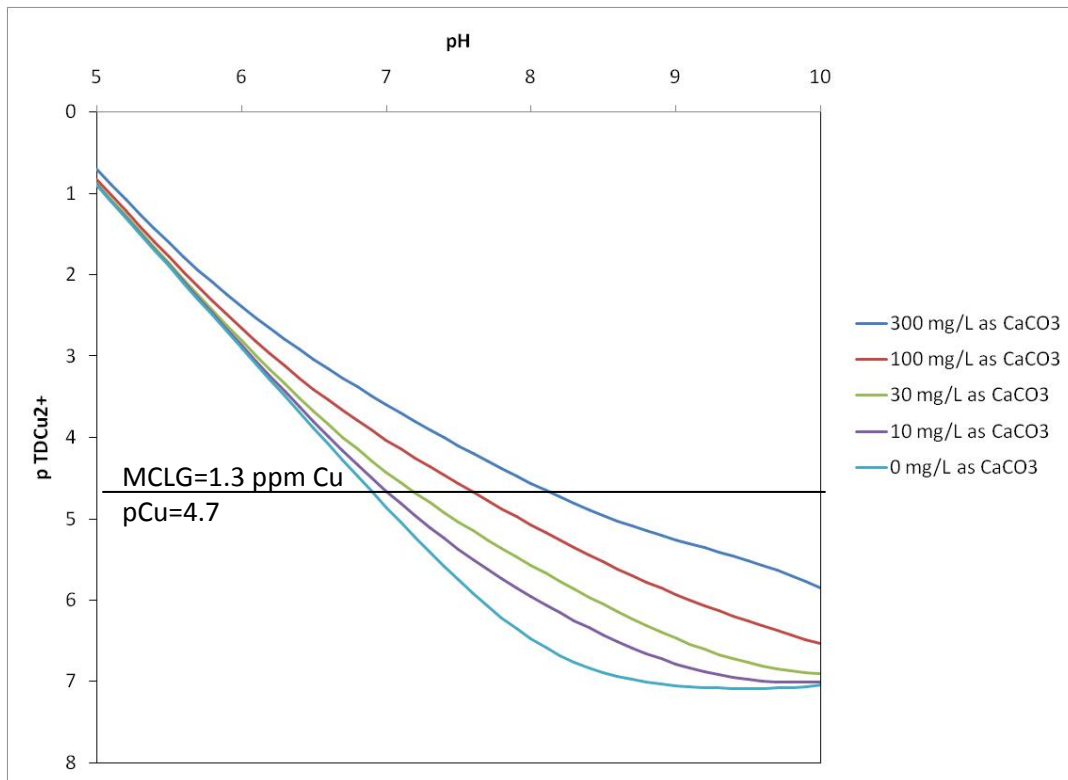


Figure 3.2 pC-pH diagram depicting effect of alkalinity on cuprosolvency with a  $\text{Cu}(\text{OH})_2$  controlling solid without consideration of inhibitors

The speciation of dissolved copper at pH 8.0 under  $\text{Cu}(\text{OH})_2$  control was calculated for zero alkalinity and 30 mg/L as  $\text{CaCO}_3$ . Pie charts showing the relative distribution of copper (II) under each condition are shown in Figure 3.3 and Figure 3.4, respectively.

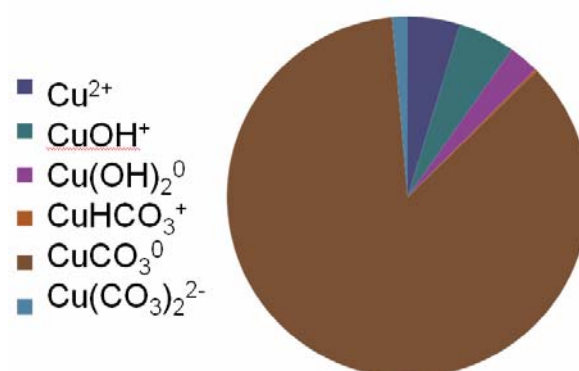
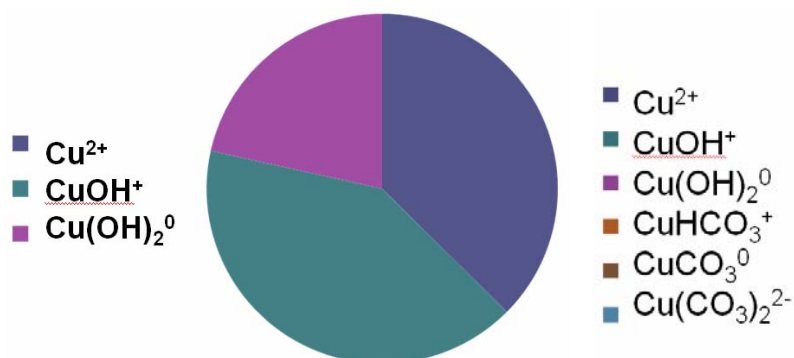


Figure 3.3 Speciation of copper (II) at pH 8.0 under  $\text{Cu(OH)}_2$  control without alkalinity

Figure 3.4 Speciation of copper (II) at pH 8.0 under  $\text{Cu(OH)}_2$  control with alkalinity 30 mg/L as  $\text{CaCO}_3$

When there is no alkalinity,  $\text{Cu}^{2+}$  composes 37% of all the dissolved copper; however, after addition of 30 mg/L of  $\text{CaCO}_3$  alkalinity,  $\text{Cu}^{2+}$  composes only 5% of all the dissolved copper whereas  $\text{CuCO}_3^0$  composes 86% of all dissolved copper. This demonstrates the significant role of alkalinity in increasing cuprosolvency by carbonatocopper (II) complexes.

## CHAPTER 4 MATERIALS AND METHODS

This dissertation is based on research that was part of a larger research effort by the University of Central Florida (UCF) Environmental Systems Engineering Institute (ESEI) jointly supported by the member governments of Tampa Bay Water (TBW) and by the American Water Works Research Foundation (AwwaRF). At the time this dissertation was written, results from this research were pending publication in the AwwaRF report, “Control of Distribution System Water Quality in a Changing Water Quality Environment Using Inhibitors” conducted by Taylor et al. (2008). Throughout this dissertation, this research effort is referred to as TBW II. The pilot distribution system facility was constructed during a previous research investigation, TBW I, published in the AwwaRF report, “Effects of Blending on Distribution System Water Quality” conducted by Taylor et al. (2005).

### **Pilot Testing**

A pilot testing facility was used to test the effects of corrosion inhibitors on distribution system water quality in pilot distribution systems. The pilot distribution systems are located on the grounds of the Cypress Creek Water Treatment Facility in Pasco County, Florida, USA.

### *Source Waters*

A blend of surface water (SW), groundwater (GW), and brackish water (RO) was used for the pilot study. The following paragraphs describe the treatment process for each source water.

Surface water was treated at a surface water treatment plant by ferric sulfate coagulation and trucked to the pilot testing facility shown in Figure 4.1 and pumped into storage tanks shown

in Figure 4.2. On site, the surface water treatment process included chloramination and pH stabilization.

Raw groundwater was obtained from the Cypress Creek water treatment facility. The groundwater treatment process included aeration, chloramination, and pH stabilization.

Brackish water was artificially prepared from the raw groundwater by the addition of sea salt. The reverse osmosis desalinated water treatment process included reverse osmosis, aeration, chloramination, and pH stabilization.

The three sources were blended, aerated, chloraminated, and pH stabilized in the process tanks shown in Figure 4.3. All pilot distribution systems received the same blend of water. Three blends were studied over four operating phases, with each phase lasting three months. Blend composition, water quality, and schedule for each phase are presented in Table 4.1. A more detailed table showing the averages and range of water quality parameters is given in Table 4.2

Table 4.1  
Blend ratios and water quality by phase

	Phase I	Phase II	Phase III	Phase IV
GW (%)	62	27	62	40
SW (%)	27	62	27	40
RO (%)	11	11	11	20
Alkalinity (mg/L as CaCO <sub>3</sub> )	160	103	150	123
Chlorides (mg/L Cl <sup>-</sup> )	45	67	68	59
Sulfates (mg/L SO <sub>4</sub> <sup>2-</sup> )	62	103	67	76
Temperature (°C)	21.3	26.2	25.7	21.2
Time Period	Feb-May 2006	May-Aug 2006	Aug-Nov 2006	Nov 2006-Feb 2007

On-site chemical analyses were conducted in the field trailers shown in Figure 4.4. Off site chemical analyses were completed at UCF ESEI. Finished waters were then fed to the

influent standpipes of the pilot distribution systems. The influent standpipes for the pilot distribution systems are shown in Figure 4.5.

Table 4.2  
Water Quality Profile

Parameter	Project Minimum	Project Maximum	Phase I	Phase II	Phase III	Phase IV
Alkalinity (mg/L as CaCO <sub>3</sub> )	84	175	160	103	150	123
Calcium (mg/L as CaCO <sub>3</sub> )	53.8	220	202	105	206	168
Chloride (mg/L)	35	123	45	67	68	59
Dissolved Oxygen (mg/L)	6.6	10.9	8.7	8	8	9.1
pH	7.4	9.1	7.9	7.9	7.9	7.8
Silica (mg/L)	4	65.0*	10.9	5.1	10.2	6.4
Sodium (mg/L)	5	53.3	7	36.7	39.5	32
Sulfate (mg/L)	52	119	62	103	67	76
TDS (mg/L)	338	436	365	388	413	378
Temperature (°C)	10.4	29.7	21.3	26.2	25.7	21.2
Total Phosphorus (mg/L as P)	0	3.36*	0.2	0	0	0.1
UV-254 (cm <sup>-1</sup> )	0.007	0.105	0.071	0.069	0.077	0.063
Zinc (mg/L)	0.001	0.793	0.031	0.023	0.04	0.037

### *Corrosion Inhibitors*

Corrosion inhibitors, including, blended poly/ortho phosphate (BOP), orthophosphate (OP), zinc orthophosphate (ZOP), and silicate (SiO<sub>2</sub>) were fed from inhibitor tanks by peristaltic pumps, shown in Figure 4.6, into the influent standpipes to mix with the blend water coming from the process storage tanks. Phosphate inhibitors were dosed at 0.5, 1.0, and 2.0 mg/L as P, while silicate inhibitor was dosed at 3.0, 6.0, and 12.0 mg/L as SiO<sub>2</sub>. Phosphate inhibitors were all maintained near pH<sub>s</sub>+0.3 (about 8.0). pH in the silicate lines varied directly with inhibitor

dose., with pH in the 12 mg/L as SiO<sub>2</sub> line averaging 8.4. Two PDSs were operated as pH controls without inhibitor addition. One PDS was operated at the stability pH for calcium carbonate precipitation, pH<sub>s</sub>, while the other was operated at an elevated pH, pH<sub>s</sub>+0.3.

### *Pilot Distribution Systems*

After inhibitor addition, the water from each influent standpipe flowed into the pilot distribution systems (PDSs), shown in Figure 4.7. The PDSs were constructed to simulate the effects of variation in source waters on distribution system water quality. All pipes used in the PDSs were excavated from distribution systems of TBW member governments. Each of 14 pilot distribution systems (PDS) was composed of four materials, laid out sequentially as:

Approximately 20 feet (6.1 m) of 6-inch (0.15 m) diameter polyvinylchloride (PVC) pipe,

Approximately 20 feet (6.1 m) of 6-inch (0.15 m) diameter lined cast iron (LCI) pipe,

Approximately 12 feet (3.7 m) of 6-inch (0.15 m) diameter unlined cast iron (UCI) pipe,

Approximately 40 feet (12.2 m) of 2-inch (0.05 m) diameter galvanized iron (G) pipe

### *Pipe Coupons*

G, LCI, PVC, and UCI coupons for biofilm and surface analyses were incubated in the corrosion cradles shown in Figure 4.8. The coupons were cut from pipes like those used in the PDSs. The corrosion cradles received a parallel feed from the influent standpipes. Coupons were mounted on PVC sleeves as shown in Figure 4.9.

### *Corrosion Shed*

At the end of each PDS water flowed from the effluent standpipe into a corrosion shed, shown in Figure 4.10. Inside the corrosion shed, there were 14 separate 5/8 inch inner diameter copper tubes, shown in Figure 4.11, with each loop of copper tubing being 30 feet (9.1 m) long. Hence the surface area of copper tubing was 707 in<sup>2</sup> (4560 cm<sup>2</sup>). Hence each copper tube held about 1.81 L (1810 cm<sup>3</sup>) of water. The ratio of surface area to volume was thus 40 m<sup>-1</sup> (0.4 cm<sup>-1</sup>). Typical values for surface area to volume ratios for copper tubing experiments are summarized by Merkel and Pehkonen (2006).

One lead-tin coupon, having 3.38 in<sup>2</sup> (21.8 cm<sup>2</sup>) surface area, was placed between two standard brass fittings within each copper loop assembly to simulate lead release from lead/tin solder in a copper plumbing system. Hence the surface area of lead tin was about 0.5% that of copper.

### *Corrosion Coupons*

Copper, lead/tin, and iron corrosion coupons for surface analyses were stored in noise cradles or “naddles” which were inside the electrochemical noise trailer shown in Figure 4.12. The copper coupons measured 1/2 inch by 3 inch by 1/16 inch (1.27 cm by 7.6 cm by 0.16 cm). The lead/tin coupons measured 3/8 inch by 3 inch by 1/16 inch (0.95 cm by 7.6 cm by 0.16 cm). The naddles also contained copper, lead/tin, and iron electrodes that were used in electrochemical studies.



Figure 4.1 Truck and stainless steel trailer used to haul raw surface water



Figure 4.2 Raw surface water storage



Figure 4.3 Covered tanks for process treatment



Figure 4.4 Field trailers



Figure 4.5 Influent standpipes



Figure 4.6 Inhibitor tanks and feed pumps



Figure 4.7 Pilot distribution systems



Figure 4.8 Cradles for housing coupons



Figure 4.9 Mounted coupons



Figure 4.10 Corrosion shed

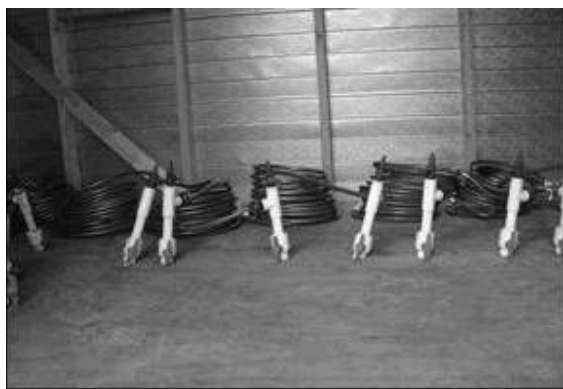


Figure 4.11 Copper lines with lead coupons



Figure 4.12 Electrochemical Noise Trailer

## Surface Characterization

### *Surface Structure*

#### Optical Profilometry

An optical profiler, WYKO NT 3300 (Veeco Instruments, Woodbury, N.Y.) was used to measure surface roughness of galvanized iron (G), lined cast iron (LCI), polyvinyl chloride (PVC), unlined cast iron (UCI), and copper (Cu), and lead/tin (PbSn). The instrument, shown in Figure 4.13, is a non-contact optical profiler capable of producing three dimensional surface measurements with 4.14  $\mu\text{m}$  horizontal resolution and 0.1 nm vertical resolution.



Figure 4.13 WYKO NT 3300 optical profiler

The surface roughness of each coupon was measured both before and after incubation in its corresponding cradle or nadle. Table 4.3 shows the number of surface roughness coupons by material and by phase. In Phase I, three surface roughness measurements were made per coupon both before and after incubation in the PDSs. In Phase II, five measurements per coupon were

made for all materials. In Phases III and IV, eight measurements were made per metal coupon and five measurements were made per nonmetal coupon.

Table 4.3  
Number of surface roughness coupons by material and phase

<b>Material</b>	<b>Phase I</b>	<b>Phase II</b>	<b>Phase III</b>	<b>Phase IV</b>	<b>Total</b>
<i>Pipe Coupons</i>					
Galvanized iron (G)	14	14	14	14	56
Lined Cast Iron (LCI)	6	14	14	14	48
Polyvinyl Chloride (PVC)	6	14	14	14	48
Unlined Cast Iron (UCI)	14	14	14	14	56
<i>Metal Coupons</i>					
Copper (Cu)	-	-	14	14	28
Lead-Tin (Pb/Sn)	-	-	14	14	28
<i>Total by Phase</i>	40	56	98	98	292

Table 4.4  
Number of measurements per coupon by material and phase

<b>Material</b>	<b>Phase I</b>	<b>Phase II</b>	<b>Phase III</b>	<b>Phase IV</b>
<i>Pipe Coupons</i>				
Galvanized iron (G)	3	5	8	8
Lined Cast Iron (LCI)	3	5	5	5
Polyvinyl Chloride (PVC)	3	5	5	5
Unlined Cast Iron (UCI)	3	5	8	8
<i>Metal Coupons</i>				
Copper (Cu)	-	-	8	8
Lead-Tin (Pb/Sn)	-	-	8	8

Note: "3" indicates a total of six measurements, with three before incubation and three after incubation.

Table 4.4 shows the number of measurements made per coupon by material and phase both before incubation and after incubation. For example, in Phase II, five measurements were made of each G coupon before incubation and after incubation, totaling ten measurements. Only for the coupons of Phase I, a stripe of reflective paint was applied to the edge of each pipe

coupon to help bring the coupon surface into focus, improving scan quality. Surface roughness was only measured on the unpainted portions of the coupons. After Phase I, no paint was applied to any coupon. Instead, a flashlight was used to help bring the surface into focus. One of the most significant findings of this work was that this instrument, typically used with highly reflective specimens in the semiconducting industry, has application to the imaging of dull, non-reflective, heterogeneous surfaces like corroded pipe. This finding shows that this pipe may have further application in industries like drinking water or petrochemicals, which deal with corroded pipelines.

### Scanning Electron Microscopy

A scanning electron microscope, JEOL 6400F SEM, (JEOL Ltd, Tokyo, Japan) was used to take micrographs of galvanized iron (G), copper (Cu), iron (Fe), and lead/tin (PbSn) coupons. The SEM emits an energized electron beam which interacts with a surface causing the surface to reemit electrons and photons. The microscope produces the image by analyzing the reemitted electrons. The SEM shown in Figure 4.14 was used to take micrographs up to 5000x with a horizontal resolution of 10nm. All sample surfaces were Au/Pd sputtered before analysis. Images were taken from a working distance of 14 mm.

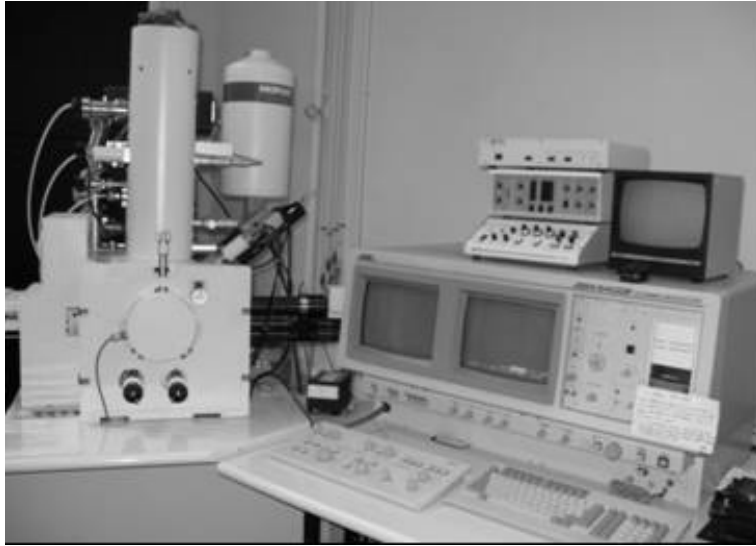


Figure 4.14 SEM JEOL 6400F

### *Surface Composition*

#### X-Ray Photoelectron Spectroscopy

Following each phase of operations, chemical compositions of corrosion scales on the surface of metal coupons (iron, copper, lead, and galvanized iron) were characterized by X-ray Photoelectron Spectroscopy (Physical Electronics 5400 ESCA) (Figure 4.15). In XPS, a Mg anode (1254 eV  $K\alpha$ ) bombards the coupon surface with high energy X-rays that interact with atoms in the top 5-6 nm of the surface (Seal and Barr 2001). Then, according to the photoelectric effect, these atoms emit high energy electrons. An electron analyzer counts the number of electrons emitted over a range of energies, producing scan spectra which may be used for surface composition analysis.

Coupons were inserted into the pilot distribution systems (PDS) at the beginning of each phase of pilot plant operation, and then retrieved at the end of the phase. The XPS scanning consists of a two-step process: an initial “survey” scan followed by a “high resolution” scan.

The survey scan, conducted over a broad range of energy levels, is useful for confirming the presence or absence of elements on the surface of the coupon. In contrast, a high resolution scan, conducted over a narrow range of energy levels is useful for establishing the chemical states present for a given element.



Figure 4.15 Physical Electronics 5400 ESCA XPS

Elements are indicated by pronounced peaks above the background. Elements of interest, such as those associated with inhibitors, coupon material, or water quality, were analyzed with high resolution scans. Possible compounds associated with a given element were determined through deconvolution of the high resolution scan.

#### Energy Dispersive X-Ray Spectroscopy

The scanning electron microscope, has an energy dispersive spectroscope (EDS), which analyzes the emitted photons to determine chemical composition of the surface. EDS enables one to identify the chemical composition of surface features detected in a micrograph.

## Thermodynamic Modeling

### *Copper Solubility*

#### Theory

Thermodynamic models were developed to evaluate if the beneficial effect of corrosion inhibitors results from a change in the controlling solid phase of copper. The thermodynamic model is inherently limited to consideration of dissolved copper at equilibrium. Copper release kinetics and particulate copper are not evaluated in this technique. The total dissolved cupric ion concentration is the sum of the free dissolved cupric ions and the complexed dissolved cupric ions.

The free dissolved cupric ion concentration,  $[Cu^{2+}]$ , is evaluated by assuming a copper controlling solid and solving the solubility equilibrium equation for the cupric ion concentration. For example, cupric phosphate,  $Cu_3(PO_4)_2$ , has a solubility equilibrium equation as shown in Equation 4.1. The predicted free dissolved cupric ion concentration can then be found algebraically as shown in Equation 4.2. It also follows that when cupric phosphate is the controlling solid phase, the free cupric ion concentration can be expected to vary with the negative two-thirds power of the phosphate concentration.

$$K_{sp} = [Cu^{2+}]^3 [PO_4^{3-}]^2 \quad \text{Equation 4.1}$$

$$[Cu^{2+}] = \left( \frac{K_{sp}}{[PO_4^{3-}]^2} \right)^{\frac{1}{3}} \quad \text{Equation 4.2}$$

Once in solution the free dissolved cupric ion can interact with other dissolved species to form copper complexes. A copper complex results when these other dissolved species act as ligands and associate with electron pairs on the central atom, the cupric ion. The propensity of these ligands to complex cupric ion can be described using equilibrium relations like that shown in Equation 4.3 describing the relationship between free dissolved cupric ion and the  $\text{CuCO}_3^0$  complex.

$$[\text{CuCO}_3^0] = \frac{K_f}{[\text{Cu}^{2+}][\text{CO}_3^{2-}]} \quad \text{Equation 4.3}$$

### Application

Feasible copper controlling solid phases were identified with the aid of XPS for further thermodynamic modeling. Chemical water quality data for each phase blend were compiled to provide the necessary information to predict the free and complexed cupric ion concentrations. The thermodynamic model, shown in Equation 4.4, assumed that all dissolved copper is present entirely as copper (II), cupric, ion. This model is similar to the thermodynamic model used during TBW I (Taylor et al., 2005); however, it was expanded to include phosphate, sulfate, chloride, and ammonia. A review of literature concerning coordination chemistry did not reveal any thermodynamic data corresponding to a copper-silica complex.

$$\begin{aligned} \text{Cu}_T = & [\text{Cu}^{2+}] + [\text{CuOH}^+] + [\text{Cu}(\text{OH})_2^0] + [\text{Cu}(\text{OH})_3^-] + [\text{CuHCO}_3^+] + [\text{CuCO}_3^0] \\ & + [\text{Cu}(\text{CO}_3)^{2-}] + [\text{Cu}(\text{OH})\text{CO}_3^-] + [\text{Cu}(\text{OH})_2\text{CO}_3^{2-}] + [\text{CuH}_2\text{PO}_4^+] \\ & + [\text{CuHPO}_4^0] + [\text{CuSO}_4^0] + [\text{Cu}(\text{NH}_3)^{2+}] + [\text{Cu}(\text{NH}_3)_2^{2+}] + [\text{Cu}(\text{NH}_3)_3^{2+}] \\ & + [\text{Cu}(\text{NH}_3)_4^{2+}] + [\text{Cu}(\text{NH}_3)_5^{2+}] + [\text{CuCl}^+] + [\text{CuCl}^0] \end{aligned} \quad \text{Equation 4.4}$$

Thermodynamic modeling of phosphate, sulfate, and ammonia complexes of copper demonstrated that these complexes were insignificant to total dissolved copper release. Of these complexes, copper phosphate complexes were the most abundant yet only comprised 0.5% of total dissolved copper.

Consideration of the different water quality parameters present in Equation 4.4 gives insight into how these water quality parameters may act as factors increasing dissolved copper release. The complexes considered within Equation 4.4 demonstrate the various water quality parameters. An empirical model, developed as a part of this study (Taylor et al. 2008), identified pH, chloride, and alkalinity as the main water quality factors influencing dissolved copper release. Increasing the pH tended to reduce copper release; whereas, raising chloride or alkalinity tended to increase copper release.

Despite being significant in the empirical model (Taylor et al. 2008), thermodynamic modeling suggests that copper chloride complexes are not a significant factor, per se, in dissolved copper release.  $\text{CuCl}^+$  and  $\text{CuCl}^0$  complexes accounted for less than 0.0001% of total dissolved copper release, for the water quality conditions of this study. Hence, some other explanation would be required to explain the effect of chlorides on copper release.

In contrast, thermodynamic modeling suggests that copper alkalinity complexes are a significant factor in dissolved copper release.  $\text{CuCO}_3^0$ ,  $\text{Cu}(\text{CO}_3)_2^{2-}$ ,  $\text{Cu}(\text{OH})\text{CO}_3^-$ , and  $\text{Cu}(\text{OH})_2\text{CO}_3^{2-}$  complexes accounted for about 90% of all total dissolved copper. Charged complexes could play a role in the formation of malachite. Hence, alkalinity is an important factor understanding and controlling total dissolved copper release.

## CHAPTER 5 SURFACE ROUGHNESS OF COMMON WATER DISTRIBUTION SYSTEM MATERIALS

### Abstract

The effects of phosphate inhibitors on surface roughness of galvanized iron, lined cast iron, polyvinyl chloride, and unlined cast iron pipe were evaluated as part of a yearlong pilot study investigating the influence of corrosion inhibitors on distribution system water quality.

Inhibitors included blended poly/ortho phosphate, sodium orthophosphate, zinc orthophosphate, sodium silicate, and pH elevation. An optical profiler was used to measure surface roughness both before and after exposure to inhibitors during a three month phase.

Change in surface roughness of G and UCI tended to vary with the initial surface roughness toward an equilibrium roughness. For G, LCI, and PVC, no statistically significant relationship was found between inhibitor addition or water quality and surface roughness. Water quality and inhibitors appeared to influence UCI surface roughness. Increased alkalinity and increased temperature tended to correspond with increases in UCI surface roughness. UCI coupons receiving phosphate inhibitors tended to have significant changes in surface roughness more frequently than UCI coupons not receiving phosphate inhibitors.

## **Introduction**

### *Distribution System Water Quality*

Management of water quality in the distribution system is an essential task for utilities who must deliver a reliable supply of drinking water that meets consumer expectations and regulatory requirements. Public health concerns include release of copper and lead from plumbing as well as regrowth of microorganisms, and formation of disinfection by products. In addition, release of iron from unlined pipes can cause consumer complaints over “red water.” These problems can be exacerbated when new source waters are introduced into the finished water blend.

A recent AWWARF study entitled “Control of Distribution System Water Quality in a Changing Water Quality Environment Using Inhibitors” investigated the use of corrosion inhibitors to control metal release in distribution systems receiving a blend of groundwater, surface water, and reverse osmosis desalinated water. Significant decreases in copper and lead release were observed with the addition of phosphate or silicate inhibitors. The study also looked at the impact of inhibitors on iron release, chloramine demand, and biological regrowth.

This paper examines the effect of inhibitors on surface roughness of common water distribution system materials. Conceptually, it is reasonable that reductions in metal release would result from a decrease in the corrosion reaction which supplies dissolved metal at the anode. Because corroded surfaces tend to be relatively rough, it is reasonable to expect that surfaces exposed to corrosion inhibitors may be smoother than surfaces not exposed to inhibitors. The following section discusses the effects of surface roughness in the distribution system.

### *Effects of Surface Roughness*

Surface roughness increases pipe pressure losses. It is also a suspected factor in water quality phenomena at the pipe wall including biofilm density, chlorine decay, and polyphosphate reversion.

### Pipe Pressure Losses

Water flowing through a pipe encounters resistance along the pipe wall. This resistance to flow increases as the pipe roughness increases. Rough pipes tend to have higher pressure losses for a given flow and are said to have reduced hydraulic capacity. Nikuradse was the first to quantify the relationship between pipe surface roughness and pressure losses. He simulated rough pipes by gluing sieved sand grains of relatively uniform diameter to the pipe walls and measuring pressure drop at each roughness (Nikuradse 1950). The average sand grain diameter,  $e$ , corresponds to the absolute roughness of a pipe. The Colebrook equation (Equation 5.1) relates the absolute roughness,  $e$ , to the Darcy friction factor,  $f$  (Colebrook 1939).

$$\frac{1}{\sqrt{f}} = -2 \log \left( \frac{e/D}{3.7} + \frac{2.51}{\text{Re} \sqrt{f}} \right) \quad \text{Equation 5.1}$$

where  $f$  = Darcy friction factor (-)  
 $e$  = absolute roughness, equivalent to sand grain diameter (ft)  
 $D$  = pipe diameter (ft)  
 $\text{Re}$  = Reynolds number (-)

Because the equation is implicit in  $f$ , it must be solved iteratively.  $f$  increases with increasing  $e/D$ , while decreasing asymptotically with increasing  $\text{Re}$ . Alternatively, engineers may use other approximating formulas or the Moody chart for friction factor (Moody 1944). This

friction factor is then used to compute head loss by the Darcy-Weisbach equation for head loss (Equation 5.2)

$$h_f = f \frac{L V^2}{D 2g}$$

Equation 5.2

where  $h_f$  = head loss (ft)  
 $f$  = Darcy-Weisbach friction coefficient  
 $D$  = equivalent diameter (ft)  
 $V$  = average velocity (ft/s)  
 $g$  = acceleration due to gravity, 32.2 (ft/s<sup>2</sup>)

The most common formula used to relate hydraulic capacity and head loss is the empirically based Hazen-Williams equation, which is presented in Equation 5.2. Utilities commonly conduct flow tests in order to determine the Hazen-Williams coefficient for given lengths of pipe (Walski et al. 2003). Higher  $C_{HW}$  correspond with a higher hydraulic capacity, like that found in new pipe. Thus, the  $C_{HW}$  is inversely proportional to pipe surface roughness. The  $C_{HW}$  is also a function of fluid velocity, fluid kinematic viscosity, and pipe diameter (Sharp and Walski 1988).

$$h_f = 3.04 C_{HW}^{-1.85} D^{-1.17} V^{1.85} L$$

Equation 5.3

where  $h_f$  = head loss (ft)  
 $C_{HW}$  = Hazen-Williams Coefficient  
 $D$  = diameter of circular conduit (ft)  
 $V$  = average velocity (ft/s)  
 $L$  = length of circular conduit (ft)

There are few studies in the literature investigating the relationship between surface roughness in a distribution system and distribution system water quality. Hudson (1966) examined the decline in carrying capacity of water distribution systems in seven cities. He found

that the decline in Hazen-Williams coefficient varied between cities, suggesting that roughness growth rates may depend on local water quality.

Larson and Sollo (1967) examined the relationship between water quality and corrosion rate of unlined cast iron. They recommended that the pH be adjusted to maintain a zero calcium carbonate saturation index in order to avoid losses in pipe carrying capacity.

Sharp and Walski (1988) developed a model for predicting the increase in roughness of unlined metal pipes and water quality. The model assumed that roughness increased linearly with time, and the rate of roughness increase was dependent on Langelier index (LI), with more negative LIs corresponding with greater rates of roughness increase. By incorporating the LI into the roughness growth model, Sharp and Walski, demonstrated that calcium hardness and alkalinity, in addition to pH, are factors affecting the roughness growth rate. Taken together, these studies suggest roughness growth rate is largely influenced by water quality.

### Biofilm Density

Historically, surface roughness in the distribution system has been considered for its effect on flow capacity. However, surface roughness may also be a factor influencing various water quality phenomena occurring at the pipe wall, such as biofilms and chlorine dissipation.

Fletcher and Marshall (1982) found the rate of biofilm formation to be dependent on surface chemistry, surface roughness, and the organism. LePuil et al. (2005) measured biofilm density using the protein exoproteolytic activity (PEPA) assay by Laurent and Servais (1995) and found that biofilm density was greatest for UCI pipe, followed by LCI and G pipe. Finally the least biofilm density was observed for PVC pipe. Visual observations of the roughness of

these materials suggest that differences in biofilm density by material can be related to differences in material surface roughness.

### Chlorine Decay

Surface roughness has been proposed as a factor affecting chlorine decay at the pipe wall; however, published studies seem to suggest that material is more important than surface roughness in determining wall rate constants.

Doshi, Grayman, and Guastella (2003) conducted a series of simultaneous chlorine loss and head loss tests within the water distribution system of Detroit, Mich. Most of the pipes were unlined cast iron, from 70 to 135 years old. Using a first-order mass-transfer model, they reported that the wall decay coefficient of chlorine,  $k_w$  ( $L/time^{-1}$ ), did not appear to be related to the Hazen-Williams coefficient (i.e. pipe roughness), but rather  $k_w$  increased directly with increasing flow.

Vasconcelos et al. (1997) developed a distribution system chlorine decay model for unlined cast iron pipe that took both bulk and wall chlorine decay into account. The both zero order and first order wall rate constants were determined assuming that the wall rate constant for each pipe varied inversely with the Hazen-Williams coefficient on record for that pipe. However, inclusion of the roughness term in the model provided only a minimal improvement in the predictive power of the chlorine decay model.

Furthermore, there is evidence suggesting that pipe material is the most important factor affecting wall rate constants. Arevalo (2003) and Ki  n  , Lu, and L  vi (1998) have all found that old cast iron and steel pipes had a higher chlorine demand than plastic pipes, suggesting that

oxidation of ferrous iron to ferric iron is a key factor responsible for decay of chlorine residual at the pipe wall.

### *Measurement of Surface Roughness*

There are two common methods for the measurement of pipe surface roughness. Flow testing is an indirect technique that measures the reduction in flow due to pipe surface roughness; whereas, profilometry is a direct technique that measures the actual shape of the pipe surface.

### Flow Testing

Flow tests may also be used to quantify pipe surface roughness. They are helpful because they directly measure hydraulic head losses. By measuring the flow of water through a pipe under a known pressure gradient it is possible to deduce the surface roughness of that pipe using empirical relationships of fluid mechanics. This method was mentioned previously in the subsection on pipe pressure losses.

### Profilometry

This study used a surface profiler to directly measure the physical surface roughness of pipes. There are two common kinds of surface profilers available for measurement of pipe surface roughness. Results from either kind of profiler can be used to calculate surface roughness parameters, such as  $R_a$ . With a stylus profiler, a stylus is traced in a line across the surface, and the displacement of the stylus is recorded along the trace line. In contrast, an optical profiler uses the interference of light to measure surface roughness over a scanning area. A monochromatic beam of light is split and directed towards a flat reference surface and the measurement surface.

The light is reflected from each surface and recombined within the profiler. When the beams of light recombine, interference fringes form because the phase of the light reflected from the measurement surface depends on the distance of the optical path, which depends on the surface elevation. Optical profilometry works best with uniformly reflective materials. Measurement of dull or non-uniformly reflective materials is more difficult. Optical profilometry has the advantage of being able to rapidly generate a map of the surface elevation over a given area of the coupon without contacting the coupon surface.

When surface roughness is measured by a profiler, a roughness statistic can then be computed from the profile data (Lippold and Podlesny, 1998). Most of these statistics describe either the height or the spacing of peaks and valleys in the profile. In this paper,  $R_a$ , the roughness average is used. It is the arithmetic mean of the surface deviations from the mean plane. For an array of  $M$  by  $N$  elevation points, it is calculated according to Equation 5.4. Figure 5.1 shows a surface profile with average  $R_a$  roughness of  $83.2 \mu\text{m}$ , calculated over the  $2.3 \text{ mm} \times 3.0 \text{ mm}$  scan area.

$$R_a = \frac{1}{MN} \sum_{j=1}^M \sum_{i=1}^N |Z_{ij}| \quad \text{Equation 5.4}$$

where  $R_a$  = roughness average ( $\mu\text{m}$ )  
 $M$  = number of rows in the array  
 $N$  = number of columns in the array  
 $Z_{ij}$  = the absolute value of the deviation of the surface from the mean zero plane at the cell where the  $i^{\text{th}}$  column and  $j^{\text{th}}$  row of the array intersect ( $\mu\text{m}$ )

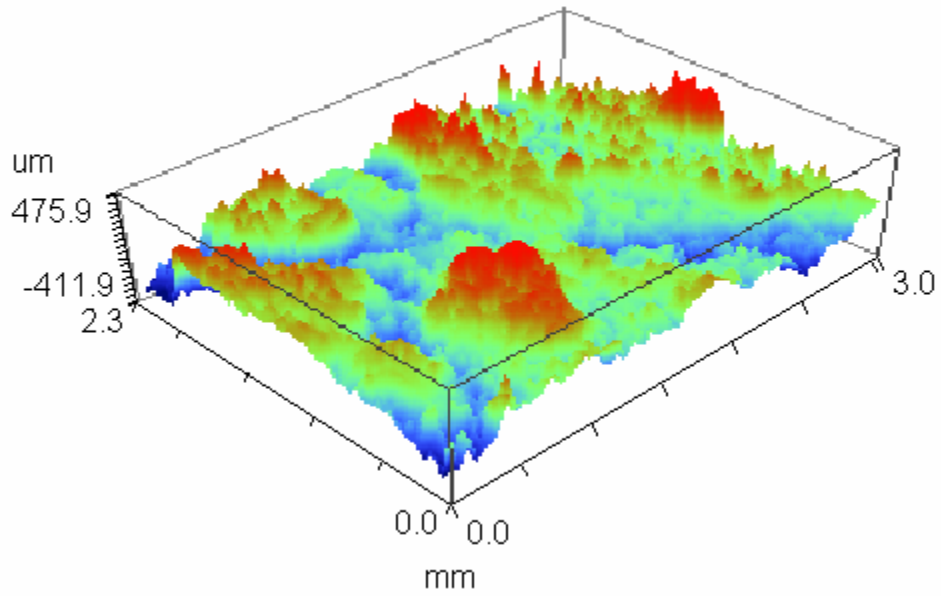


Figure 5.1 Sample OIP Scan of UCI pipe surface with  $R_a$  of  $83.2 \mu\text{m}$

## **Materials and Methods**

### *Pilot Testing*

A pilot testing facility was used to test the effects of corrosion inhibitors on distribution system water quality in pilot distribution systems. The pilot distribution systems are located in Pasco County, Florida, USA on the grounds of the Cypress Creek Water Treatment Facility.

### Source Waters

A blend of surface water, groundwater, and brackish water was used for the pilot study. The following paragraphs describe the treatment process for each source water.

Surface water was treated at a surface water treatment plant by ferric sulfate coagulation and trucked to the pilot testing. On site, additional surface water treatment process included chloramination and pH stabilization.

Raw groundwater was obtained from the Cypress Creek water treatment facility. The groundwater treatment process included aeration, chloramination, and pH stabilization.

Brackish water was artificially prepared from the raw groundwater by the addition of sea salt. The reverse osmosis desalinated water (RO) treatment process included reverse osmosis, aeration, chloramination, and pH stabilization.

The three sources were blended, aerated, chloraminated, and pH stabilized in the process tanks shown in Figure 5.2. Within each phase, all pilot distribution systems received the same blend of water. Three blends were studied over four operating phases, with each phase lasting three months. Blend composition, water quality, and schedule for each phase are presented in Table 5.1.

Table 5.1  
Blend ratios and water quality by phase

	Phase I	Phase II	Phase III	Phase IV
GW (%)	62	27	62	40
SW (%)	27	62	27	40
RO (%)	11	11	11	20
Alkalinity (mg/L as CaCO <sub>3</sub> )	160	103	150	123
Chlorides (mg/L Cl <sup>-</sup> )	45	67	68	59
Sulfates (mg/L SO <sub>4</sub> <sup>2-</sup> )	62	103	67	76
Temperature (°C)	21.3	26.2	25.7	21.2
Time Period	Feb-May 2006	May-Aug 2006	Aug-Nov 2006	Nov 2006-Feb 2007

### Corrosion Inhibitors

Corrosion inhibitors, including, blended poly/ortho phosphate (BOP), orthophosphate (OP), zinc orthophosphate (ZOP), and silicate (SiO<sub>2</sub>) were fed from inhibitor tanks by peristaltic pumps, into influent standpipes to mix with blended water coming from the process storage tanks. Phosphate inhibitors were dosed at 0.5, 1.0, and 2.0 mg/L as P, while silicate inhibitor was dosed at 3.0, 6.0, and 12.0 mg/L as SiO<sub>2</sub>. Two PDSs were operated as pH controls without inhibitor addition. One PDS was operated at the stability pH for calcium carbonate precipitation, pH<sub>s</sub>, while the other was operated at an elevated pH, pH<sub>s</sub>+0.3.

### Pilot Distribution Systems

After inhibitor addition, the water from each influent standpipe flowed into the pilot distribution systems (PDSs), shown in Figure 5.3. The PDSs were constructed to simulate the effects of variation in source waters on distribution system water quality. All pipes used in the PDSs were excavated from TBW member government distribution systems. Each of 14 pilot distribution systems (PDS) was composed of four materials, laid out sequentially as:

Approximately 20 feet (6.1 m) of 6-inch (0.15 m) diameter polyvinylchloride (PVC) pipe,

Approximately 20 feet (6.1 m) of 6-inch (0.15 m) diameter lined cast iron (LCI) pipe,  
Approximately 12 feet (3.7 m) of 6-inch (0.15 m) diameter unlined cast iron (UCI) pipe,  
Approximately 40 feet (12.2 m) of 2-inch (0.05 m) diameter galvanized iron (G) pipe



Figure 5.2 Covered tanks for process treatment



Figure 5.3 Pilot distribution systems



Figure 5.4 Cradles for housing coupons

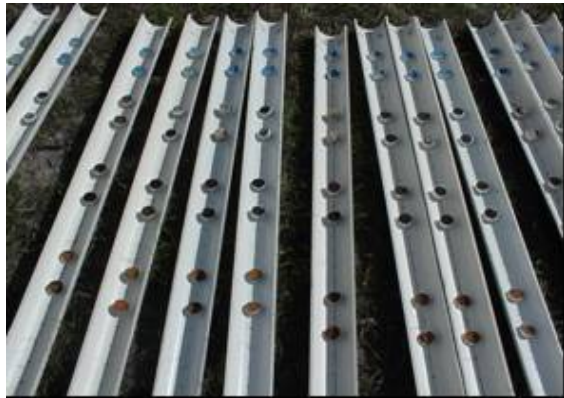


Figure 5.5 Mounted coupons

### Pipe Coupons

G, LCI, PVC, and UCI coupons for biofilm and surface analyses were incubated in the corrosion cradles shown in Figure 5.4. The coupons were cut from pipes like those used in the

PDSs. The corrosion cradles received a parallel feed from the influent standpipes. Coupons were mounted on PVC sleeves as shown in Figure 5.5.

### *Surface Characterization*

#### Optical Profilometry

An optical profiler, WYKO NT 3300 (Veeco Instruments, Woodbury, N.Y.) was used to measure the surface roughness of galvanized iron (G), lined cast iron (LCI), polyvinyl chloride (PVC), and unlined cast iron (UCI). The WYKO NT 3300, shown in Figure 5.6, is a non-contact optical profiler capable of producing three dimensional surface measurements with 4.14  $\mu\text{m}$  horizontal resolution and 0.1 nm vertical resolution. An example output of the optical profiler was shown previously in Figure 5.1, which depicted the surface of an unlined cast iron coupon having  $R_a$  of 83.2  $\mu\text{m}$ . Post processing of raw outputs included corrections for tilt and cylindrical curvature. Noise in the output was reduced using a 3x3 window median filter.



Figure 5.6 WYKO NT 3300 optical profiler

The surface roughness of each coupon was measured both before and after incubation in its corresponding cradle or nadle. Table 5.2 shows the number of surface roughness coupons by material and by phase. Table 5.3 shows the number of measurements made per coupon by material and phase both before incubation and after incubation. For example, in Phase II, five measurements were made of each G coupon before incubation and after incubation, totaling ten measurements. Because all of the coupons were made of relatively dull materials, a thin strip of reflective paint was applied to coupon to help bring the surface into focus. After Phase I, no paint strips were applied to any coupon. Instead, a flashlight was used to help bring the surface into focus.

Table 5.2  
Number of surface roughness coupons by material and phase

<b>Material</b>	<b>Phase I</b>	<b>Phase II</b>	<b>Phase III</b>	<b>Phase IV</b>	<b>Total</b>
Galvanized iron (G)	14	14	14	14	56
Lined Cast Iron (LCI)	6	14	14	14	48
Polyvinyl Chloride (PVC)	6	14	14	14	48
Unlined Cast Iron (UCI)	14	14	14	14	56
<i>Total</i>	<i>40</i>	<i>56</i>	<i>56</i>	<i>56</i>	<i>208</i>

Table 5.3  
Number of measurements per coupon by material and phase

<b>Material</b>	<b>Phase I</b>	<b>Phase II</b>	<b>Phase III</b>	<b>Phase IV</b>
<i>Pipe Coupons</i>				
Galvanized iron (G)	3	5	8	8
Lined Cast Iron (LCI)	3	5	5	5
Polyvinyl Chloride (PVC)	3	5	5	5
Unlined Cast Iron (UCI)	3	5	8	8

Note: "3" indicates a total of six measurements, with three before incubation and three after incubation.

## Results and Discussion

Surface roughness of G, UCI, LCI, and PVC coupons taken from used water distribution system pipes was measured before and after exposure to inhibition. The changes in surface roughness were analyzed with respect to inhibitor type and dose, water quality, initial and final roughness. For this study, the change in surface roughness of all materials was independent of inhibitor type or dose, but was dependent on the initial surface roughness. Coupons that were initially smooth tended to become rougher during incubation, whereas coupons that were initially rough tended to become smoother during incubation. This is not unreasonable since the coupons had been exposed to dry air before being placed within the pilot distribution systems and would need to come into “equilibrium” with the water environment. Hence, during incubation, the scale on the roughest coupons tended to flake off, whereas the smoothest coupons tended to become rougher.

Table 5.4  
Roughness summary by material

		UCI	G	LCI	PVC
$R_i$	$\mu\text{m}$	86.1	25.5	25.4	1.5
$\sigma_i$	$\mu\text{m}$	21.7	7.4	10.4	0.5
$R_f$	$\mu\text{m}$	93.3	26.3	26.7	1.7
$\sigma_f$	$\mu\text{m}$	18.7	7.6	9.0	0.5
$\Delta R$	$\mu\text{m}$	7.9	0.3	1.5	0.2
$\sigma_\Delta$	$\mu\text{m}$	20.9	6.5	6.0	0.2

Where:  $R_i$  = Initial roughness  
 $\sigma_i$  = Standard deviation Initial roughness  
 $R_f$  = Final roughness  
 $\sigma_f$  = Standard deviation final roughness  
 $\Delta R$  = Delta roughness  
 $\sigma_\Delta$  = Standard deviation delta roughness

The change in roughness of UCI and G coupons was correlated to alkalinity and temperature, but the change in roughness was otherwise independent of water quality. As shown in Table 5.4, the decreasing order of surface roughness was UCI>G≈LCI>PVC. Although there was significant variability in roughness measurements as shown by the standard deviations ( $\sigma$ ) in Table 5.4, measurement of mean roughness of replicate coupons after inhibition exposure showed repeatability within 20 %.

Effects of inhibitors, pH, and water quality on surface roughness were considered. Major differences in water quality by phase are shown in Table 5.1. Phase I and Phase III had the same blend of mostly groundwater (GW 62%) with surface water (SW 27%) and desalinated water (RO 11%). Phase I and III had elevated alkalinities (160 mg/L as CaCO<sub>3</sub> and 150 mg/L as CaCO<sub>3</sub>) and relatively low sulfates (62 mg/L and 67 mg/L). In contrast, chlorides (45 mg/L and 68 mg/L) and temperature (21.3 °C and 25.7 °C) were different for each Phase. Because Phase I and III have the same blend of source waters, comparison of roughness from these two phases shows the effect of temperature and chlorides on surface roughness.

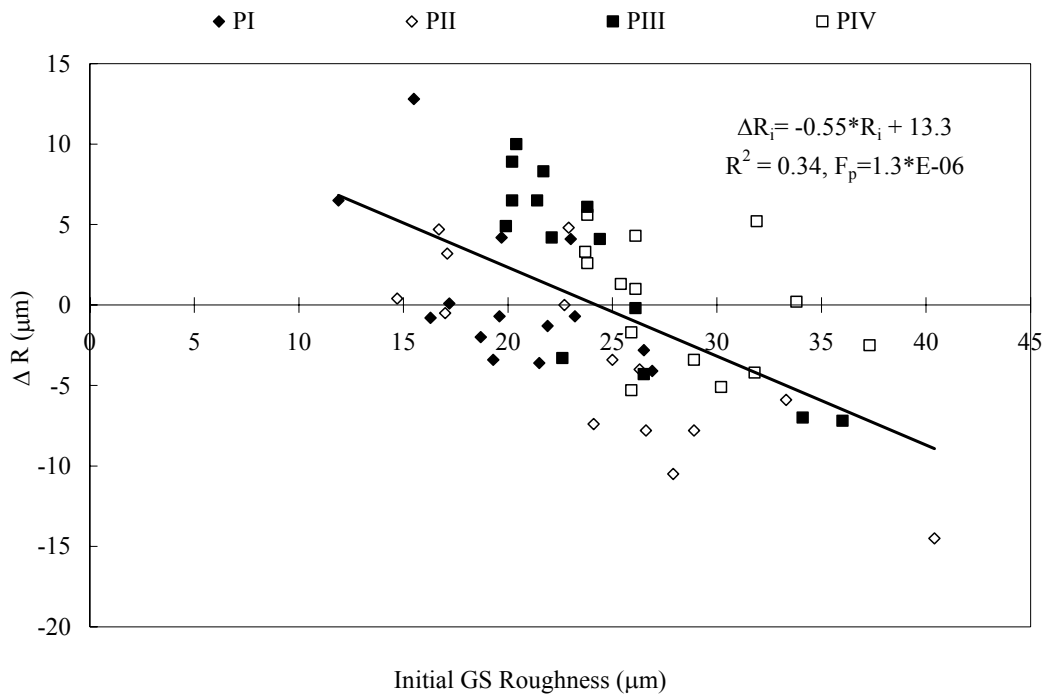
Phase II had a blend of mostly surface water (SW 62%), with groundwater (GW 27%), and desalinated water (RO 11%). Because it was predominately surface water, Phase II had lower alkalinity (103 mg/L as CaCO<sub>3</sub>), and higher sulfate (103 mg/L). Phase IV had a blend of desalinated water (RO 40%), with groundwater (GW 20%), and surface water (SW 20%). Phase IV had moderate alkalinity (123 mg/L as CaCO<sub>3</sub>) and relatively low sulfate (76 mg/L).

### *Galvanized Iron*

The surface roughness of galvanized iron (G) coupons was measured for Phases I, II, III, and IV. Galvanized iron coupons were cut from galvanized iron pipe that had been in service

underground for more than two decades. Before cutting, the pipe had been stored in an open atmosphere for several years. The initial surface roughness of galvanized iron coupons varied from 11.9  $\mu\text{m}$  to 37.3  $\mu\text{m}$  and averaged 24.7  $\mu\text{m}$ . The change in surface roughness of galvanized iron coupons varied from +12.8  $\mu\text{m}$  to -14.5  $\mu\text{m}$  and averaged -0.4  $\mu\text{m}$ . There was no relationship to inhibitor or inhibitor dose.

The change in G roughness,  $\Delta R$ , relative to initial roughness,  $R_i$  is shown in Figure 5.7.  $\Delta R$  was well described by a linear model incorporating the initial surface roughness. Corrosion inhibitors and water quality were not statistically significant factors influencing G surface roughness.



### *Lined Cast Iron*

Surface roughness of lined cast iron (LCI) coupons was measured in all four phases. LCI coupons were cut from lined cast iron pipe that had been in the ground for more than two decades, extracted and stored in an open atmosphere. The initial surface roughness of lined cast iron coupons varied from 13.3  $\mu\text{m}$  to 68.5  $\mu\text{m}$  and averaged 25.2  $\mu\text{m}$ . The change of surface roughness of lined cast iron coupons varied from +16.7 to -25.1  $\mu\text{m}$  and averaged +1.52  $\mu\text{m}$ .

There was no clear relationship between inhibitor dose and surface roughness. Linear and non-linear (power) models for correlating water quality and  $R_i$  to  $\Delta R$  and  $R_f$  of lined cast iron were evaluated for all phases. As with G coupons, the variation of  $R_f$  for LCI coupons was described by a linear model that depended on the initial LCI roughness,  $R_i$ , and a mean roughness term  $R_{\text{mu}}$ , and was independent of inhibitors or water quality.

### *Polyvinyl Chloride*

Polyvinyl chloride coupons were cut from polyvinyl chloride pipe that had been in the ground for more than two decades, extracted and stored in an open atmosphere. The initial surface roughness of polyvinyl chloride coupons varied from 0.64 to 2.98  $\mu\text{m}$  and averaged 1.52  $\mu\text{m}$ . The change of surface roughness of polyvinyl chloride coupons varied from +1.19 to -0.31  $\mu\text{m}$  and averaged 0.16  $\mu\text{m}$ .

The change in polyvinyl chloride surface roughness and the ratio of the initial polyvinyl chloride surface roughness to the change in polyvinyl chloride surface roughness decreased as surface roughness increased. The variation of  $R_f$  for PVC was described by a linear model that depended on the initial PVC roughness,  $R_i$ , and a mean roughness term,  $R_{\text{mu}}$ , and was independent of inhibitors, including pH, or inhibitor dose or water quality.

Photographs of the PVC coupon surfaces showed a scattered red-brown precipitate on several PVC coupons. After incubation, the surface of most PVC coupons was covered with a scatter of orange-brown precipitates, indicating deposition of a metal present in the source water or iron released from biofilm coupons upstream of the roughness coupons. Metal precipitation is presumed to explain significant increases in surface roughness of PVC, which is a relatively inert material.

#### *Unlined Cast Iron*

Surface roughness of unlined cast iron (UCI) coupons was measured for Phases I, II, III, and IV. UCI coupons were cut from sections of pipe which had been excavated from within the distribution system and held in indoor storage for a few years exposed to air. Therefore, the initial roughness of UCI coupons varied significantly between coupons. Also the initial roughness varied between Phases I-II and Phases III-IV because the scan length in Phases I-II was often not great enough to capture the entire highest and lowest portions in the scan area. Scan length was increased starting in Phase III, providing a more accurate representation of UCI surface roughness. In Phases III and IV, the initial surface roughness of UCI was on average 85.5  $\mu\text{m}$  with a minimum and maximum of 46.6  $\mu\text{m}$  and 122.8  $\mu\text{m}$  respectively. Surface roughness data for UCI from Phases I-IV are shown in Table 5.5 and Table 5.6.

Surface roughness of UCI coupons receiving phosphate inhibitors had significant changes in surface roughness more often than UCI coupons not receiving phosphate inhibitors. Photographs of UCI coupons demonstrated the decreases and increases in surface roughness for Phases II and III. Although the mechanism of phosphate inhibitors on UCI surface roughness is unclear, it seems that the addition of phosphate inhibitors may destabilize iron scales.

Linear and non-linear (power) models relating water quality and  $R_i$  to  $\Delta R$  and  $R_f$  were evaluated for all phases and for Phases I-II and III-IV. These models indicated that alkalinity, chlorides or temperature were all significantly correlated to  $\Delta R$  and  $R_f$ , and did not provide any practical interpretation of relationships among water quality and  $R_i$  to  $\Delta R$  and  $R_f$ .

Table 5.5  
Statistical comparison of UCI initial and final surface roughness

Phase	Parameter	PDS	PDS	PDS	PDS	PDS	PDS	PDS	PDS	PDS	PDS	PDS	PDS	PDS	PDS	AVG
		01 BOP	02 BOP	03 BOP	04 OP	05 OP	06 OP	07 ZOP	08 ZOP	09 ZOP	10 Si	11 Si	12 Si	13 pH <sub>s</sub>	14 pH <sub>s</sub> +0.3	
I†	R <sub>i</sub>	29.9	32.1	28.5	37.3	34.8	43.2	34.6	38.0	33.5	24.6	23.9	42.2	39.3	41.4	34.5
	N	5	3	3	3	3	3	3	4	4	3	3	3	3	3	-
	R <sub>f</sub>	29.2	37.0	29.3	31.0	36.4	38.7	31.7	39.9	34.0	29.7	22.6	34.1	38.1	37.5	33.5
	N	6	5	5	5	5	5	5	5	5	5	5	5	5	5	-
	ΔR	-0.7	4.8	0.8	-6.3	1.5	-4.5	-2.9	1.9	0.5	5.0	-1.3	-8.1	-1.1	-3.9	-1.0
	ΔR p-values	0.85	0.20	0.89	0.36	0.80	0.46	0.61	0.71	0.91	0.31	0.78	0.18	0.81	0.52	-
	ΔR/R <sub>i</sub>	-0.02	0.15	0.03	-0.17	0.04	-0.10	-0.08	0.05	0.02	0.20	-0.05	-0.19	-0.03	-0.10	-0.02
II	R <sub>i</sub>	53.5	64.0	40.7	43.7	60.8	53.0	59.8	40.6	44.2	58.9	41.0	52.7	58.5	62.1	52.4
	N	9	5	5	5	5	5	5	5	5	5	5	5	5	5	-
	R <sub>f</sub>	35.7	44.4	48.6	31.0	34.4	41.4	38.0	22.9	39.4	44.3	42.7	45.0	43.2	62.4	41.0
	N	5	5	5	6	8	5	6	7	7	5	8	6	5	5	-
	ΔR	-17.8	-19.6	8.0	-12.7	-26.4	-11.6	-21.8	-17.7	-4.8	-14.6	1.7	-7.6	-15.3	0.3	-11.4
	ΔR p-values	<b>&lt;0.01</b>	<b>0.03</b>	0.19	<b>0.05</b>	<b>&lt;0.01</b>	0.23	<b>0.01</b>	<b>0.01</b>	0.69	0.20	0.81	0.25	0.17	0.97	-
	ΔR/R <sub>i</sub>	-0.33	-0.31	0.20	-0.29	-0.43	-0.22	-0.36	-0.44	-0.11	-0.25	0.04	-0.14	-0.26	0.00	-0.21

†Surface roughness of UCI in Phases I and II was measured using a small scan length, hence underestimating the actual surface roughness.

Table 5.6  
Statistical comparison of UCI initial and final surface roughness

Phase	Parameter	PDS	PDS	PDS	PDS	PDS	PDS	PDS	PDS	PDS	PDS	PDS	PDS	PDS	PDS	AVG
		01 BOP	02 BOP	03 BOP	04 OP	05 OP	06 OP	07 ZOP	08 ZOP	09 ZOP	10 Si	11 Si	12 Si	13 pH <sub>s</sub>	14 pH <sub>s</sub>	
		0.5	1.0	2.0	0.5	1.0	2.0	0.5	1.0	2.0	3.0	6.0	12.0	+0.3		
III	R <sub>i</sub>	46.6	72.8	68.3	74.6	66.2	68.5	82.3	78.0	47.6	86.4	87.6	75.5	71.6	74.5	71.5
	N	5	5	5	5	5	5	5	5	5	5	6	5	5	5	-
	R <sub>f</sub>	90.3	102.0	91.2	95.7	116.7	98.8	90.8	91.6	76.3	96.4	88.7	92.0	87.7	101.6	94.2
	N	5	6	5	5	5	5	5	5	5	5	6	5	5	5	-
	ΔR	43.6	29.1	22.9	21.1	50.4	30.2	8.5	13.6	28.7	10.0	1.1	16.5	16.0	27.1	22.8
	ΔR p-values	<b>0.04</b>	<b>0.01</b>	0.14	0.14	<b>&lt;0.01</b>	<b>0.03</b>	0.43	0.23	0.11	0.31	0.90	0.14	0.12	<b>&lt;0.01</b>	-
	ΔR/R <sub>i</sub>	0.94	0.40	0.34	0.28	0.76	0.44	0.10	0.17	0.60	0.12	0.01	0.22	0.22	0.36	0.36
IV	R <sub>i</sub>	93.3	91.2	115.7	99.4	96.4	93.4	98.4	86.7	89.4	100.3	108.5	99.5	103.5	95.8	98.0
	N	5	5	5	5	5	5	5	5	5	5	5	5	5	5	-
	R <sub>f</sub>	82.7	101.1	90.2	102.8	89.3	97.7	108.7	73.4	97.5	72.8	100.0	101.2	115.4	78.9	93.7
	N	8	5	5	5	5	5	5	5	6	5	6	5	5	5	-
	ΔR	-10.6	9.9	-25.5	3.3	-7.1	4.4	10.3	-13.3	8.1	-27.5	-8.5	1.7	11.9	-16.9	-4.3
	ΔR p-values	<b>0.05</b>	0.27	<b>&lt;0.01</b>	0.48	0.23	0.58	0.08	0.18	0.26	<b>0.03</b>	0.28	0.83	0.35	0.06	-
	ΔR/R <sub>i</sub>	-0.11	0.11	-0.22	0.03	-0.07	0.05	0.10	-0.15	0.09	-0.27	-0.08	0.02	0.12	-0.18	-0.04

## **Conclusions**

Optical profilometry can be used to measure surface roughness of pipe materials common in water distribution systems, including galvanized iron, lined cast iron, polyvinyl chloride, unlined cast iron. Corrosion inhibitor addition and water quality were not found to be significant factors affecting G, LCI, and PVC surface roughness. UCI surface roughness appeared to be influenced by phosphates, temperature, and alkalinity. For all materials, the most significant factor influencing the change in surface roughness was the initial surface roughness. The initial roughness varied greatly between materials. PVC was the smoothest material. LCI and G had similar roughnesses, and UCI was the roughest material.

## **Recommendations**

The development of standard methods for the measurement of surface roughness of corrosion coupons by optical profilometry would help standardize the collection and interpretation of results. An optical profiler could be used for further studies investigating the relationship between surface roughness and biofilm density, chlorine wall decay rates, and polyphosphate reversion.

Although, in this study, models did not indicate a statistically significant effect of inhibitors on surface roughness over three months, similar studies with longer incubation times for corrosion coupons, such as six months to one year, may demonstrate some effect.

Also, whereas the pilot distribution systems was operated to simulate dead end conditions, similar studies operated under turbulent flow conditions may have different results for iron surface roughness.

Head loss tests within the distribution system would be more sensitive to the practical effect of corrosion inhibitors on surface roughness. A utility collecting Hazen-Williams coefficients as part of hydrodynamic modeling efforts could compare head loss data before and after introduction of inhibitors to directly measure the practical effect of inhibitors on pipe surface roughness. If corrosion inhibitors had a beneficial effect on surface roughness of unlined iron in the distribution system, then one would also expect to see decreases in energy consumption for the high-service pumps and booster pumps throughout the system.

## CHAPTER 6 SURFACE CHARACTERIZATION AND SOLUBILITY MODELING OF COPPER LOOPS RECEIVING PHOSPHATE INHIBITORS

### Abstract

The effect of phosphate inhibitors on copper release in copper tubing receiving a varying blend of ground, surface and brackish water was investigated. Blended poly/ortho phosphate, sodium orthophosphate, and zinc orthophosphate were used from about 0.5 to 2 mg P/L and reduced copper release compared to the no inhibitor pH controls at  $\text{pH}_s$  and  $\text{pH}_{s+0.3}$ .

All phosphate inhibitors reduced copper release relative to the no inhibitor treatments, keeping total copper below the 1.3 mg/L MCLG for all water quality blends. Addition of 1 mg/L as P phosphorus reduced both total and dissolved copper by about 60% relative to no inhibitor addition. This effect was consistent even with seasonal changes in source water blends. Solubility models were developed to predict copper release concentration assuming  $\text{Cu}(\text{OH})_2$  or  $\text{Cu}(\text{PO}_4)_3$  as the controlling solid phase. The  $\text{Cu}(\text{OH})_2$  model consistently under predicted copper release for pH controls whereas the  $\text{Cu}_2(\text{PO}_4)_3$  model adequately fit the data for P inhibitors.

A plot of cupric ion concentration versus orthophosphate concentration showed a decrease in copper release consistent with mechanistic control by either cupric phosphate solubility or a diffusion limiting phosphate film.

## **Introduction**

Management of water quality in distribution systems is an essential task for utilities to deliver a reliable supply of drinking water that meets consumer expectations and complies with regulatory requirements. It is desirable for utilities to find a corrosion control strategy that can mitigate copper release below LCR action levels despite seasonal variations in source water quality, which can potentially disrupt existing copper scales. A recent AwwaRF study entitled “Control of Distribution System Water Quality in a Changing Water Quality Environment Using Inhibitors” (Taylor et al., 2007) investigated the use of corrosion inhibitors to mitigate adverse impacts of varying water quality in distribution systems receiving seasonally varied source water blends. Significant decreases in copper release were observed with the addition of phosphate or silicate inhibitors.

This paper examines the effect of phosphate inhibitors on copper release. Surface characterization and water quality data were used to evaluate possible mechanisms whereby phosphate inhibitors reduced copper release.

### *Copper Corrosion*

Copper corrodes from its noble metallic form of  $\text{Cu}^0$  to the, cuprous,  $\text{Cu(I)}$  and cupric,  $\text{Cu(II)}$  ions. The maximum contaminant level goal (MCLG) and action level for LCR compliance for copper in potable water systems is 1.3 mg/L. Elevated copper can cause gastrointestinal distress, liver damage, and/or kidney damage (Barceloux and Barceloux 1999).

In new piping generally up to 5 years of use, copper (II) concentrations are controlled by  $\text{Cu(OH)}_2$  solid phases, which can age with time to form less soluble tenorite,  $\text{CuO}$ , or malachite,

$\text{Cu}_2(\text{OH})_2\text{CO}_3$  scales (Schock, Lytle, and Clement; 1995). Although copper (I) can exist in solution, for the pH and ORP associated with drinking water systems, it is usually oxidized to copper (II).

In 2003, a similar study was conducted using the same pilot facility described in this article; which investigated treatment process impacts on water quality without use of inhibitors. Cuprite ( $\text{Cu}_2\text{O}$ ) was identified as a crystalline structure found in the corrosion layer using XRD (Taylor et al.; 2005). Cupric hydroxide ( $\text{Cu}(\text{OH})_2$ ), tenorite ( $\text{CuO}$ ), and cuprite ( $\text{Cu}_2\text{O}$ ), made up the bulk surface composition on copper coupons identified by XPS. Thermodynamic modeling indicated that copper release was well described by equilibrium with  $\text{Cu}(\text{OH})_2$  acting as the controlling solid (Xiao; 2004). Alkalinity increased copper release; whereas pH elevation above  $\text{pH}_s$  and silica reduced copper release.

Often, in domestic systems, copper concentrations do not fully reach equilibrium between use. It can take 48 to 72 hours to reach equilibrium copper levels in a disinfected copper loop (Schock, Lytle, and Clement 1995). The authors also suggested that orthophosphate would be most effective in controlling copper release in the pH range of 6.5 to 7.5. Orthophosphate inhibitors are suggested to function by forming a cupric phosphate scale (Edwards, McNeill, and Holm 2001); however, data on cupric phosphate solids is scarce (Schock, Lytle, and Clement 1995).

When inhibitors are not added, other methods for controlling copper release include raising the pH, and or reducing the alkalinity.  $\text{CO}_2$  stripping has been recommended as one way to increase the pH without increasing alkalinity (Edwards, Hidmi, and Gladwell; 2003). However, decreasing the alkalinity can increase lead solubility (Taylor et al. 2005). Inhibitors are

an attractive alternative as they may overcome the apparent tradeoff between control of copper or lead release concentration.

## **Materials and Methods**

### *Pilot Testing*

A pilot testing facility comprised of pilot distribution systems (PDSs), copper corrosion loops, and PVC pipe cradles to house corrosion and biological coupons were used to test the effects of corrosion inhibitors on distribution system water quality. The pilot testing facility was located on the grounds of the Cypress Creek Water Treatment Facility , located in Pasco County, Florida, USA.

### Source Waters

Blends of surface water, groundwater, and brackish water were used for the pilot study. Surface water was treated at a surface water treatment plant by ferric sulfate coagulation and trucked to the pilot testing site. On site, additional surface water treatment process included chloramination and pH stabilization. Raw groundwater was obtained from the Cypress Creek water treatment facility. The groundwater treatment process included aeration, chloramination, and pH stabilization. Brackish water was artificially prepared from the raw groundwater by the addition of sea salt after RO treatment. The reverse osmosis desalinated water (RO) treatment process included reverse osmosis, aeration, chloramination, and pH stabilization.

The three sources were blended, aerated, chloraminated, and pH stabilized in the process tanks shown in Figure 6.1. Three blends were studied over four operating phases, with each phase lasting three months. Within each phase, all pilot distribution systems received the same blend of water. Blend composition, water quality, and schedule for each phase are presented in Table 6.1.

Table 6.1  
Blend ratios and water quality by phase

	Phase I	Phase II	Phase III	Phase IV
GW (%)	62	27	62	40
SW (%)	27	62	27	40
RO (%)	11	11	11	20
Alkalinity (mg/L as CaCO <sub>3</sub> )	160	103	150	123
Chlorides (mg/L Cl <sup>-</sup> )	45	67	68	59
Sulfates (mg/L SO <sub>4</sub> <sup>2-</sup> )	62	103	67	76
Temperature (°C)	21.3	26.2	25.7	21.2
Time Period	Feb-May 2006	May-Aug 2006	Aug-Nov 2006	Nov 2006-Feb 2007

### Corrosion Inhibitors

Blended poly/ortho phosphate (BOP), orthophosphate (OP), zinc orthophosphate (ZOP), and silicate (SiO<sub>2</sub>) were fed from inhibitor tanks by peristaltic pumps, into influent standpipes to mix with blended water coming from the process storage tanks. Phosphate inhibitors were dosed at 0.5, 1.0, and 2.0 mg/L as P, while silicate inhibitor was dosed at 3.0, 6.0, and 12.0 mg/L as SiO<sub>2</sub>. Two PDSs were operated as pH controls without inhibitor addition, one at the stability pH for calcium carbonate precipitation i.e. pH<sub>s</sub>, while the other at an elevated pH of pH<sub>s+0.3</sub>.

### Pilot Distribution Systems

After inhibitor addition, the water from each influent standpipe flowed into the pilot distribution systems (PDSs), shown in Figure 6.2. The PDSs were constructed to simulate the effects of variation in source waters on distribution system water quality. All pipes used in the PDSs were excavated from TBW member government distribution systems. The 14 hybrid PDSs each about 92 feet long, consisted of polyvinylchloride (PVC), lined cast iron (LCI), unlined cast iron (UCI) pipe, and galvanized iron (G) in series.

## Copper Loops

Copper loops were housed (Figure 6.3) in series at the end of each PDS to simulate a home plumbing system. Copper tubes (Figure 6.4) were 5/8 in. (1.6 cm) in diameter and 30 ft. (9.1 m) in length. Copper loops were flushed every morning with 2 gallons (7.6 L) of water at an average velocity of 1 fps. Copper concentration was measured weekly from water from copper loops after a standing time of six to seven hours.



Figure 6.1 Covered tanks for process treatment



Figure 6.2 Pilot distribution systems



Figure 6.3 Corrosion shed



Figure 6.4 Copper lines

### *X-Ray Photoelectron Spectroscopy*

Chemical composition of corrosion scales on the surface of metal coupons copper exposed to the various inhibitors were characterized by XPS or X-ray Photoelectron Spectroscopy (Physical Electronics 5400 ESCA) shown in Figure 6.5. In XPS, an Mg anode (1254 eV  $K\alpha$ ) bombards the coupon surface with high energy X-rays that interact with atoms in the top 5-6 nm of the surface (Seal and Barr 2001). Then, according to the photoelectric effect, these atoms emit high energy electrons. An electron analyzer counts the number of electrons emitted over a range of energies, producing scan spectra which may be used for surface composition analysis.

The effluent from the PDS was split in two parts. One part was directed to the copper corrosion loops and the other was directed to a trailer which housed electrochemical noise electrodes and copper corrosion coupons. These coupons were inserted at the beginning of each phase, and then retrieved at the end of the phase, about 90 days later. The XPS scanning consists of a two-step process: an initial “survey” scan followed by a “high resolution” scan. The survey scan, conducted over a broad range of energy levels, is useful for confirming the presence or absence of elements on the surface of the coupon. In contrast, a high resolution scan, conducted over a narrow range of energy levels, is useful for establishing the chemical states present for a given element.



Figure 6.5 Physical Electronics 5400 ESCA XPS

The elements are indicated on the survey scan by pronounced peaks above the background of the survey, and these peaks are then selected individually for a “high resolution” scan for each element. Additionally, elements of interest, such as those associated with inhibitors, coupon material, or water quality, were analyzed with high resolution scans. Possible compounds associated with a given element were determined through deconvolution of the high resolution scan.

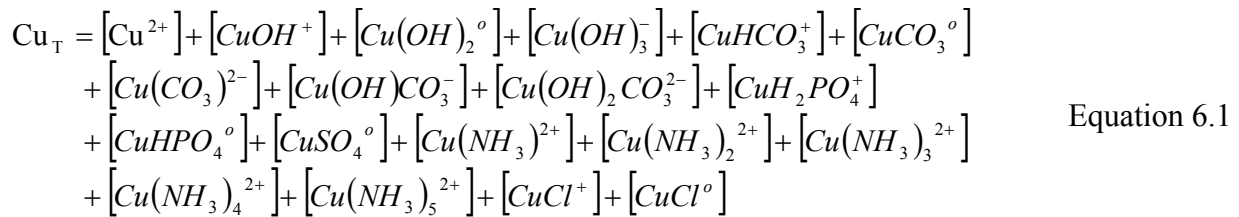
### *Thermodynamic Modeling*

$\text{Cu}(\text{OH})_2$  has been identified as a metastable intermediate that forms in new copper pipe, and has been used as the basis for thermodynamic models of copper (Schock, Lytle, and Clement 1995)(Xiao 2004). Cupric hydroxide can age to its dehydrated form tenorite,  $\text{CuO}$ , which is less soluble. In the presence of alkalinity, old copper pipe tends to form the more stable, less soluble cupric hydroxycarbonate  $\text{Cu}_2(\text{OH})_2\text{CO}_3$ , malachite (Schock, Lytle, and Clement. 1995). Cupric

phosphate has also been identified as a possible controlling solid for copper release in the presence of phosphate inhibitors.

### Thermodynamic Model Development

The thermodynamic model for dissolved copper that had been developed in TBW I (Taylor et al., 2005) was expanded to include phosphate, sulfate, chloride, and ammonia complexes and is given in Equation 6.1. The equilibrium model assumed the presence of Cu (II) species. Silica complexation of copper was also considered; however, a review of literature concerning coordination chemistry did not reveal any thermodynamic data corresponding to a copper-silica complex.



The complexes considered within Equation 6.1 demonstrate the various water quality parameters governing copper release. The free dissolved cupric ion concentration at equilibrium depends on the controlling solid; however, other water quality parameters, such as alkalinity, chloride, sulfate, ammonia, and phosphate form copper complexes in equilibrium with the free cupric ion, and thus amplify the natural level of dissolved copper. Empirical models developed as a part of this study, and reported elsewhere (Taylor et al. 2007) identified pH, chloride, and alkalinity as the main water quality effects. Increased pH was beneficial in controlling copper release, whereas increasing the chlorides or alkalinity increased copper release.

The effect of chlorides on dissolved copper did not appear to be explained by formation of a copper-chloride complex., because  $\text{CuCl}^+$  and  $\text{CuCl}^0$  complexes accounted for approximately  $1/1000^{\text{th}}$  of a percent of the dissolved copper. Rather, the effect may relate to associated changes in solution conductivity and ionic strength that accompany elevated chloride concentrations. It is speculated that chlorides may have reduced carbonate/ hydroxide scale passivity by promoting local pH drops near copper surfaces and may cause pitting corrosion; however for the moderate alkalinity (84-175 as  $\text{CaCO}_3$ ) waters used in this study large pits were not observed on copper surfaces.

For this study, copper-alkalinity complexes accounted for approximately 90% of all dissolved copper. Copper-alkalinity complexes included  $\text{CuHCO}_3^-$ ,  $\text{CuCO}_3^0$ ,  $\text{Cu}(\text{CO}_3)_2^{2-}$ ,  $\text{Cu}(\text{OH})\text{CO}_3^-$ , and  $\text{Cu}(\text{OH})_2\text{CO}_3^{2-}$ . Equilibrium calculations demonstrated that alkalinity had a tremendous effect on copper release, capable of increasing the total dissolved copper to several times the level of free dissolved copper.

For this study, copper-phosphate complexes accounted for only about 0.5% of total dissolved copper, indicating little adverse effect. Copper-phosphate complexes included  $\text{CuH}_2\text{PO}_4^+$  and  $\text{CuHPO}_4^0$ .

### Model Implementation

Separate runs of the model were performed assuming considering the following compounds as candidate controlling solids: cupric hydroxide ( $\text{Cu}(\text{OH})_2$ ), tenorite ( $\text{CuO}$ ), and two forms of cupric phosphate,  $\text{Cu}_3(\text{PO}_4)_2$  and its dihydride  $\text{Cu}_3(\text{PO}_4)_2 \cdot 2\text{H}_2\text{O}$ . Calculations were performed for the  $\text{pH}_s$  controls and all phosphate inhibitor types using average water quality data

for each phase. The middle dose (1.0 mg/L as P) phosphate inhibitor lines were modeled which corresponded with the coupons tested by XPS analysis.

### *Mechanistic Investigation of Copper Release*

Water quality data for copper release were compared against two mechanistic models derived from cupric phosphate solubility and from diffusion theory. The purpose of this investigation was to identify the most plausible mechanism to explain the reduction in copper release with phosphate inhibitor addition.

### Solubility Model

If cupric phosphate solubility controlled dissolved copper, then the expected copper concentration should vary as function of the orthophosphate concentration. Solving the solubility product equation of cupric phosphate (Equation 6.2) for free dissolved copper yielded Equation 6.3 which predicted that free dissolved copper varied with the  $-2/3^{\text{rd}}$  power of the orthophosphate concentration.

$$K_{sp} = [Cu^{2+}]^3 [PO_4^{3-}]^2 \quad \text{Equation 6.2}$$

$$[Cu^{2+}] = \left( \frac{K_{sp}}{[PO_4^{3-}]^2} \right)^{1/3} \quad \text{Equation 6.3}$$

Under cupric phosphate control, the free dissolved copper would depend primarily on the orthophosphate concentration, which is a function of the phosphoric acid concentration ( $C_{T,PO_4}$ ), and pH. In contrast, the total dissolved copper depends on the free dissolved copper and the concentration of copper ligands, especially alkalinity. Free dissolved copper concentrations were solved using the water quality data and back calculating with complexation coefficients

assembled by Shock, Lytle, and Clement (1995). Hence, instead of total dissolved copper, it is most appropriate to consider a plot of free dissolved copper versus orthophosphate, because the effect of alkalinity is removed. If cupric phosphate acts as a controlling solid for copper release, then the data should be consistent with a -2/3rd order power model like that shown in Equation 6.4.

$$[Cu^{2+}] = a \times [PO_4^{3-}]^{-2/3} \quad \text{Equation 6.4}$$

### Film Diffusion Model

If cupric phosphate was not the controlling solid for copper release, then phosphate inhibitor addition may have reduced copper release by formation of a film over the controlling copper solid. Whatever the composition of this phosphate film, the film thickness might be approximated as a linear function of the orthophosphate concentration. Hence, increased phosphate inhibitor addition would result in thicker phosphate films, which would reduce the rate of diffusion of dissolved copper to the bulk.

Fick's first law (Equation 6.5), describes the diffusion flux,  $J$ , as a function of a diffusion coefficient,  $D$ , and concentration gradient  $d\phi/dx$ . The negative sign indicates that the diffusion flux goes against the concentration gradient.

$$J = -D \frac{d\phi}{dx} \quad \text{Equation 6.5}$$

where:  $J$  = diffusion flux ( $ML^{-2}T^{-1}$ )  
 $D$  = diffusion coefficient ( $L^2/T$ )  
 $\phi$  = concentration ( $ML^{-3}$ )  
 $x$  = position ( $L$ )

Applying this equation to copper diffusion through a phosphate film an equation (Equation 6.6) describing the effect of phosphate film thickness on free dissolved copper was

developed. This equation assumes that the copper diffusion flux is directly proportional to the dissolved copper in the bulk. It also assumes that the film thickness is directly proportional to the orthophosphate concentration.

$$[Cu^{2+}]_{bulk} = \frac{[Cu^{2+}]_{surface}}{1 + a[PO_4^{3-}]} \quad \text{Equation 6.6}$$

where:  $[Cu^{2+}]_{bulk}$  = dissolved copper concentration in the bulk (ML)  
 $[Cu^{2+}]_{surface}$  = dissolved copper concentration at the copper surface (ML)  
 $a$  = proportionality constant  
 $[PO_4^{3-}]$  = orthophosphate concentration in the bulk (ML<sup>-3</sup>)

## Results and Discussion

### *Effect of Phosphate Inhibitor on Copper Release*

The average copper release observed during the study is shown in Table 6.2 by phase for each phosphate inhibitor and relative to the pH<sub>s</sub>+0.3 control. In all cases, inhibitors reduced copper release relative to the control. Phosphate inhibitors reduced copper release to about 40% that observed with the control. Time series plots for BOP, OP, ZOP, and the no inhibitor controls are shown in Figure 6.6 through Figure 6.9. The plots show that the addition of 0.5, 1.0, or 2.0 mg/L as P of phosphate inhibitor tended to reduce copper release in proportion to the copper release observed with the no inhibitor control pH<sub>s</sub>+0.3.

Table 6.2  
Comparison of observed copper release from inhibitor PDSs to pH<sub>s</sub>+0.3

Phase	Inhibitor	Average Release (mg/L)		% Ratio to pH <sub>s</sub> +0.3	
		Dissolved Cu	Total Cu	Dissolved Cu	Total Cu
I	pH <sub>s</sub> +0.3	0.89	1.00		
	BOP	0.34	0.36	38%	36%
	OP	0.38	0.41	42%	41%
	ZOP	0.34	0.36	38%	36%
II	pH <sub>s</sub> +0.3	0.73	0.82		
	BOP	0.29	0.33	40%	40%
	OP	0.28	0.35	39%	43%
	ZOP	0.32	0.39	44%	48%
III	pH <sub>s</sub> +0.3	0.79	0.85		
	BOP	0.30	0.32	38%	38%
	OP	0.29	0.35	37%	41%
	ZOP	0.30	0.34	37%	40%
IV	pH <sub>s</sub> +0.3	0.83	0.93		
	BOP	0.31	0.37	38%	39%
	OP	0.32	0.36	38%	39%
	ZOP	0.32	0.38	38%	41%

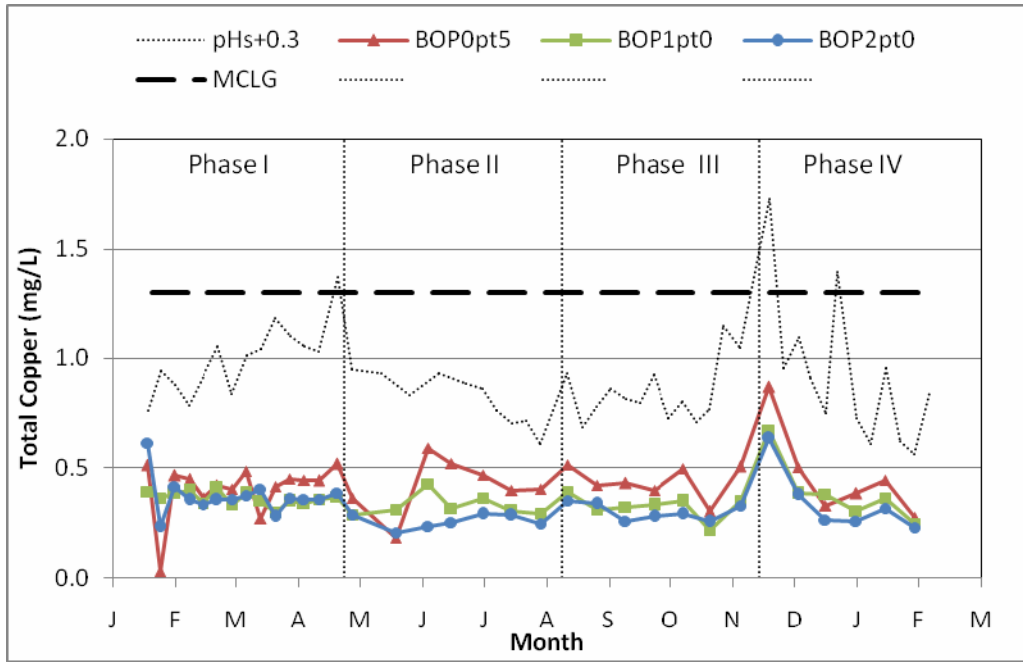


Figure 6.6 Time series plot of copper release with BOP inhibitor addition

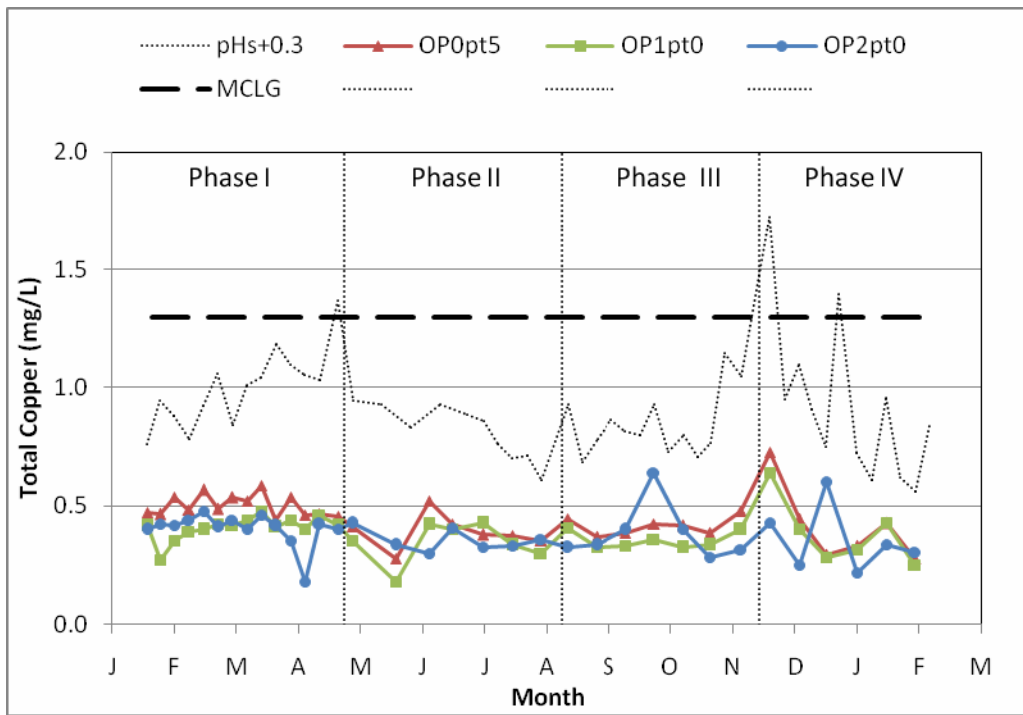


Figure 6.7 Time series plot of copper release with OP inhibitor addition

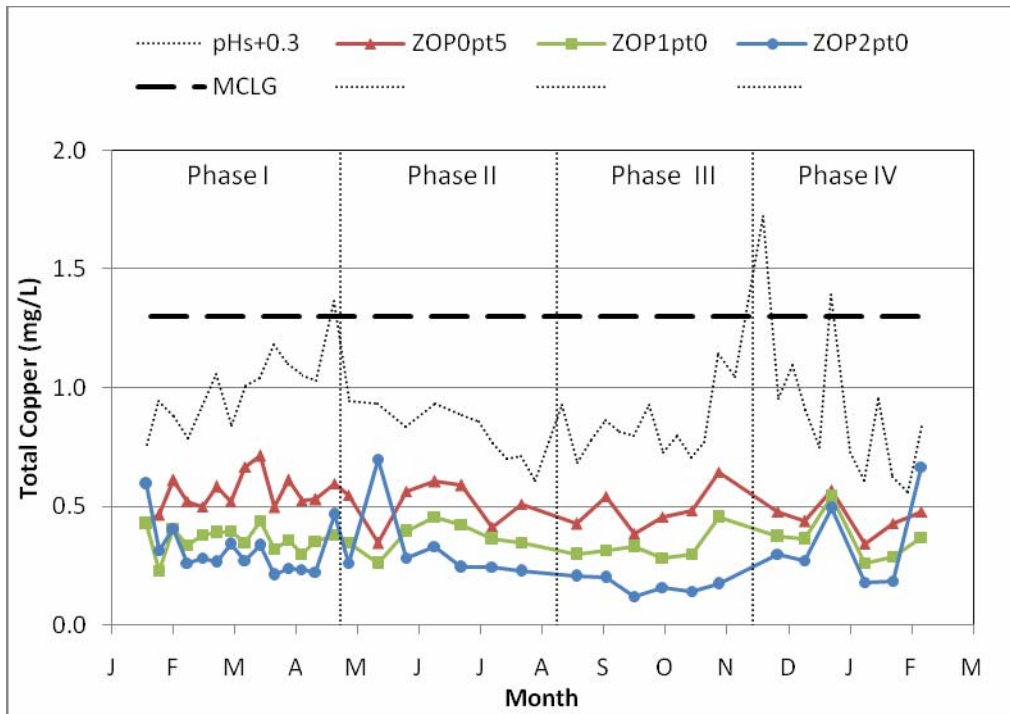


Figure 6.8 Time series plot of copper release with ZOP inhibitor addition

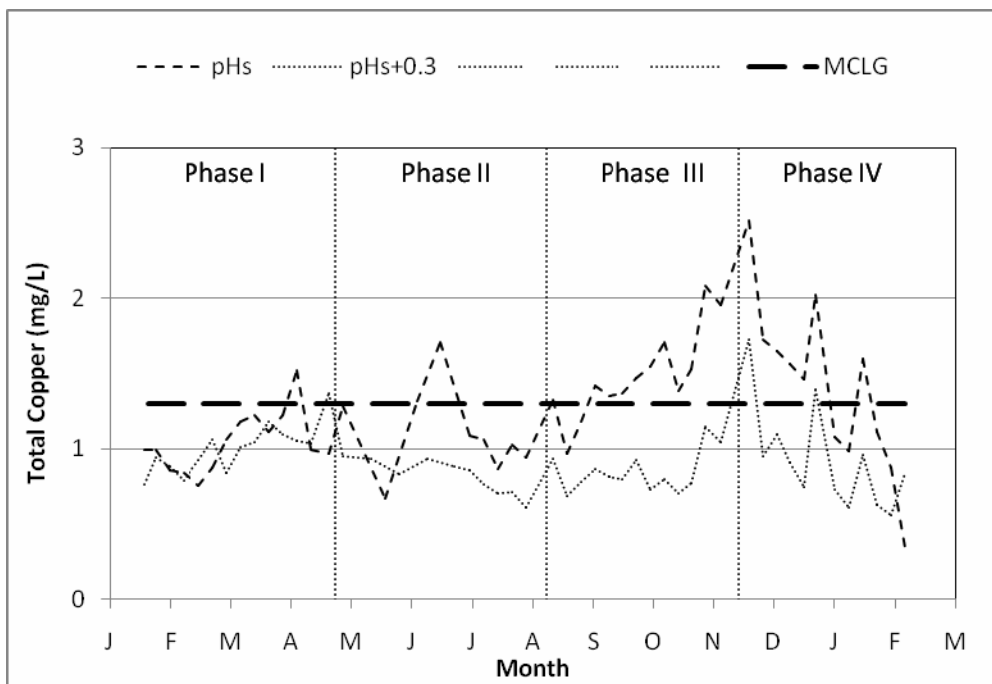


Figure 6.9 Time series plot of copper release by pH without inhibitor addition

### *XPS Identification of Copper Corrosion Products*

An example XPS survey spectrum for copper is shown in Figure 6.10. Peaks were dependent on the inhibitor to which the coupon had been exposed and were typically pronounced for copper, carbon, oxygen, calcium, phosphorus, and zinc.

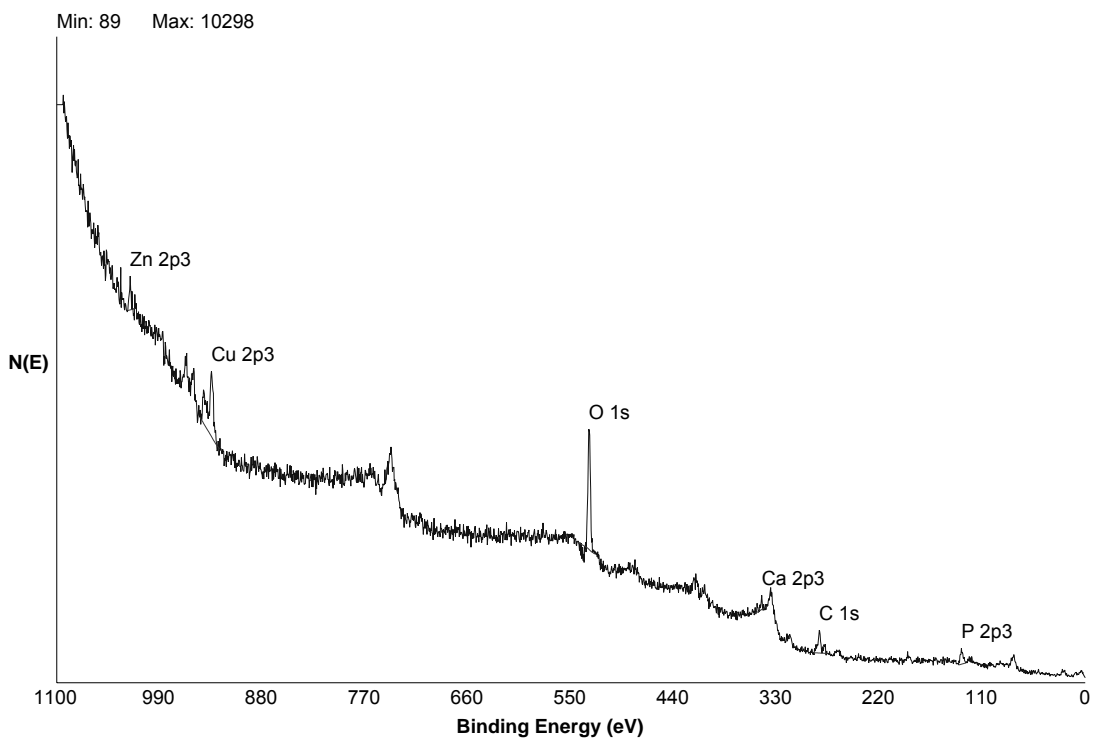


Figure 6.10 Survey spectrum of a copper coupon from 1.0 ZOP, Phase III

### Identification of Copper Corrosion Products

High resolution spectra for copper were deconvoluted (Figure 6.11) to identify copper corrosion products and to determine their relative abundance. Copper compounds detected included:  $\text{Cu}_2\text{O}$ ,  $\text{CuO}$ ,  $\text{Cu}(\text{OH})_2$ ; and cupric salts  $\text{Cu}(\text{II})$  (Xiao, 2004). Binding energy data from the NIST database (Wagner et al., 2003) support the inclusion of  $\text{CuCl}_2$ ,  $\text{CuSO}_4$ ,  $\text{CuCO}_3$ , and  $\text{CuSiO}_3$  under the  $\text{Cu}(\text{II})$  curve given by Xiao (2003). In addition  $\text{Cu}_3(\text{PO}_4)_2$ ,  $\text{Cu}_2(\text{OH})_2\text{CO}_3$

(malachite), and  $\text{Cu}_4\text{SO}_4(\text{OH})_6\text{H}_2\text{O}$  (a cupric hydroxysulfate) are all feasible cupric salts (Schock, Lytle, and Clement 1995); however, no published XPS binding energies were identified for these compounds. It should be noted that the surface composition of copper coupons is not uniform. Failure to detect a compound by XPS in one scan did not imply the compound was not likely to be present in the scale.

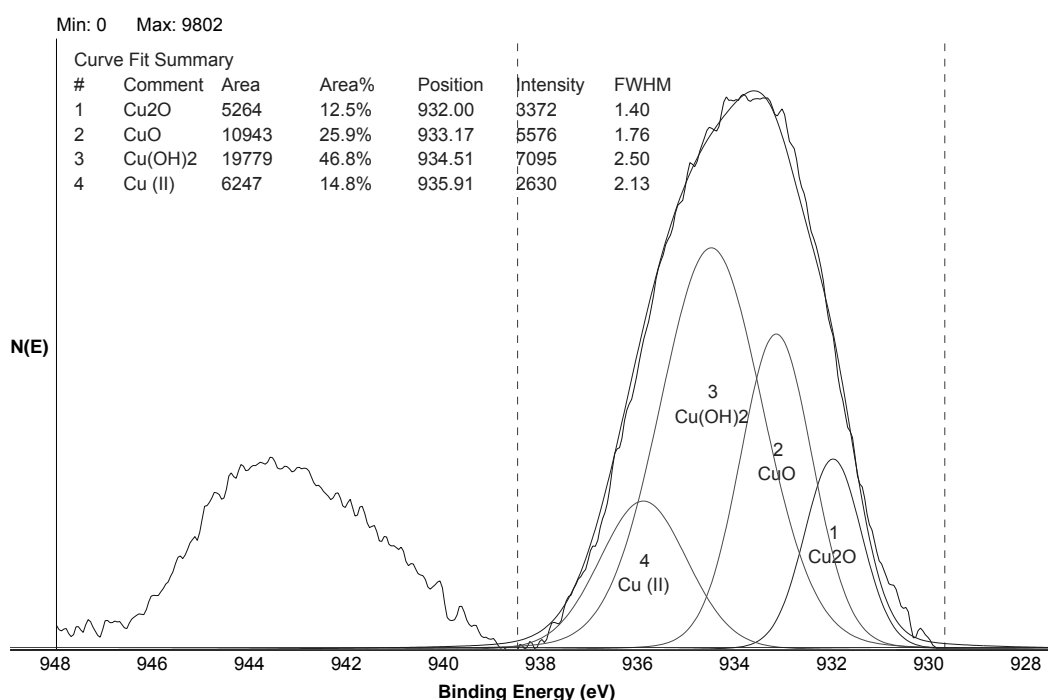


Figure 6.11 Deconvolution of copper for the coupon exposed to BOP during Phase IV

A combination of these four compounds was sufficient to describe the high resolution spectra for the copper coupons. Figure 6.12 depicts the percent area of the various compounds over all phases by inhibitor treatment. Cupric hydroxide was the most abundant copper surface compound. This may imply that  $\text{Cu}(\text{OH})_2$  was the controlling solid phase for copper solubility (Schock, 1999)(Xiao, 2004). However, as shown in the thermodynamic models for copper, the cupric phosphate dihydride,  $\text{Cu}_3(\text{PO}_4)_2 \cdot 2\text{H}_2\text{O}$  model provided reasonable predictions of dissolved

copper release from copper loops receiving phosphate inhibitors. It should be noted that this compound corresponds stoichiometrically with a cupric biphosphate dihydroxide,  $\text{CuHPO}_4(\text{OH})_2$ , solid. This may indicate that biphosphate plays a role in the controlling solid for copper release.  $\text{Cu}(\text{OH})_2$  commonly forms in new copper pipe. Tenorite is more thermodynamically stable than cupric hydroxide; however, the rate of transformation of cupric hydroxide to tenorite is slow, resulting in cupric hydroxide being present as a metastable intermediate. Older copper pipe tends to form the more stable, less soluble cupric hydroxycarbonate  $\text{Cu}_2(\text{OH})_2\text{CO}_3$ , malachite (Schock, Lytle, and Clement; 1995); nonetheless, increased levels of alkalinity can aggravate copper release (Taylor et Al.,; 2005), even in older copper pipe (Schock and Fox; 2001). This results is reasonable since the primary effect of alkalinity on cuprosolvency is to multiply copper concentrations by complexing free dissolved copper. Changes in the controlling solid phase with ageing of copper pipe may reduce the free uncomplexed dissolved copper; however, the effect of alkalinity on dissolved copper is largely independent of the controlling solid phase since it acts to increase dissolved copper by complexing cupric ions already in solution.

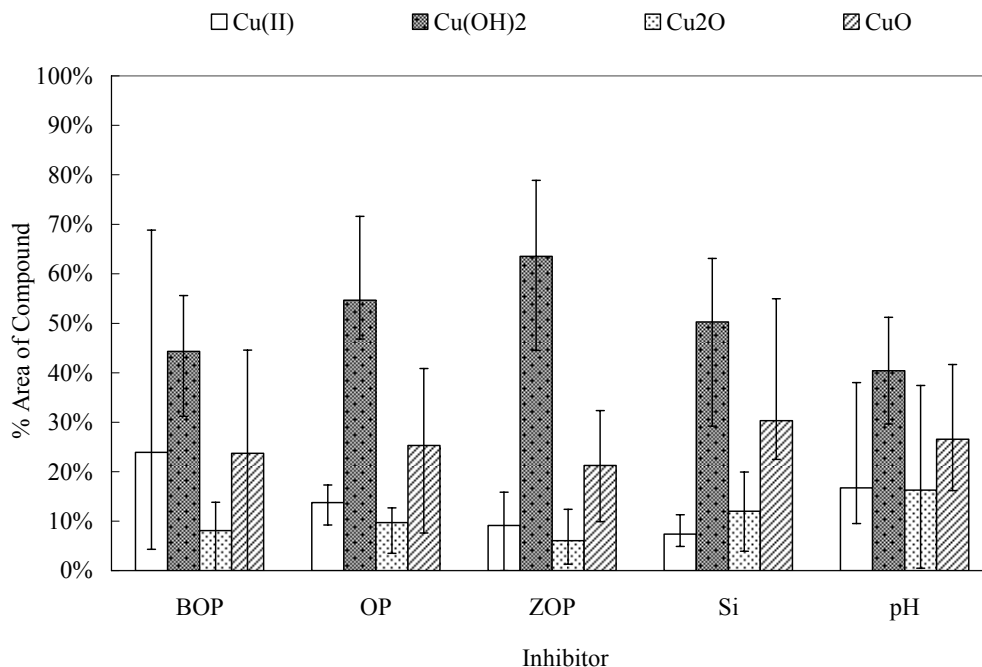


Figure 6.12 Distribution of copper compounds for all phases

#### Effect of Inhibitor on Copper Scale Corrosion Products

Copper coupons exposed to BOP, OP, and ZOP were analyzed for the elements shown in Table 6.3. One copper coupon was tested for each phase. For brevity, only the results of OP are presented. The main differences observed with BOP and ZOP inhibitors were the presence of polyphosphates and zinc oxides respectively.

*Phosphate Inhibitor.* For the OP coupons, carbon was detected in the copper scale on four out of four coupons as carbonate. Calcium was detected on two out of four coupons as  $\text{CaCO}_3$  in Phase I and in Phase III. This indicated that in the presence of a similar predominantly groundwater blend conditions may favor the formation of  $\text{CaCO}_3$  films. Other calcium compounds, such as  $\text{Ca}_3(\text{PO}_4)_2$  were not detected on copper coupons in the presence of OP inhibitor.

Table 6.3  
Compounds identified in scale on copper coupons in the presence of OP inhibitor

Element	Compound	Phase I	Phase II	Phase III	Phase IV
C	CO <sub>3</sub> <sup>2-</sup>	X	X	X	X
Ca	CaCO <sub>3</sub>	X		X	
	Ca <sub>3</sub> (PO <sub>4</sub> ) <sub>2</sub>				
Cu	CaO				
	Cu <sub>2</sub> O	X	X	X	X
	CuO	X	X	X	X
	Cu(OH) <sub>2</sub>	X	X	X	X
O	Cu(II)		X	X	X
	O <sup>2-</sup>	X	X	X	X
	CO <sub>3</sub> <sup>2-</sup>	X	X	X	X
	OH <sup>-</sup>	X	X	X	X
	PO <sub>4</sub> <sup>3-</sup>	X	X	X	
P	PO <sub>4</sub> <sup>3-</sup>	X	X	X	
	Meta				
	Pyro				
Si					
Zn	ZnO			X	

Copper was detected on four out of four coupons, as a mixture of Cu<sub>2</sub>O, CuO, Cu(OH)<sub>2</sub>, and Cu(II) salts, except for Phase I. Cu(II) salts were not detected on the copper coupon for Phase I. In Phases, II, III, and IV, Cu (II) may be present as a copper carbonate compound, such as CuCO<sub>3</sub> or Cu<sub>2</sub>(OH)<sub>2</sub>CO<sub>3</sub>, since carbonate was detected for all these phases, but calcium was detected only in Phase III. Similarly, since it is not precipitated with calcium, phosphate may be present as Cu<sub>2</sub>(PO<sub>4</sub>)<sub>3</sub>. However, it is also possible that phosphate was adsorbed to the scale surface as a liquid-solid film. Oxygen was detected on four out of four coupons as a mixture of O<sup>2-</sup>, CO<sub>3</sub><sup>2-</sup>, OH<sup>-</sup>, and PO<sub>4</sub><sup>3-</sup>, except for Phase IV. PO<sub>4</sub><sup>3-</sup> was not detected on the copper coupon for Phase IV. This result was consistent with observations for BOP, where PO<sub>4</sub><sup>3-</sup> was not detected on the copper coupon in Phase IV.

Phosphorus was detected on three out of four coupons as  $\text{PO}_4^{3-}$  in Phases I, II, and III only. Phosphorus was not detected on the Phase IV coupon, which is consistent with the results for oxygen. As mentioned in the thermodynamic modeling section, phosphate may also be present as a copper phosphate solid. Although the actual form of such a solid in distribution systems has not been established in the literature, the thermodynamic model for  $\text{Cu}_3(\text{PO}_4)_2 \cdot 2\text{H}_2\text{O}$  gave reasonable predictions for dissolved copper release for all phosphate inhibitors. Silica was not detected on any of the four coupons. Zinc was detected on one of the four coupons, found in the form of ZnO, for Phase III. This zinc might have come from the G pipe section of the PDSs which was upstream of the PVC pipe which housed these corrosion coupons. .

*No Inhibitor - pH control.* Four copper coupons exposed to the  $\text{pH}_{\text{s}+0.3}$  treatment were analyzed for the elements shown in Table 6.4. One copper coupon was tested for each of the four phases. Carbon was detected on four out of four coupons, always appearing as carbonate. Calcium was not detected on the four coupons tested, indicating that  $\text{CaCO}_3$  films were not formed in the absence of phosphate and/or silicate inhibitors.

Copper was detected on four out of four coupons as a mixture of  $\text{Cu}_2\text{O}$ ,  $\text{CuO}$ ,  $\text{Cu}(\text{OH})_2$ , and Cu(II) salts, for all phases. Cu (II) salts may be present as a cupric carbonate compound such as  $\text{CuCO}_3$  or  $\text{Cu}_2(\text{OH})_2\text{CO}_3$ , given that  $\text{CO}_3^{2-}$  is present, and no significant calcium was detected. Oxygen was detected on four out of four coupons as a mixture of  $\text{O}^{2-}$ ,  $\text{CO}_3^{2-}$ , and  $\text{OH}^-$ . It should be noted that  $\text{PO}_4^{3-}$  was not detected on any of the four coupons for the  $\text{pH}_{\text{s}}$  treatment, confirming that phosphate inhibitor addition is the primary source for phosphorus on the copper surfaces for the given water qualities studied.

Phosphorus was detected on none of the four coupons, consistent with the results from oxygen. Silica was not detected on the four coupons tested, indicating that silicate inhibitor

addition is the primary source for crystalline silicate compounds on the copper surfaces for the given water qualities studied. Zinc was not detected on any of the four coupons.

Table 6.4  
Compounds identified in scale on copper coupons in the presence of pH<sub>s</sub>+0.3 treated waters

Element	Compound	Phase I	Phase II	Phase III	Phase IV
C	CO <sub>3</sub> <sup>2-</sup>	X	X	X	X
Ca	CaCO <sub>3</sub>				X
	Ca <sub>3</sub> (PO <sub>4</sub> ) <sub>2</sub>				
	CaO				
Cu	Cu <sub>2</sub> O	X	X	X	X
	CuO	X	X	X	X
	Cu(OH) <sub>2</sub>	X	X	X	X
	Cu(II)	X	X	X	X
O	O <sup>2-</sup>	X	X	X	X
	CO <sub>3</sub> <sup>2-</sup>	X	X	X	X
	OH <sup>-</sup>	X	X	X	X
	PO <sub>4</sub> <sup>3-</sup>				
P	PO <sub>4</sub> <sup>3-</sup>				
	Meta				
	Pyro				
Si					
Zn					

Four copper coupons exposed to the pH<sub>s</sub>+0.3 treatment were analyzed for the elements shown in Table 6.4. One copper coupon was tested for each of the four phases. Carbon was detected on four out of four coupons, always appearing as carbonate. Calcium was detected on one of the four coupons, appearing in Phase IV as CaCO<sub>3</sub>. This result is counterintuitive given the lower calcium and alkalinity levels of Phase IV.

Copper was detected on four out of four coupons, appearing as a mixture of Cu<sub>2</sub>O, CuO, Cu(OH)<sub>2</sub>, and Cu(II) salts, for all phases. Cu (II) salts may be present as a cupric carbonate compound such as CuCO<sub>3</sub> or Cu<sub>2</sub>(OH)<sub>2</sub>CO<sub>3</sub>, given that CO<sub>3</sub><sup>2-</sup> is present, and no significant

calcium was detected in Phases I, II, and III. Oxygen was detected on four out of four coupons, appearing as a mixture of  $O^{2-}$ ,  $CO_3^{2-}$ , and  $OH^-$ . No  $PO_4^{3-}$  was detected on any of the four coupons for the  $pH_s+0.3$  treatment, establishing that phosphate inhibitor addition is the primary source for phosphorus on the copper surfaces for the given water qualities studied. Phosphorus was detected on none of the four coupons, consistent with the results from oxygen.

Silica was not detected on the four coupons tested, indicating that silicate inhibitor addition is the primary source for crystalline silicate compounds on the copper surfaces for the given water qualities studied. Zinc was not detected on any of the four coupons. Similar results were observed for the  $pH_s$  treatment except  $CaCO_3$  was not detected and  $Cu_2O$  was not detected in Phase III.

### *Thermodynamic Modeling*

#### Expected Copper Release from Thermodynamic Models

$pH_s+0.3$ . Table 6.2 compared copper release observed with inhibitor addition to copper release observed with the initial source water. A thermodynamic model was developed to consider copper release as a function of a copper controlling solid phase. The prediction of copper release was determined from the previously defined thermodynamic model for copper release.

From the XPS analysis, it was determined that cupric hydroxide ( $Cu(OH)_2$ ) was the predominant copper corrosion product present on the copper coupons. Tenorite ( $CuO$ ), cuprous oxide ( $Cu_2O$ ), and cupric salts ( $Cu(II)$ ) were also present on the copper coupons.

Binding energy data from the NIST database (Wagner et al. 2003) support the inclusion of  $CuCl_2$ ,  $CuSO_4$ ,  $CuCO_3$ , and  $CuSiO_3$  under the Cu (II) curve given by Xiao. In addition

$\text{Cu}_3(\text{PO}_4)_2$ ,  $\text{Cu}_2(\text{OH})_2\text{CO}_3$  (malachite), and  $\text{Cu}_4\text{SO}_4(\text{OH})\cdot 6\text{H}_2\text{O}$  (a cupric hydroxysulfate) are all feasible cupric solids (Schock, Lytle, and Clement 1995); however, no published XPS binding energies were identified for these three compounds.

Both cupric hydroxide and tenorite were considered as the controlling solid phase during thermodynamic modeling. Table 6.5 shows that the cupric hydroxide thermodynamic model under-predicted the dissolved copper concentrations by about 0.3 mg/L Cu. Similarly, the tenorite thermodynamic model under-predicted the dissolved copper concentrations by about 0.7 mg/L Cu. Equation 6.7 describes the equilibrium of dissolved cupric ion with cupric hydroxide solids. A log equilibrium constant of 8.89 was used to predict copper dissolution from cupric hydroxide scales. This same value has been used in other studies modeling cupric hydroxide as a controlling solid phase for copper release (Shock, Lytle, and Clement 1995) (Xiao 2004).



Table 6.5  
Copper thermodynamic modeling of  $\text{pH}_s+0.3$

Inhibitor	Phase	Actual Copper Release (mg/L)		Modeled Copper Release (mg/L)	
		Diss Cu	Total Cu	$\text{Cu}(\text{OH})_2$	CuO
$\text{pH}_s+0.3$	1	0.89	1.00	0.59	0.07
	2	0.73	0.82	0.46	0.06
	3	0.79	0.85	0.48	0.06
	4	0.83	0.93	0.54	0.07
	All	0.81	0.90	0.54	0.07

The dissolved copper samples were collected six hours after flushing of the copper loops, and six hours is less than the time required for copper concentrations to reach equilibrium values

(Schock, Lytle, and Clement; 1995). In both this study and TBW I (Taylor et al.,; 2007, 2005), which were conducted using the same pilot distribution system and copper loops, the cupric hydroxide model, with log equilibrium constant 8.89, consistently under-predicted dissolved copper release (Xiao 2004). The variability of equilibrium constants for copper scales, including copper hydroxide, was discussed by Schock, Lytle and Clement (1995). Using earlier work by Schindler et al., (1965,1967) they found the range of log equilibrium constants for cupric hydroxide to vary from 8.67 to 8.89, when corrected for ionic strength. Hidmi and Edwards reported a log equilibrium constant of  $9.36 \pm 0.02$  for freshly precipitated  $\text{Cu}(\text{OH})_2$  (1999).

The observed copper concentrations presented in these results are consistent with what would be expected using a greater log equilibrium constant. The log equilibrium constant for  $\text{Cu}(\text{OH})_2$  has been observed to decrease with aging of the cupric hydroxide solids (Hidmi and Edwards 1999). Other reported values for the  $\text{Cu}(\text{OH})_2$  log equilibrium constant include 8.3, 8.7, 9.2, and 9.4 (King 1959) (Hahn and Welcher 1969) (Hogness and Johnson 1957) (Schenk 1996). A unit variation in log equilibrium constant would result in a log order variation in predicted copper release.

The dramatic reductions in copper release with the addition of phosphate inhibitor, as shown in Table 6.2 , suggest that a less soluble copper phosphate solid may form; however, very little information on solid forms of copper orthophosphate solids is available (Schock, Lytle, and Clement 1995). A review of the literature confirmed the lack of information identifying copper orthophosphate solids in water distribution systems. Thermodynamic data was available for the two forms  $\text{Cu}_3(\text{PO}_4)_2 \cdot 2\text{H}_2\text{O}$  and  $\text{Cu}_3(\text{PO}_4)_2$ , hence these were used to model cupric phosphate solubility (Shock, Lytle, and Clement 1995).

For the range of pH values considered in this study with phosphate inhibitors, 7.7-8.0, tenorite ( $\text{CuO}$ ), is thermodynamically favored; however, tenorite usually forms by aging of cupric hydroxide ( $\text{Cu}(\text{OH})_2$ ) solids. Tenorite was detected by XPS on copper coupons for all inhibitors but not as abundant as cupric hydroxide. This indicates cupric solids are slow to reach equilibrium form as  $\text{CuO}$ . Therefore cupric hydroxide solids can persist as a metastable solid (Xiao 2004). Near pH 8, cupric phosphate dihydride,  $\text{Cu}_3(\text{PO}_4)_2 \cdot 2\text{H}_2\text{O}$  and cupric hydroxide,  $\text{Cu}(\text{OH})_2$  have similar predicted copper solubility, indicating that neither compound is thermodynamically favored over the other.

*OP.* Copper corrosion products identified by the XPS analysis for the four copper coupons exposed to OP found  $\text{Cu}(\text{OH})_2$ ,  $\text{CuO}$ ,  $\text{Cu}_2\text{O}$  and Cu (II) copper scales. However,  $\text{Cu}(\text{OH})_2$  and  $\text{CuO}$  were the most predominant scales. Orthophosphate was found on three of four copper coupons. Calcium phosphate was not detected on any of these coupons, although calcium carbonate was detected on two of the three coupons with orthophosphate present. The formation of tenorite is thermodynamically favored, but this solid is not as abundant as cupric hydroxide due to kinetic limitations. For these conditions, given available thermodynamic constants, cupric hydroxide and cupric phosphate dihydride are equally favored thermodynamically.

Equilibrium calculations are provided in Table 6.6 considering cupric hydroxide, tenorite, cupric phosphate dihydride, and cupric phosphate as the possible controlling solid phases. From Table 6.2 there is a clear improvement with the control of copper release with the addition of OP when compared to  $\text{pH}_s+0.3$ . Both cupric hydroxide and cupric phosphate dihydride solids over predict the observed dissolved copper release.

If the effective log equilibrium constant for cupric hydroxide were elevated to be consistent with observed dissolved copper release for  $\text{pH}_s+0.3$ , then the cupric phosphate dihydride model would explain the decrease in copper release with OP addition. No data on the XPS binding energies for cupric phosphate dihydride were located in the literature; however, they may be represented as part of the Cu (II) salts curve.

Table 6.6  
Copper thermodynamic modeling of OP

Inhibitor	Phase	Actual Copper Release (mg/L)		Modeled Copper Release (mg/L)			
		Diss Cu	Total Cu	Cu(OH) <sub>2</sub>	CuO	Cu <sub>3</sub> (PO <sub>4</sub> ) <sub>2</sub> ·2H <sub>2</sub> O	Cu <sub>3</sub> (PO <sub>4</sub> ) <sub>2</sub>
OP	1	0.38	0.41	0.56	0.07	0.67	2.88
	2	0.28	0.35	0.52	0.06	0.41	1.75
	3	0.29	0.35	0.53	0.07	0.63	2.70
	4	0.32	0.36	0.64	0.08	0.47	2.01
	All	0.32	0.37	0.60	0.07	0.56	2.42

#### *Mechanistic Investigation of Copper Release*

Figure 6.13 shows the results of the mechanistic analysis comparing the diffusion model and the solubility model as explanations for the observed reductions in free dissolved copper with increasing orthophosphate. Both models make predictions consistent with the data. The phosphate film diffusion model (-1<sup>st</sup> order) tends to under predict copper when orthophosphate is greater than about  $0.04 \times 10^6$  mg/L as P; however, the cupric phosphate solubility model (-2/3<sup>rd</sup> order) appears to better fit the data within this range. Both models provided a plausible description of the reduction in copper concentration with increasing phosphate inhibitor dose. However, the low concentrations of orthophosphate ion near pH 8, suggest that biphosphate ion,  $\text{HPO}_4^{2-}$ , may play a more important role in inhibition of copper release.

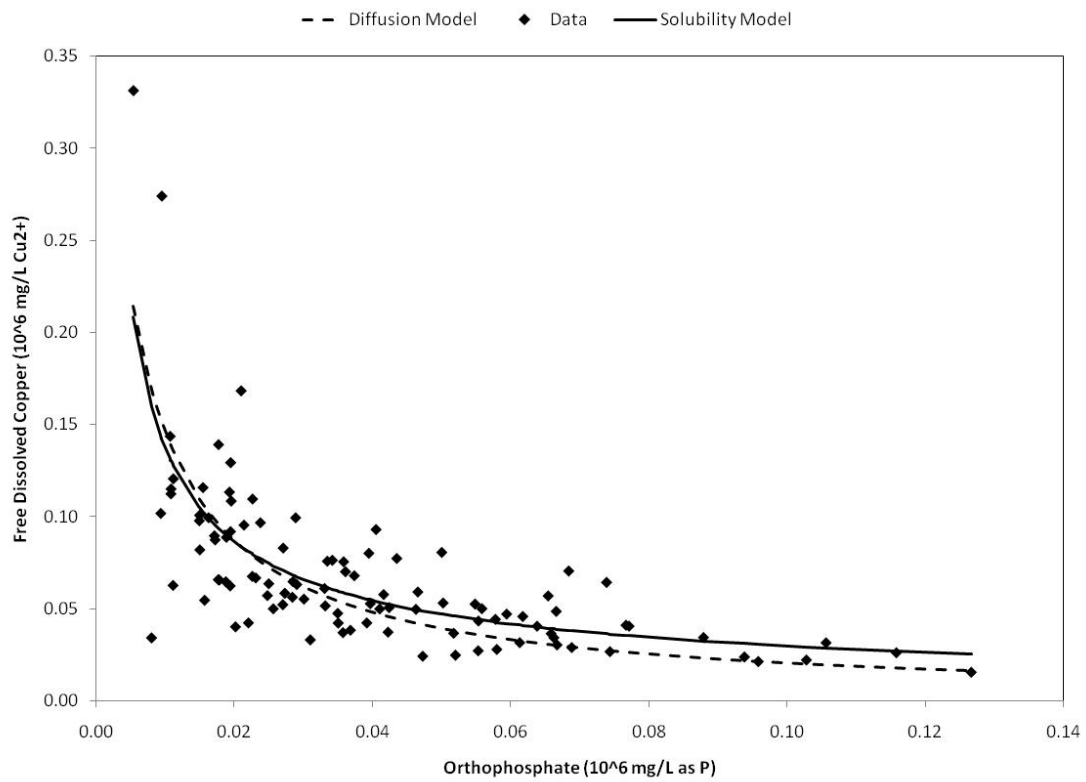


Figure 6.13 Comparison of diffusion model and solubility model as mechanisms for the effect of orthophosphate on copper Release

## Conclusions

A yearlong investigation of the effects of phosphate inhibitors on copper release was undertaken using a specially constructed pilot plant and array of pilot distribution systems. The effect of inhibitors was investigated under a range of blended waters including groundwater, surface water, and reverse osmosis desalinated water.

Pilot distribution systems were tested with phosphate inhibitors including blended poly/orthophosphate, sodium orthophosphate, and zinc orthophosphate and waters that had received no inhibitors. On average, all phosphate inhibitors tended to reduce copper release by about 60% at a 1 mg/L as P dose. This effect was consistent, even with seasonal changes in the source water blend.

Surface characterization of copper coupons by x-ray photoelectron spectroscopy (XPS) indicated that  $\text{Cu}_2\text{O}$ ,  $\text{CuO}$ ,  $\text{Cu}(\text{OH})_2$ , and cupric salts were the main copper compounds on the surface of the copper coupons. Orthophosphate was found on all copper coupons exposed to phosphate inhibitors. A lack of published XPS binding energies precluded positive identification of  $\text{Cu}_2(\text{PO}_4)_3$ ; however,  $\text{Ca}_3(\text{PO}_4)_2$  was ruled out by XPS analysis as the phosphate compound.

Thermodynamic models for copper release, based on  $\text{Cu}(\text{OH})_2$ ,  $\text{CuO}$ ,  $\text{Cu}_3(\text{PO}_4)_2$ , and its dihydride,  $\text{Cu}_3(\text{PO}_4)_2 \cdot 2\text{H}_2\text{O}$  controlling solids were developed using reported thermodynamic data. In all cases, copper-alkalinity complexes accounted for about 90% of predicted dissolved copper. The  $\text{Cu}(\text{OH})_2$  model was the closest fit for the no inhibitor line; however, it tended to under predict copper concentrations. Considerable variation in  $\text{Cu}(\text{OH})_2$  solubility products has been reported in the literature.

$\text{Cu}(\text{OH})_2$  and  $\text{Cu}_3(\text{PO}_4)_2 \cdot 2\text{H}_2\text{O}$  models provided similar copper release predictions for copper loops receiving phosphate inhibitors. However, when the results with  $\text{Cu}(\text{OH})_2$  and the no

inhibitor loops are considered, the cupric phosphate dihydride model provides the closest prediction of copper release. The cupric phosphate dihydride solid corresponds stoichiometrically with a cupric biphosphate dihydroxide,  $\text{CuHPO}_4(\text{OH})_2$ , solid. The role of biphosphate in the effect of phosphate inhibitors should be considered since it is the predominant phosphate species at  $7.2 < \text{pH} < 12.3$ .

Two mechanisms were proposed to explain how phosphate inhibitors control copper release: a diffusion model, and a solubility model. The diffusion model was derived from Fick's first law of diffusion, assuming that phosphate inhibitors form a film that acts as a diffusion barrier over the underlying controlling solid and that the film thickness varies with orthophosphate concentration. The solubility model was derived from the solubility product equation for cupric phosphate. The free uncomplexed cupric ion concentration was calculated from the dissolved copper using the water quality data and published thermodynamic data. Orthophosphate concentration was calculated using the phosphoric acid concentration and pH. A plot of both models against the data from the orthophosphate loops showed that the copper concentration decreased in a manner consistent with control by either cupric phosphate solubility or a diffusion limiting phosphate film.

## CHAPTER 7 SURFACE CHARACTERIZATION AND SOLUBILITY MODELING OF COPPER IN WATER DISTRIBUTION SYSTEMS RECEIVING SILICATE INHIBITORS

### Abstract

A yearlong investigation of the effects of silicate inhibitor on copper release was undertaken using a specially constructed pilot plant and array of pilot distribution systems. A range of blended waters were used including groundwater, surface water, and reverse osmosis desalinated water.

Pilot distribution systems were run comparing silicate inhibitor doses ranging from 3 to 12 mg/L as SiO<sub>2</sub>, treated with silicate inhibitor and waters that had received no inhibitors. When compared to no inhibitor addition, silicate inhibitor addition at 6.0 mg/L as SiO<sub>2</sub> reduced copper release by about 25-40%.

Surface characterization of copper coupons by x-ray photoelectron spectroscopy (XPS) indicated that Cu<sub>2</sub>O, CuO, Cu(OH)<sub>2</sub>, and cupric salts were the main copper compounds on the surface of the copper coupons. Oxidized silicon (SiO<sub>x</sub>) was detected on copper coupons exposed to phosphate inhibitors. A lack of published XPS binding energies precluded positive identification of the silicon as an adsorbed silicate film or as cupric silicate.

Thermodynamic models for copper release, based on Cu(OH)<sub>2</sub>, CuO, and CuSiO<sub>3</sub> · H<sub>2</sub>O were developed using published thermodynamic data. In all cases, copper-alkalinity complexes accounted for about 90% of predicted dissolved copper. The Cu(OH)<sub>2</sub> model was the closest fit for the no inhibitor line; however, it tended to under predict copper concentrations.. The CuSiO<sub>3</sub> · H<sub>2</sub>O models provided the closest prediction of copper release for the silicate inhibitor line, whereas the Cu(OH)<sub>2</sub> model tended to under predict copper release. Solubility constants for Cu(OH)<sub>2</sub> have been reported to vary with particle size.

## **Introduction**

This paper examines the effect of sodium silicate inhibitor on copper release. A recent AwwaRF study entitled “Control of Distribution System Water Quality in a Changing Water Quality Environment Using Inhibitors” (Taylor et al. 2007) investigated the use of corrosion inhibitors to mitigate adverse impacts of varying water quality in distribution systems. Significant decreases in copper release were observed with the addition of phosphate or silicate inhibitors. Control of copper release was maintained even with changes in season and water quality. Surface characterization and water quality data were used to evaluate possible mechanisms whereby silicate inhibitors reduced copper release.

### *Copper Corrosion*

Copper corrodes from its metallic form of  $\text{Cu}^0$  to the, cuprous,  $\text{Cu(I)}$  and cupric,  $\text{Cu(II)}$  ions. The maximum contaminant level goal (MCLG) and action level for LCR compliance for copper in potable water systems is 1.3 mg/L. Elevated copper can cause gastrointestinal distress, liver damage, and/or kidney damage (Barceloux and Barceloux 1999). Hence, utilities have a motivation to produce nonaggressive waters that will not result in excessive copper release.

In new piping generally up to 5 years of use, copper (II) concentrations are controlled by  $\text{Cu(OH)}_2$  solid phases, which can age with time to form less soluble tenorite,  $\text{CuO}$ , or malachite,  $\text{Cu}_2(\text{OH})_2\text{CO}_3$  scales (Schock, Lytle, and Clement; 1995). Although copper (I) can exist in solution, for the pH and ORP associated with drinking water systems, it is usually oxidized to copper (II).

In 2003, a similar study was conducted using the same pilot facility described in this paper which investigated treatment process impacts on water quality without use of inhibitors.

XRD identified cuprite ( $\text{Cu}_2\text{O}$ ) crystalline structures in the corrosion layer (Taylor et al., 2005). Cuprite ( $\text{Cu}_2\text{O}$ ), cupric hydroxide ( $\text{Cu}(\text{OH})_2$ ), tenorite ( $\text{CuO}$ ), and, made up the bulk surface composition on copper coupons identified by XPS. Thermodynamic modeling indicated that copper release was well described by equilibrium with  $\text{Cu}(\text{OH})_2$  acting as the controlling solid (Xiao; 2004). Alkalinity increased copper release; whereas pH elevation above  $\text{pH}_s$  and silica reduced copper release.

Often, in domestic systems, copper concentrations do not fully reach equilibrium between use. It can take 48 to 72 hours to reach equilibrium copper levels in a disinfected copper loop (Schock, Lytle, and Clement 1995). When inhibitors are not added, other methods for controlling copper release include raising the pH, and or reducing the alkalinity.  $\text{CO}_2$  stripping has been recommended as one way to increase the pH without increasing alkalinity (Edwards, Hidmi, and Gladwell; 2003). However, decreasing the alkalinity can increase lead solubility (Taylor et al. 2005). Inhibitors may overcome the apparent tradeoff between control of copper or lead release concentration.

### *Silicate Inhibitors*

The form of dissolved silica in water has not been clearly established; however, it does not behave as a charged anion such as  $\text{SiO}_3^{2-}$  or as a colloid (Hem 1971). In contrast, silicate inhibitor manufacturers claim that a negatively charged silica monomer, represented as  $\text{SiO}_3^{2-}$  adsorbs as a surface film on anodic sites (PQ Corp 2001) High passivation doses during the first month of dosing were recommended to help in formation of a passivating silicate film. The formation of a film was supported by scanning electron microscopy and x-ray photoelectron spectroscopy.

Because silicate acts as an anodic inhibitor, there is the danger that insufficient dosages could result in incomplete coverage of the anodic areas, leading to pitting corrosion. Silicate inhibitor films tend to be self-limiting and do not form thick layers (Vic et al. 1996).

## Materials and Methods

### *Pilot Testing*

A pilot testing facility comprised of pilot distribution systems (PDSs), copper corrosion loops, PVC pipe cradles to house corrosion and biological coupons were used to test the effects of corrosion inhibitors on distribution system water quality. The PDSs were located in Pasco County, Florida, USA on the grounds of the Cypress Creek Water Treatment Facility.

### Source Waters

Blends of surface water, groundwater, and brackish water was used for the pilot study. Surface water was treated at a surface water treatment plant by ferric sulfate coagulation and trucked to the pilot testing site. On site, additional surface water treatment process included chloramination and pH stabilization. Raw groundwater was obtained from the Cypress Creek water treatment facility. The groundwater treatment process included aeration, chloramination, and pH stabilization. Brackish water was artificially prepared from the raw groundwater by the addition of sea salt after RO treatment. The reverse osmosis desalinated water (RO) treatment process included reverse osmosis, aeration, chloramination, and pH stabilization.

The three sources were blended, aerated, chloraminated, and pH stabilized in the process tanks shown in Figure 5.2. Three blends were studied over four operating phases, with each phase lasting three months. Within each phase, all pilot distribution systems received the same blend of water. Blend composition, water quality, and schedule for each phase are presented in Table 5.1.

Table 7.1  
Blend ratios and water quality by phase

	Phase I	Phase II	Phase III	Phase IV
GW (%)	62	27	62	40
SW (%)	27	62	27	40
RO (%)	11	11	11	20
Alkalinity (mg/L as CaCO <sub>3</sub> )	160	103	150	123
Chlorides (mg/L Cl <sup>-</sup> )	45	67	68	59
Sulfates (mg/L SO <sub>4</sub> <sup>2-</sup> )	62	103	67	76
Temperature (°C)	21.3	26.2	25.7	21.2
Time Period	Feb-May 2006	May-Aug 2006	Aug-Nov 2006	Nov 2006-Feb 2007

### Corrosion Inhibitors

Blended poly/ortho phosphate (BOP), orthophosphate (OP), zinc orthophosphate (ZOP), and silicate (SiO<sub>2</sub>) were fed from inhibitor tanks by peristaltic pumps, into influent standpipes to mix with blended water coming from the process storage tanks. Phosphate inhibitors were dosed at 0.5, 1.0, and 2.0 mg/L as P, while silicate inhibitor was dosed at 3.0, 6.0, and 12.0 mg/L as SiO<sub>2</sub>. Two PDSs were operated as pH controls without inhibitor addition, one at the stability pH for calcium carbonate precipitation i.e. pH<sub>s</sub>, while the other at an elevated pH of pH<sub>s+0.3</sub>.

### Pilot Distribution Systems

After inhibitor addition, the water from each influent standpipe flowed into the pilot distribution systems (PDSs), shown in Figure 7.2. All pipes used in the PDSs were excavated from distribution systems. The 14 hybrid PDSs each about 92 feet long, consisted of polyvinylchloride (PVC), lined cast iron (LCI), unlined cast iron (UCI) pipe, and galvanized iron (G) in series.

## Copper Loops

Copper loops were housed (Figure 7.3) in series at the end of each PDS to simulate a home plumbing system. Copper tubes (Figure 7.4) were 5/8 in. (1.6 cm) in diameter and 30 ft. (9.1 m) in length. Copper loops were flushed daily with 2 gallons (7.6 L) of water at an average velocity of 1 fps. Copper concentration was measured weekly from water from copper loops after a standing time of six to seven hours.



Figure 7.1 Covered tanks for process treatment



Figure 7.2 Pilot distribution systems



Figure 7.3 Corrosion shed

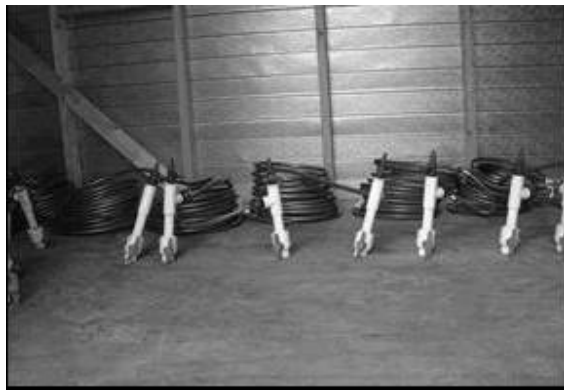


Figure 7.4 Copper lines

### *X-Ray Photoelectron Spectroscopy*

Chemical composition of corrosion scales on the surface of metal coupons copper exposed to the various inhibitors were characterized by XPS or X-ray Photoelectron Spectroscopy (Physical Electronics 5400 ESCA) following each phase of operations. In XPS, an Mg anode (1254 eV  $K\alpha$ ) bombards the coupon surface with high energy X-rays that interact with atoms in the top 5-6 nm of the surface (Seal and Barr 2001). Then, according to the photoelectric effect, these atoms emit high energy electrons. An electron analyzer counts the number of electrons emitted over a range of energies, producing scan spectra which may be used for surface composition analysis

The effluent from the PDS was split in two parts. One part was directed to the copper corrosion loops and the other was directed to a trailer which housed 4 in diameter PVC pipes with copper corrosion coupons. These coupons were inserted at the beginning of each phase, and then retrieved at the end of the phase. The XPS scanning consists of a two-step process: an initial survey scan followed by a high resolution scan. The survey scan, conducted over a broad range of energy levels, is useful for confirming the presence or absence of elements on the surface of the coupon. In contrast, a high resolution scan is conducted over a narrow range of energy levels is useful for establishing the chemical states present for a given element.

The elements are indicated on the survey scan by pronounced peaks above the background of the survey, and these peaks are then selected individually for a “high resolution” scan for each element. Additionally, elements of interest, such as those associated with inhibitors, coupon material, or water quality, were analyzed with high resolution scans. Possible compounds associated with a given element were determined through deconvolution of the high resolution scan.

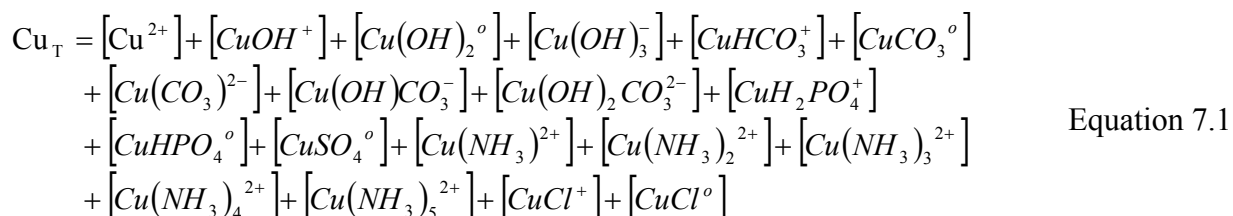
## Scanning Electron Microscopy

### *Thermodynamic Modeling*

Cu(OH)<sub>2</sub> has been identified as a metastable intermediate that forms in new copper pipe, and has been used as the basis for thermodynamic models of copper (Schock, Lytle, and Clement 1995)(Xiao 2004). Cupric hydroxide can age to its dehydrated form tenorite, CuO, which is less soluble. In the presence of alkalinity, old copper pipe tends to form the more stable, less soluble cupric hydroxycarbonate Cu<sub>2</sub>(OH)<sub>2</sub>CO<sub>3</sub>, malachite (Schock, Lytle, and Clement. 1995).

### Thermodynamic Model Development

The thermodynamic model for dissolved copper that had been developed in TBW I (Taylor et al., 2005) was expanded to include phosphate, sulfate, chloride, and ammonia complexes and is given in Equation 4.4. The equilibrium model assumed the presence of Cu (II) species. Silica complexation of copper was also considered; however, a review of literature concerning coordination chemistry did not reveal any thermodynamic data corresponding to an aqueous copper-silica complex.



The complexes considered within Equation 4.4 demonstrate the various water quality parameters governing copper release. The free dissolved cupric ion concentration at equilibrium depends on the controlling solid; however, other water quality parameters, such as alkalinity, chloride, sulfate, ammonia, and phosphate form copper complexes in equilibrium with the free

cupric ion, and thus amplify the natural level of dissolved copper. Empirical models developed as a part of this study, and reported elsewhere (Taylor et al. 2007) identified pH, chloride, and alkalinity as the main water quality effects. Increased pH was beneficial in controlling copper release, whereas increasing the chlorides or alkalinity increased copper release.

The effect of chlorides on dissolved copper did not appear to be explained by formation of a copper-chloride complex, because  $\text{CuCl}^+$  and  $\text{CuCl}^0$  complexes accounted for approximately 1/1000<sup>th</sup> of a percent of the dissolved copper. Rather, the effect may relate to associated changes in solution conductivity and ionic strength that accompany elevated chloride concentrations. It is speculated that chlorides may have reduced carbonate/ hydroxide scale passivity by promoting local pH drops near copper surfaces and may cause pitting corrosion; however for the moderate alkalinity (84-175 mg/L as  $\text{CaCO}_3$ ) waters used in this study large pits were not observed on copper surfaces.

For this study, copper-alkalinity complexes accounted for approximately 90% of all dissolved copper. Copper-alkalinity complexes included  $\text{CuHCO}_3^-$ ,  $\text{CuCO}_3^0$ ,  $\text{Cu}(\text{CO}_3)_2^{2-}$ ,  $\text{Cu}(\text{OH})\text{CO}_3^-$ , and  $\text{Cu}(\text{OH})_2\text{CO}_3^{2-}$ . Equilibrium calculations demonstrated that alkalinity had a tremendous effect on copper release, capable of increasing the total dissolved copper to several times the level of free dissolved copper.

For this study, copper-phosphate complexes accounted for only about 0.5% of total dissolved copper, indicating little adverse effect. Copper-phosphate complexes included  $\text{CuH}_2\text{PO}_4^+$  and  $\text{CuHPO}_4^0$ .

## Model Implementation

Separate runs of the model were performed assuming considering the following compounds as candidate controlling solids: cupric hydroxide ( $\text{Cu}(\text{OH})_2$ ), tenorite ( $\text{CuO}$ ), and cupric silicate hydrate ( $\text{CuSiO}_3 \cdot \text{H}_2\text{O}$ ). Calculations were performed for the  $\text{pH}_s$  controls and all phosphate inhibitor types using average water quality data for each phase. The middle dose (5.0 mg/L as  $\text{SiO}_2$ ) silicate inhibitor lines were modeled because the coupons from these lines are the ones studied by XPS analyses.

## Results and Discussion

### *Effect of Silicate Inhibitor on Copper Release*

The average copper release observed during the study is shown in Table 7.2 by phase for each inhibitor and relative to the  $\text{pH}_s+0.3$  control. In all cases, inhibitors reduced copper release relative to the control. Phosphate inhibitors, at dose 1 mg/L as P, reduced copper release to about 40% that observed with the control. Silicate inhibitors, at dose 6 mg/L as  $\text{SiO}_2$ , reduced copper release to about 70% of that observed with the control.

Time series plots for Si, and the no inhibitor controls are shown in Figure 7.5 and Figure 7.6. The plots show that the addition of 3, 6, or 12 mg/L as  $\text{SiO}_2$  of silicate inhibitor tended to reduce copper release in proportion to the copper release observed with the no inhibitor control  $\text{pH}_s+0.3$ .

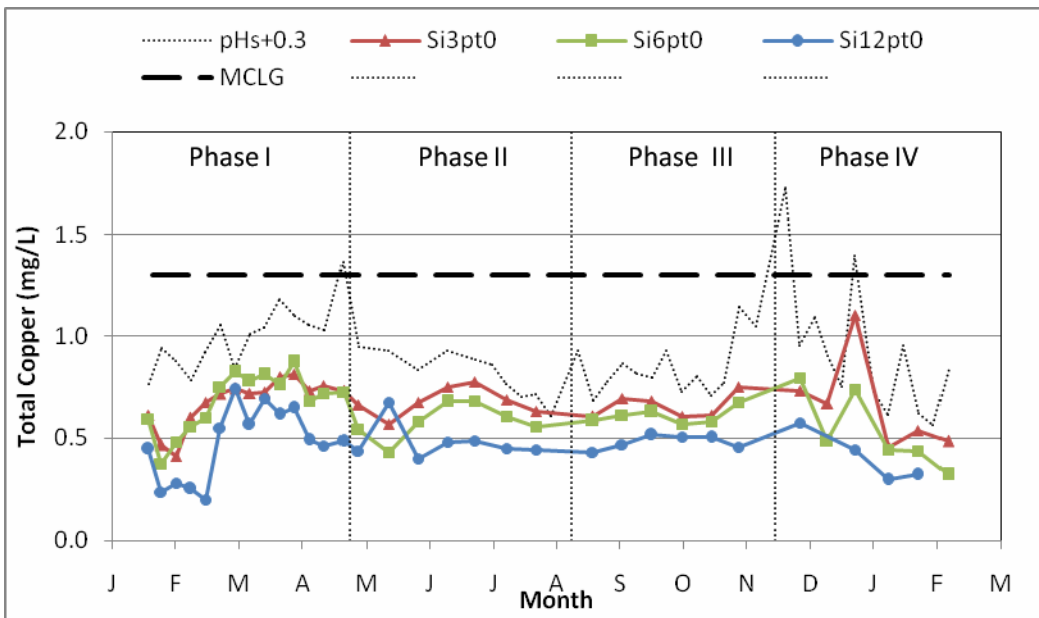


Figure 7.5 Time series plot of copper release with Si inhibitor addition

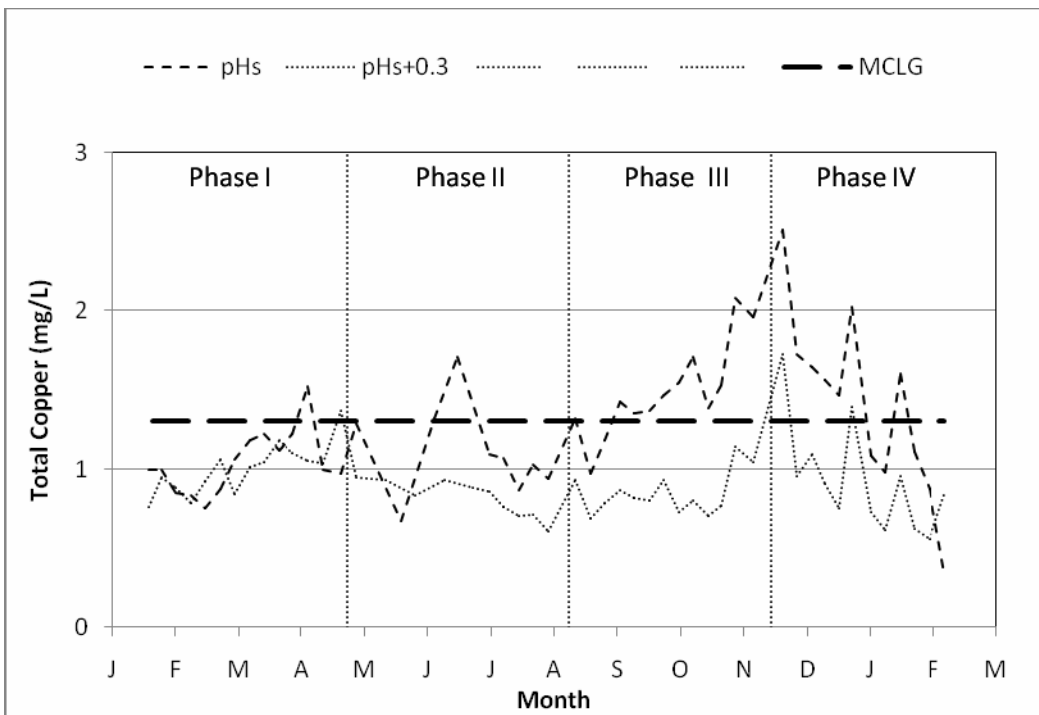


Figure 7.6 Time series plot of copper release by pH without inhibitor addition

Table 7.2  
Comparison of observed copper release from inhibitor PDSs to pH<sub>s</sub>+0.3

Phase	Inhibitor	Average Release (mg/L)		% Ratio to pH <sub>s</sub> +0.3	
		Dissolved Cu	Total Cu	Dissolved Cu	Total Cu
I	pH <sub>s</sub> +0.3	0.89	1.00		
	OP	0.38	0.41	42%	41%
	Si	0.61	0.68	68%	68%
II	pH <sub>s</sub> +0.3	0.73	0.82		
	OP	0.28	0.35	39%	43%
	Si	0.51	0.60	69%	73%
III	pH <sub>s</sub> +0.3	0.79	0.85		
	OP	0.29	0.35	37%	41%
	Si	0.58	0.65	74%	77%
IV	pH <sub>s</sub> +0.3	0.83	0.93		
	OP	0.32	0.36	38%	39%
	Si	0.51	0.58	62%	63%

#### *XPS Identification of Copper Corrosion Products*

Five copper coupons exposed to Si inhibitor were analyzed for the elements shown in Table 7.3. One copper coupon was tested for Phases I, II, and IV. Two coupons were tested for Phase III, with one coupon being receiving a 6mg/L as SiO<sub>2</sub> inhibitor dose (PDS 11) and the other receiving a 12 mg/L as SiO<sub>2</sub> inhibitor dose (PDS 12).

Carbon was detected on five out of five coupons, always appearing as carbonate. Calcium was detected on two out of five coupons, appearing as CaCO<sub>3</sub> in Phase IV and CaO in Phase III for the higher 12 mg/L as SiO<sub>2</sub> dose. No calcium was detected on either the Phase I or the Phase III coupons. Thus, in the presence of Si inhibitor, CaCO<sub>3</sub> films were only detected for Phase IV water quality conditions.

Table 7.3  
Compounds identified in scale on copper coupons in the presence of Si inhibitor

Element	Compound	Phase I	Phase II	Phase III (PDS 12)	Phase IV
C	CO <sub>3</sub> <sup>2-</sup>	X	X	X(X)	X
Ca	CaCO <sub>3</sub>				X
	Ca <sub>3</sub> (PO <sub>4</sub> ) <sub>2</sub>				
Cu	CaO			(X)	
	Cu <sub>2</sub> O	X	X	X(X)	X
	CuO	X	X	X(X)	X
	Cu(OH) <sub>2</sub>	X	X	X(X)	X
	Cu(II)	X	X	X(X)	X
O	O <sup>2-</sup>	X	X	X(X)	X
	CO <sub>3</sub> <sup>2-</sup>	X	X	X(X)	X
	OH <sup>-</sup>	X	X	X(X)	X
P	PO <sub>4</sub> <sup>3-</sup>				
	PO <sub>4</sub> <sup>3-</sup>				
	Meta				
	Pyro				
Si	SiO <sub>x</sub>	X		(X)	X
Zn					

Copper was detected on five out of five coupons, appearing as a mixture of Cu<sub>2</sub>O, CuO, Cu(OH)<sub>2</sub>, and Cu(II) salts, for all phases. Cu (II) salts may be associated with carbonates (detected for five out of five coupons), and cupric silicate (detected on three out of five coupons). It has been suggested that CuSiO<sub>3</sub> can form from malachite exposed to SiO<sub>2</sub> inhibitor (Schock et al. 2005).

Oxygen was detected on five out of five coupons, appearing as a mixture of O<sup>2-</sup>, CO<sub>3</sub><sup>2-</sup>, and OH<sup>-</sup>. It should be noted that no PO<sub>4</sub><sup>3-</sup> was detected on any of the five coupons for Si inhibitor, indicating that phosphate inhibitor addition is the primary source for phosphorus on the copper surfaces for the given water qualities studied.

Phosphorus was detected on none of the five coupons, consistent with the results from oxygen. Even though orthophosphate is not present, some Cu(II) salts were still present in the Si

inhibitor lines, comprising about 8% of all copper corrosion products. Average relative percent areas of copper for Cu(II) were approximately 23%, 13%, and 10% for BOP, OP, and ZOP inhibitors respectively. Similarly, the average relative percent area for the pH lines was approximately 15%. The results from the phosphate inhibitors suggest that increasing phosphorus levels may correspond with increased percent areas of Cu(II); however, Cu(II) levels are also elevated for the pH lines, suggesting that sulfate, carbonate, silicate or some other anion may also account for increased levels of Cu(II) deposits.

Silica was detected on three out of five coupons, including Phase I, Phase III (PDS 12 only), and Phase IV. In all cases Si was found as  $\text{SiO}_x$ . No silica was found on the coupons for Phase II and Phase III (PDS 11). Absence of silica from the XPS results for Phase II and Phase III (PDS 11), does not imply that silica is not present on the copper surface. Rather, non uniformity in silica surface deposits may explain this result. The presence of  $\text{SiO}_x$  may indicate a mixed silica film of  $\text{SiO}_2$  monomers, and polymers, and/or the presence of a cupric silicate,  $\text{CuSiO}_3$ . Zinc was not detected on any of the five coupons. As mentioned in the thermodynamic modeling section, silicate may also be present as a copper silicate solid. Although the actual form of such a solid in distribution systems has not been established in the literature, the thermodynamic model for, cupric silicate hydride,  $\text{CuSiO}_3 \cdot \text{H}_2\text{O}$ , gave reasonable predictions for dissolved copper release with silicate inhibitor.

### *Thermodynamic Modeling*

The XPS analysis for the five copper coupons exposed to silicate inhibitor during four phases of operation indicated the presence of  $\text{Cu}(\text{OH})_2$ ,  $\text{CuO}$ ,  $\text{Cu}_2\text{O}$ , and Cu(II) salts for all four

phases. An additional copper coupon was placed in PDS 12 during Phase III. Of the five copper coupons analyzed by XPS, three of the coupons contained amorphous silica.

Upon precipitation of silica, copper ions may be incorporated into the lattice of the amorphous structure, precipitated on the copper surface. Copper silicate hydrate ( $\text{CuSiO}_3 \cdot \text{H}_2\text{O}$ ) was modeled to represent a possible bond between copper and silica. Cupric hydroxide and tenorite were also considered as possible controlling solids for copper release in the presence of silicate inhibitor.

Cupric hydroxide, tenorite, and the cupric silicate hydrate were considered separately as the controlling solid phases for copper release. Table 7.4 shows the actual copper release and modeled copper release for the three controlling solid forms. Predicted copper release from cupric hydroxide and the cupric silicate hydrate provided the most reasonable prediction of copper release, with both solids slightly under predicting dissolved copper release. Cupric silicate hydrate more accurately predicted dissolved copper concentrations; however, the predicted solubility for the cupric hydroxide and the cupric silicate hydrate model are very close.

Table 7.4  
Copper thermodynamic modeling of Si

Inhibitor	Phase	Actual Copper Release (mg/L)		Modeled Copper Release (mg/L)		
		Diss Cu	Total Cu	$\text{Cu}(\text{OH})_2$	CuO	$\text{CuSiO}_3 \cdot \text{H}_2\text{O}$
Si	1	0.61	0.68	0.32	0.04	0.51
	2	0.51	0.60	0.25	0.03	0.40
	3	0.58	0.65	0.31	0.04	0.51
	4	0.51	0.58	0.29	0.04	0.47
	All	0.55	0.63	0.31	0.04	0.50

## Conclusions

A yearlong investigation of the effects of silicate inhibitor on copper release was undertaken using a specially constructed pilot plant and array of pilot distribution systems. A range of blended waters were used including groundwater, surface water, and reverse osmosis desalinated water.

Pilot distribution systems were run comparing silicate inhibitor doses ranging from 3 to 12 mg/L as SiO<sub>2</sub>. treated with silicate inhibitor and waters that had received no inhibitors. When compared to no inhibitor addition, silicate inhibitor addition at 6.0 mg/L as SiO<sub>2</sub> reduced copper release by about 25-40%.

Surface characterization of copper coupons by x-ray photoelectron spectroscopy (XPS) indicated that Cu<sub>2</sub>O, CuO, Cu(OH)<sub>2</sub>, and cupric salts were the main copper compounds on the surface of the copper coupons. Oxidized silicon (SiO<sub>x</sub>) was detected on copper coupons exposed to phosphate inhibitors. A lack of published XPS binding energies precluded positive identification of the silicon as an adsorbed silicate film or as cupric silicate.

Thermodynamic models for copper release, based on Cu(OH)<sub>2</sub>, CuO, and CuSiO<sub>3</sub>·H<sub>2</sub>O were developed using published thermodynamic data. In all cases, copper-alkalinity complexes accounted for about 90% of predicted dissolved copper. The Cu(OH)<sub>2</sub> model was the closest fit for the no inhibitor line; however, it tended to under predict copper concentrations.. The CuSiO<sub>3</sub>·H<sub>2</sub>O models provided the closest prediction of copper release for the silicate inhibitor line, whereas the Cu(OH)<sub>2</sub> model tended to under predict copper release. Solubility constants for Cu(OH)<sub>2</sub> have been reported to vary with particle size.

## CHAPTER 8 EFFECTS OF PHOSPHATE AND SILICATE CORROSION INHIBITORS ON THE SURFACE MORPHOLOGY OF COPPER

### Abstract

The effects of phosphate and silicate corrosion inhibitors on surface roughness of copper coupons were evaluated as part of a yearlong pilot study investigating the influence of corrosion inhibitors on distribution system water quality.

Inhibitors included blended poly/ortho phosphate, sodium orthophosphate, zinc orthophosphate, sodium silicate, and pH elevation. An optical profiler was used to measure surface roughness both before and after exposure to inhibitors during a three month phase.

The greatest increases in surface roughness were observed with copper coupons receiving phosphate inhibitors. Smaller increases were observed with copper coupons receiving silicate inhibitor or no inhibitor. For coupons receiving phosphate inhibitors, elevated temperature and alkalinity were associated with larger increases in surface roughness.

Under elevated alkalinity and temperature blue-green scales formed on the coupons receiving phosphate inhibitors. At lower alkalinity and temperature, speckled blue-green scales formed on coupons receiving phosphate inhibitors and silicate inhibitors. Blue-green scales are associated with copper (II) solids. No blue-green scales were observed on the coupons receiving no inhibitor, rather a compact, dull red scale was observed, indicating a copper (I) solid layer had formed. These data appear to indicate a relationship between phosphate inhibitor addition and the oxidation state of copper surface solids that is indicated by visible differences in copper scale color and morphology.

Examination of surface deposits by scanning electron microscopy showed that copper surfaces receiving phosphate and silicate inhibitors formed visible deposits that varied in

thickness and particle shape. With phosphate inhibitor addition, the deposits were thicker; whereas with silicate inhibitor addition the particles were more round in appearance. In contrast to both inhibitor types, the no inhibitor treatment showed a disintegrating copper surface with mottled appearance indicating general corrosion.

## **Introduction**

This paper examines the effect of phosphate and silicate corrosion inhibitors on the morphology of copper. Optical profilometry was used to quantify the change in surface roughness due to inhibitor addition; whereas scanning electron microscopy was used to capture images of the changes in surface structure. Numerous studies have shown that copper release can be controlled by addition of phosphate inhibitors (Schock, Lytle, and Clement 1995a,b) (Lytle and Schock, 1997) (Taylor et al. 2007) or silicate inhibitors (Schenk and Weber, 1968)(Lytle, Schock, and Sorg, 1994, 1996)(Clement, Schock and Lytle, 1994) (LaRosa-Thompson et al. , 1997) (Taylor et al 2007).

With iron scales, orthophosphate has been shown to influence the stability of ferric hydroxide aggregates (He et al, 1996), indicating a possible relationship between orthophosphate and surface structure of materials. Whether or not orthophosphate, or silicate inhibition induces structural changes in existing copper films, they may alter the surface structure by formation of surface deposits. In this paper, surface roughness was used to quantify changes in copper surface morphology for different inhibitor treatments. Micrographs and x-ray spectra were collected to visualize micro-scale changes in surface structure and composition associated with inhibitor addition.

### *Color of Copper Corrosion Products*

In addition, the color of the surface scales can be an indicator of the surface composition. The primary difference in color is related to the oxidation state of copper. Cuprite, ( $\text{Cu}_2\text{O}$ ), a common copper (I) scale has been identified as red (King 1959)(Hahn & Welcher

1968)(Richardson 1997), light brown (Benedetti-Pichler 1964), and black (Richardson 1997). In contrast, copper (II) scales tend to be green, blue, or a mixture of both. Hence, it is difficult to distinguish between the copper (II) compounds by color alone. Cupric hydroxide ( $\text{Cu}(\text{OH})_2$ ) scales have been identified as blue (King 1959) or blue-green (Schenk 1996). Malachite ( $\text{Cu}_2(\text{OH})_2\text{CO}_3$ ) scales have been identified as green (King 1959) (Richardson 1997). In addition, copper (II) phosphate and silicate solids such as libethenite,  $\text{Cu}_2\text{PO}_4\text{OH}$ , and diopside, ( $\text{CuSiO}_3 \cdot \text{H}_2\text{O}$  alt.  $\text{CuSiO}_2(\text{OH})_2$ ) are blue-green in appearance (Benedetti-Pichler 1964). The color of copper scales in drinking water applications has been reported to vary with concentration of alkalinity, sulfates, and chlorides (Xiao et al. 2007).

### *Surface Roughness*

This study used a surface profiler to directly measure the physical surface roughness of pipes. There are two common kinds of surface profilers available for measurement of pipe surface roughness. Results from either kind of profiler can be used to calculate surface roughness parameters, such as  $R_a$ . With a stylus profiler, a stylus is traced in a line across the surface, and the displacement of the stylus is recorded along the trace line. In contrast, an optical profiler uses the interference of light to measure surface roughness over a scanning area. A monochromatic beam of light is split and directed towards a flat reference surface and the measurement surface. The light is reflected from each surface and recombined within the profiler. When the beams of light recombine, interference fringes form because the phase of the light reflected from the measurement surface depends on the distance of the optical path, which depends on the surface elevation. Optical profilometry works best with uniformly reflective materials. Measurement of dull or non-uniformly reflective materials is more difficult. Optical profilometry has the

advantage of being able to rapidly generate a map of the surface elevation over a given area of the coupon without contacting the coupon surface.

When surface roughness is measured by a profiler, a roughness statistic can then be computed from the profile data (Lippold and Podlesny, 1998). Most of these statistics describe either the height or the spacing of peaks and valleys in the profile. In this paper,  $R_a$ , the roughness average is used. It is the arithmetic mean of the surface deviations from the mean plane. For an array of  $M$  by  $N$  elevation points, it is calculated according to Equation 5.4. Figure 5.1 shows a surface profile of copper with average  $R_a$  roughness of  $2.96 \mu\text{m}$ , calculated over the  $2.3 \text{ mm} \times 3.0 \text{ mm}$  scan area.

$$R_a = \frac{1}{MN} \sum_{j=1}^M \sum_{i=1}^N |Z_{ij}| \quad \text{Equation 8.1}$$

where  $R_a$  = roughness average ( $\mu\text{m}$ )  
 $M$  = number of rows in the array  
 $N$  = number of columns in the array  
 $Z_{ij}$  = the absolute value of the deviation of the surface from the mean zero plane at the cell where the  $i^{\text{th}}$  column and  $j^{\text{th}}$  row of the array intersect ( $\mu\text{m}$ )

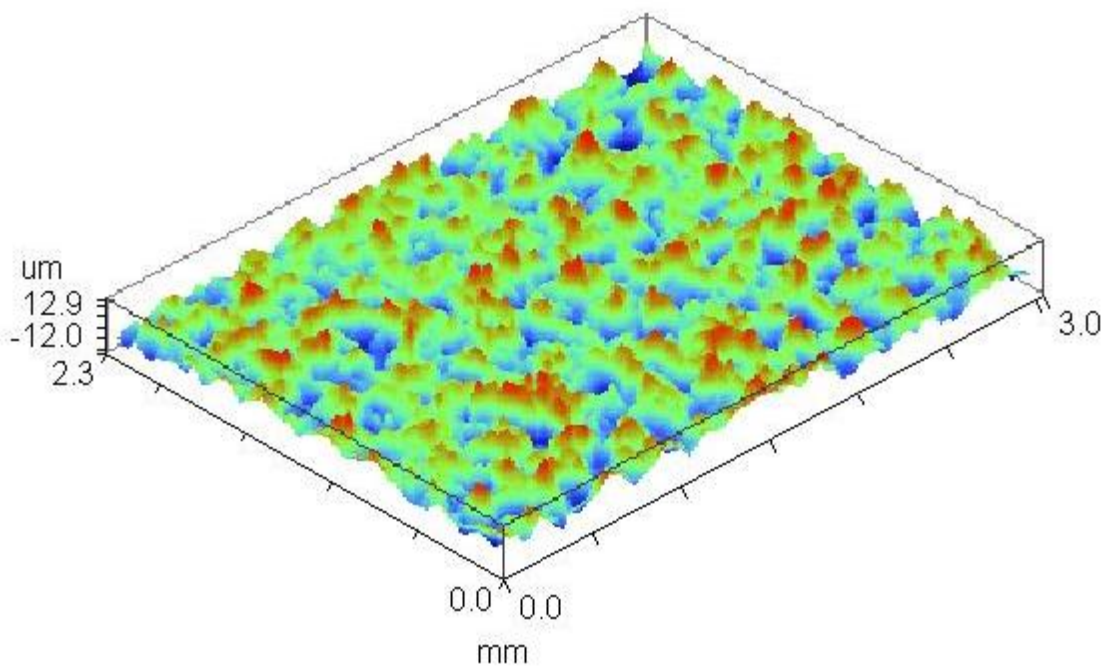


Figure 8.1 Sample optical profiler scan of copper surface with  $R_a$  of  $2.96 \mu\text{m}$

## **Materials and Methods**

### *Pilot Testing*

A pilot testing facility was used to test the effects of corrosion inhibitors on distribution system water quality in pilot distribution systems. The pilot distribution systems are located in Pasco County, Florida, USA on the grounds of the Cypress Creek Water Treatment Facility.

### Source Waters

A blend of surface water, groundwater, and brackish water was used for the pilot study. Surface water was treated at a surface water treatment plant by ferric sulfate coagulation and trucked to the pilot testing. On site, additional surface water treatment process included chloramination and pH stabilization. Raw groundwater was obtained from the Cypress Creek water treatment facility. The groundwater treatment process included aeration, chloramination, and pH stabilization. Brackish water was artificially prepared from the raw groundwater by the addition of sea salt. The reverse osmosis desalinated water (RO) treatment process included reverse osmosis, aeration, chloramination, and pH stabilization.

The three sources were blended, aerated, chloraminated, and pH stabilized in the process tanks shown in Figure 5.2. Within each phase, all pilot distribution systems received the same blend of water. Three blends were studied over four operating phases, with each phase lasting three months. Blend composition, water quality, and schedule for each phase are presented in Table 5.1.

Table 8.1  
Blend ratios and water quality by phase

	Phase I	Phase II	Phase III	Phase IV
GW (%)	62	27	62	40
SW (%)	27	62	27	40
RO (%)	11	11	11	20
Alkalinity (mg/L as CaCO <sub>3</sub> )	160	103	150	123
Chlorides (mg/L Cl <sup>-</sup> )	45	67	68	59
Sulfates (mg/L SO <sub>4</sub> <sup>2-</sup> )	62	103	67	76
Temperature (°C)	21.3	26.2	25.7	21.2
Time Period	Feb-May 2006	May-Aug 2006	Aug-Nov 2006	Nov 2006-Feb 2007

### Corrosion Inhibitors

Corrosion inhibitors, including, blended poly/ortho phosphate (BOP), orthophosphate (OP), zinc orthophosphate (ZOP), and silicate (SiO<sub>2</sub>) were fed from inhibitor tanks by peristaltic pumps, into influent standpipes to mix with blended water coming from the process storage tanks. Phosphate inhibitors were dosed at 0.5, 1.0, and 2.0 mg/L as P, while silicate inhibitor was dosed at 3.0, 6.0, and 12.0 mg/L as SiO<sub>2</sub>. Two PDSs were operated as pH controls without inhibitor addition. One PDS was operated at the stability pH for calcium carbonate precipitation, pH<sub>s</sub>, while the other was operated at an elevated pH, pH<sub>s</sub>+0.3.

### Pilot Distribution Systems

After inhibitor addition, the water from each influent standpipe flowed into the pilot distribution systems (PDSs), shown in Figure 8.3. The PDSs were constructed to simulate the effects of variation in source waters on distribution system water quality. All pipes used in the PDSs were excavated from TBW member government distribution systems. Each of 14 pilot distribution systems (PDS) was composed of four materials, laid out sequentially as:

- Approximately 20 feet (6.1 m) of 6-inch (0.15 m) diameter polyvinylchloride (PVC) pipe,
- Approximately 20 feet (6.1 m) of 6-inch (0.15 m) diameter lined cast iron (LCI) pipe,
- Approximately 12 feet (3.7 m) of 6-inch (0.15 m) diameter unlined cast iron (UCI) pipe,

Approximately 40 feet (12.2 m) of 2-inch (0.05 m) diameter galvanized iron (G) pipe

### Copper Coupons

Cu coupons for roughness and surface composition analyses were epoxied to a PVC sleeve and incubated in the electrochemical noise trailer shown in Figure 8.4. The corrosion cradles received a parallel feed from the influent standpipes. Separate coupons were used for the surface roughness analysis and surface composition analysis. Surface composition of copper coupons was investigated during Phases I-IV (MacNevin 2007c), whereas surface roughness of copper was only measured in Phases III and IV. The original experimental plan involved measurement of surface roughness for galvanized iron, unlined cast iron, lined cast iron, and polyvinyl chloride (PVC). The results from this study are reported elsewhere (MacNevin 2007b)

### Copper Loops

Copper loops were housed (Figure 8.5) in series at the end of each PDS to simulate a home plumbing system. Copper tubes (Figure 8.6) were 5/8 in. (1.6 cm) in diameter and 30 ft. (9.1 m) in length. Copper loops were flushed every morning with 2 gallons (7.6 L) of water at an average velocity of 1 fps. Copper concentration was measured weekly from water from copper loops after a standing time of six to seven hours.



Figure 8.2 Covered tanks for process treatment



Figure 8.3 Pilot distribution systems



Figure 8.4 Electrochemical noise trailer



Figure 8.5 Corrosion shed



Figure 8.6 Copper lines

### *Surface Characterization*

#### Optical Profilometry

An optical profiler, WYKO NT 3300 (Veeco Instruments, Woodbury, N.Y.) was used to measure the surface roughness of galvanized iron (G), lined cast iron (LCI), polyvinyl chloride (PVC), and unlined cast iron (UCI). The WYKO NT 3300 is a non-contact optical profiler capable of producing three dimensional surface measurements with 4.14  $\mu\text{m}$  horizontal resolution and 0.1 nm vertical resolution. An example output of the optical profiler was shown previously in Figure 5.1, which depicted the surface of a copper coupon having  $R_a$  of 2.96  $\mu\text{m}$ . Post processing of raw outputs included corrections for tilt and cylindrical curvature. Noise in the output was reduced using a 3x3 window median filter.

#### Scanning Electron Microscopy

A scanning electron microscope, SEM JEOL 6400F (JEOL Instruments, Tokyo, Japan), was used to collect micrographs and X-ray spectrums of the copper surface. The microscope

generates a coherent electron beam using a thermionic tungsten anode. The electron beam scans across the field of view in a raster, line-by line. When the electron beam strikes the surface, it interacts with the atoms in the surface causing them to emit x-rays and lower energy electrons. Differences in tilt, composition, and conductivity of the surface all affect the intensity of the remitted electron beam and hence help form an image of the surface structure.

Surface composition can be quantified using an energy dispersive x-ray spectrometer (EDS) which produces a spectrum of the reemitted x-ray energies. This spectrum can be used to confirm the presence of a particular element in the micrograph, and to get a sense of the relative abundance of different elements in the surface. EDS results are reflective of surface composition to a depth of 1-2 microns. Combined together scanning electron microscopy and electron dispersive spectrometry are powerful tools for the study of corrosion films.

## Results and Discussion

### *Surface Roughness of Copper*

All copper (Cu) coupons used in this study were new coupons, which had not been previously exposed to water like G, LCI, PVC, and UCI coupons. Therefore, there is little variation in the initial surface roughness,  $R_i$ , of the Cu coupons. All Cu coupons were of a standard size, 3" x 1/2" x 1/16" (7.6 cm x 1.27 cm x 0.16 cm). The surface roughness of Cu was examined in Phases III-IV only. A total of 35 Cu coupons were measured with average initial roughness of 3.30  $\mu\text{m}$ , with a minimum and maximum of 2.73  $\mu\text{m}$  and 3.80  $\mu\text{m}$ , respectively. The average initial roughness of copper for Phases III and IV were 3.22  $\mu\text{m}$  and 3.35  $\mu\text{m}$ , respectively. A two-tailed paired data t-test for initial roughness of Phase III-IV, had a p-value of 0.16, indicating that the initial surface roughness of copper coupons is essentially uniform. This is illustrated in Figure 8.7 which shows two copper coupons before exposure to inhibitors. The coupons are shown at actual size.



Figure 8.7 Photographs of typical copper coupons before exposure to inhibitors

A summary of the copper (Cu) surface roughness data is shown in Table 8.2. A statistical comparison of the initial and final roughness averages was completed using a two-tailed pooled-data t-test. The p-values are provided for the hypothesis tests for equality of initial and final

roughness. A reported p-value of 0.05 or less indicates there is sufficient evidence to conclude that the final roughness is different from the initial roughness (level of significance of 95%). If the p-value of the t-test is greater than 0.05, then there is no statistically significant difference in coupon surface roughness due to exposure to the inhibitor.

1  
2

Table 8.2  
Statistical comparison of Cu initial and final surface roughness

Phase	Parameter	PDS	PDS	PDS	PDS	PDS	PDS	PDS	PDS	PDS	PDS	PDS	PDS	PDS	PDS	AVG
		01 BOP	02 BOP	03 BOP	04 OP	05 OP	06 OP	07 ZOP	08 ZOP	09 ZOP	10 Si	11 Si	12 Si	13 pH <sub>s</sub>	14 pH <sub>s</sub>	
		0.5	1.0	2.0	0.5	1.0	2.0	0.5	1.0	2.0	3.0	6.0	12.0		+0.3	
III	R <sub>i</sub>	2.73	3.36	3.27	3.40	3.16	3.80	3.33	3.44	3.45	3.29	2.80	2.84	3.54	2.76	3.23
	N	8	8	8	8	8	8	8	8	8	8	8	8	8	8	-
	R <sub>f</sub>	2.90	4.19	5.22	5.45	3.62	5.59	4.53	3.76	3.98	3.27	3.15	3.45	3.74	3.18	4.00
	N	8	8	8	8	8	8	8	8	8	8	8	8	8	8	-
	ΔR	0.17	0.82	1.95	2.06	0.46	1.78	1.20	0.32	0.53	-0.03	0.34	0.61	0.20	0.43	0.77
	ΔR p-values	<b>0.01</b>	<b>0.04</b>	<b>&lt;0.01</b>	<b>&lt;0.01</b>	<b>0.05</b>	<b>&lt;0.01</b>	<b>&lt;0.01</b>	0.05	<b>&lt;0.01</b>	0.56	<b>0.02</b>	<b>&lt;0.01</b>	0.17	<b>&lt;0.01</b>	-
	ΔR/R <sub>i</sub>	0.06	0.24	0.60	0.61	0.14	0.47	0.36	0.09	0.15	-0.01	0.12	0.22	0.06	0.15	0.23
IV	R <sub>i</sub>	3.37	3.50	3.38	3.38	3.40	3.16	3.67	3.38	3.50	3.56	3.09	3.43	3.24	3.12	3.37
	N	7	8	8	8	8	8	8	8	8	8	8	8	8	8	-
	R <sub>f</sub>	3.68	4.35	4.65	4.41	3.89	4.72	3.95	3.37	3.89	3.46	3.22	3.57	3.37	3.17	3.83
	N	8	8	8	8	8	8	8	8	8	8	8	8	8	8	-
	ΔR	0.30	0.84	1.27	1.03	0.49	1.56	0.28	-0.01	0.40	-0.10	0.13	0.14	0.13	0.05	0.47
	ΔR p-values	<b>0.02</b>	<b>&lt;0.01</b>	<b>&lt;0.01</b>	<b>&lt;0.01</b>	<b>0.01</b>	<b>&lt;0.01</b>	<b>&lt;0.01</b>	0.87	<b>&lt;0.01</b>	<b>0.04</b>	0.06	0.37	0.07	0.53	-
	ΔR/R <sub>i</sub>	0.09	0.24	0.37	0.30	0.14	0.49	0.08	0.00	0.11	-0.03	0.04	0.04	0.04	0.02	0.14

125

3

4

## Effect of Inhibitors

Phase III water quality had a predominately groundwater blend with high alkalinity and high temperature. The average temperature of Phase III water was 25.8 °C. Surface roughness for eleven of fourteen copper coupons changed significantly in Phase III. Surface roughness did not change significantly for the coupons receiving 1.0 mg/L as P-ZOP, 3.0 mg/L as SiO<sub>2</sub>, and the pH<sub>s</sub> environment. The data in Table 8.2 demonstrate that surface roughness of Cu tended to increase in Phase III, with average initial and final roughness of 3.22 μm and 3.95 μm.

Phase IV water quality had the highest proportion of desalinated water (RO 20%) among all the phases. The average temperature of Phase IV water was 21.2 °C. Surface roughness for nine of fourteen copper coupons had a significant change in surface roughness during exposure to inhibitors. Surface roughness tended to increase in Phase IV, with average initial and final roughness of 3.35 μm and 3.86 μm.

Figure 8.8 shows ΔR by inhibitor and phase. The average change in roughness was calculated over all coupons receiving each inhibitor. Figure 8.8 shows that coupons receiving phosphate inhibitors tended to have greater increases in roughness than coupons receiving other inhibitors. Also, the roughness increase with phosphate inhibitor was consistently greater in Phase III than Phase IV, suggesting an interaction between water quality, inhibitor, and copper surface roughness. The change in roughness for Si, pH<sub>s</sub>, and pH<sub>s</sub>+0.3 inhibitors tended to be less than 0.5 μm and did not appear to vary between phases.

With phosphate inhibitors, elevated temperature and alkalinity were associated with larger increases in surface roughness due to precipitation of blue-green copper (II) scales.. Otherwise a compact, dull red copper (I) scale was observed. Phosphate inhibitor addition

corresponded with changes in surface morphology, and surface composition, including the oxidation state of copper solids.

In Phase III, photographs of the copper coupons showed significant blue-green scales on BOP and OP inhibitor. Similar scales were only scattered across coupons receiving ZOP inhibitor. In contrast, no blue-green scales were observed on the coupons receiving Si, pH<sub>s</sub>, and pH<sub>s</sub>+0.3 inhibitor. The top coupon in Figure 8.9 received 0.5 mg/L as P-OP inhibitor. The bottom coupon in Figure 8.9 was in the pH<sub>s</sub>+0.3 environment. In Phase IV, photographs of the copper coupons showed a speckled blue-green scale on coupons receiving BOP, OP, ZOP, and Si inhibitor. No blue-green scales were observed for the pH<sub>s</sub> and pH<sub>s</sub>+0.3 inhibitors. The top coupon in Figure 8.10 received 0.5 mg/L as P-BOP inhibitor. The bottom coupon in Figure 8.10 was in the pH<sub>s</sub> environment in Phase IV. Therefore it appears that surface roughness of copper coupons varies with inhibitor and water quality.

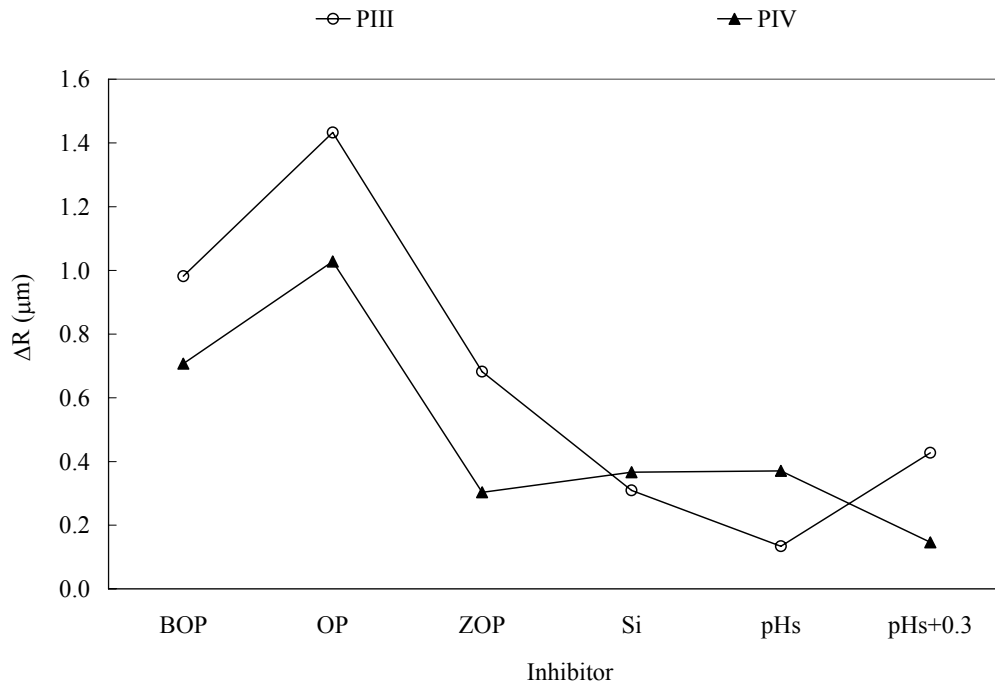


Figure 8.8  $\Delta$  roughness of copper coupons by inhibitor and phase



Figure 8.9 Visual comparison of surface scales on Phase III copper coupons



Figure 8.10 Visual comparison of surface scales on Phase IV copper coupons

## Replicates

A series of replicate Cu coupons were analyzed in Phases III-IV to gain insight into variability of the roughness experiments. The surface roughness of original and replicate copper coupons is shown in Figure 8.11 and Figure 8.12. For Phase III, one replicate coupon was placed in the pH<sub>s</sub> environment. The surface roughness of the pair of copper coupons in the pH<sub>s</sub> environment did not change significantly for either coupon. For Phase IV, replicate coupons were placed in the middle inhibitor dose, pH<sub>s</sub>, and pH<sub>s</sub>+0.3 PDSs. Roughness tended to increase in both the original and replicate copper coupons. The change in surface roughness was measured consistently within 0.6 μm between replicates.

Figure 8.11  
Paired replicate surface roughness data for copper coupons from Phase III

Parameter	PDS 13	PDS 13-R
	pH <sub>s</sub>	pH <sub>s</sub>
R <sub>i</sub>	3.54	3.16
N	8	8
R <sub>f</sub>	3.74	3.23
N	8	8
ΔR	0.20	0.07
ΔR p-values	0.17	0.37

Figure 8.12  
Paired replicate surface roughness data for copper coupons from Phase IV

Parameter	PDS 02	PDS 02-R	PDS 05	PDS 05-R	PDS 08	PDS 08-R	PDS 11	PDS 11-R	PDS 13	PDS 13-R	PDS 14	PDS 14-R
	BOP	BOP	OP	OP	ZOP	ZOP	Si	Si	pH <sub>s</sub>	pH <sub>s</sub>	pH <sub>s</sub>	pH <sub>s</sub>
	1.0	1.0	1.0	1.0	1.0	1.0	1.0	01.0			+0.3	+0.3
R <sub>i</sub>	3.50	3.34	3.40	3.30	3.38	3.42	3.09	3.27	3.24	3.36	3.12	3.22
N	8	8	8	8	8	8	8	8	8	8	8	8
R <sub>f</sub>	4.35	4.10	3.89	4.28	3.37	3.80	3.22	3.96	3.37	3.97	3.17	3.46

N	8	8	8	8	8	8	8	8	8	8	8	8
$\Delta R$	0.84	0.76	0.49	0.98	-0.01	0.39	0.13	0.70	0.13	0.61	0.05	0.24
$\Delta R$ p-values	<b>&lt;0.01</b>	<b>&lt;0.01</b>	<b>0.01</b>	<b>&lt;0.01</b>	0.87	<b>0.03</b>	0.06	<b>&lt;0.01</b>	0.07	<b>&lt;0.01</b>	0.53	<b>0.01</b>

The relative percent difference is a measure of precision and is calculated by taking the absolute difference of two values and dividing it by the average of the same two values and expressing the result as a percentage. The RPD of  $R_f$  of the copper coupons ranged from 6% to 21%.

### *Scanning Electron Microscopy*

Scanning electron micrographs of copper exposed to phosphate inhibitor (Figure 8.13), silicate inhibitor (Figure 8.14), and no inhibitor (Figure 8.15) demonstrate the differences in surface morphology between surfaces receiving inhibitor and those not receiving inhibitor. All coupons were incubated simultaneously, receiving the same blend of source waters in Phase III. The source water blend for Phase III was summarized previously (Table 5.1).

The EDS spectra (not shown) for the surface in Figure 8.13 showed high levels of Cu, O, and P with minor amounts of Si and Ca. The micrograph illustrates the tendency of phosphate inhibitors to produce large mounds of precipitates on the surface.

For the surface in Figure 8.14, the EDS spectra showed high levels of Cu and O, with moderate Si and Ca. The micrograph shows that the surface is covered with spherical particles of about 500 nm diameter. The particles are dispersed across the surface, not forming a film as dense as that of Figure 8.13. Also, the individual particles in Figure 8.14 appear more rounded than those of Figure 8.13. Both figures show a relatively smooth, uniform film underneath the particles.

For the case of no inhibitor addition, the EDS spectra indicated the presence of Cu, O, and Si, with traces of Cl and Ca. There is little evidence of particle growth/deposition on the surface, rather, the surface appears to be disintegrating. In the micrograph there are several small white structures about 100  $\mu\text{m}$  in length scattered across the surface. These structures do not resemble either type of particle seen with orthophosphate or silicate addition. Also, the surface is more mottled in appearance indicating that general corrosion has disrupted the uniformity of the surface film.

Taken together, these micrographs illustrate the differences in surface structures that form on copper surfaces exposed to different corrosion inhibitor treatments. Copper surfaces receiving phosphate or silicate inhibitors formed visible deposits that varied in thickness and particle shape, whereas the no inhibitor treatment showed a disintegrating surface with mottled appearance.

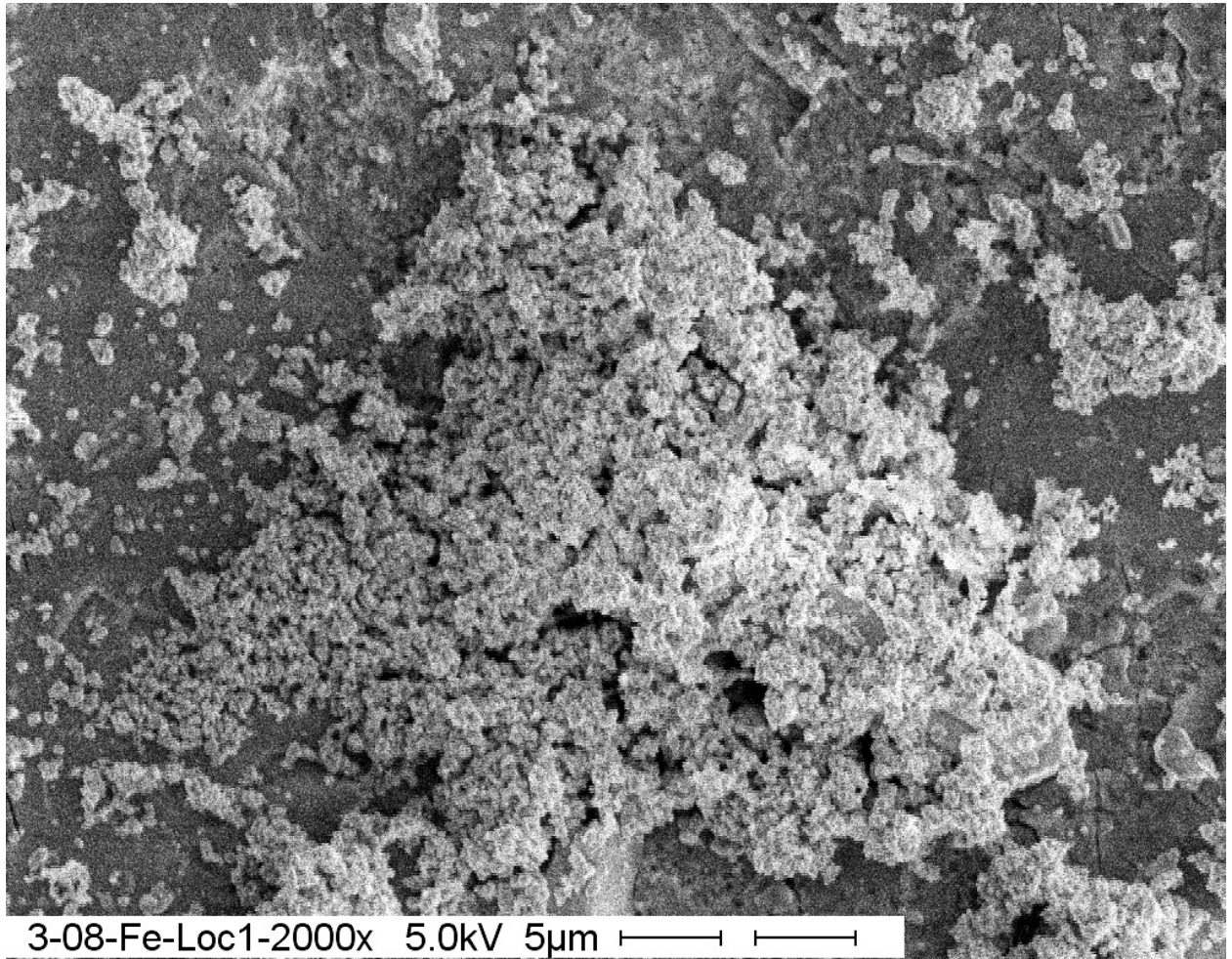


Figure 8.13 Copper surface exposed to zinc orthophosphate dose of 1.0 mg/L as  $\text{PO}_4^{3-}$  for three months

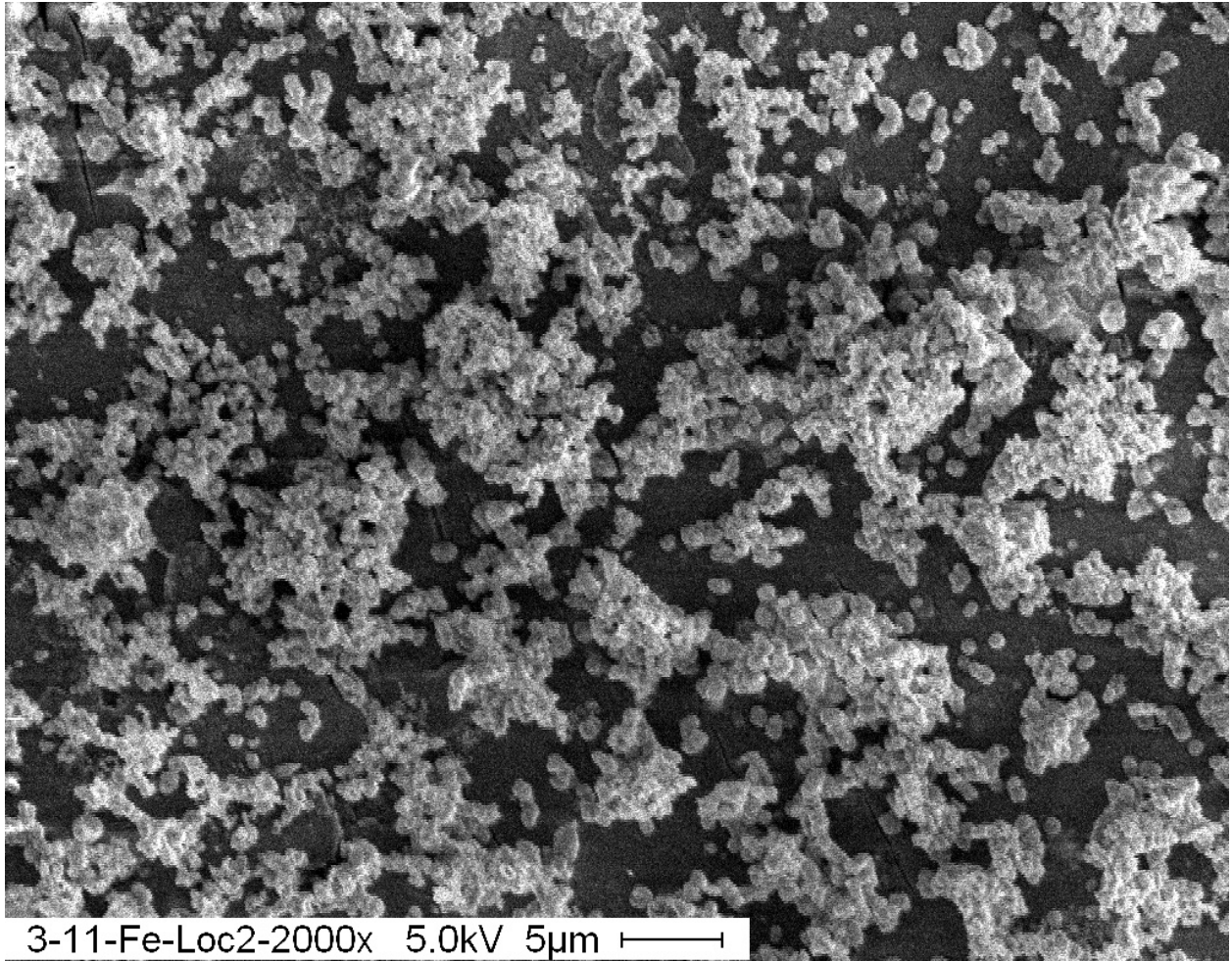


Figure 8.14 Copper surface exposed to silicate inhibitor 6.0 mg/L as SiO<sub>2</sub> for three months

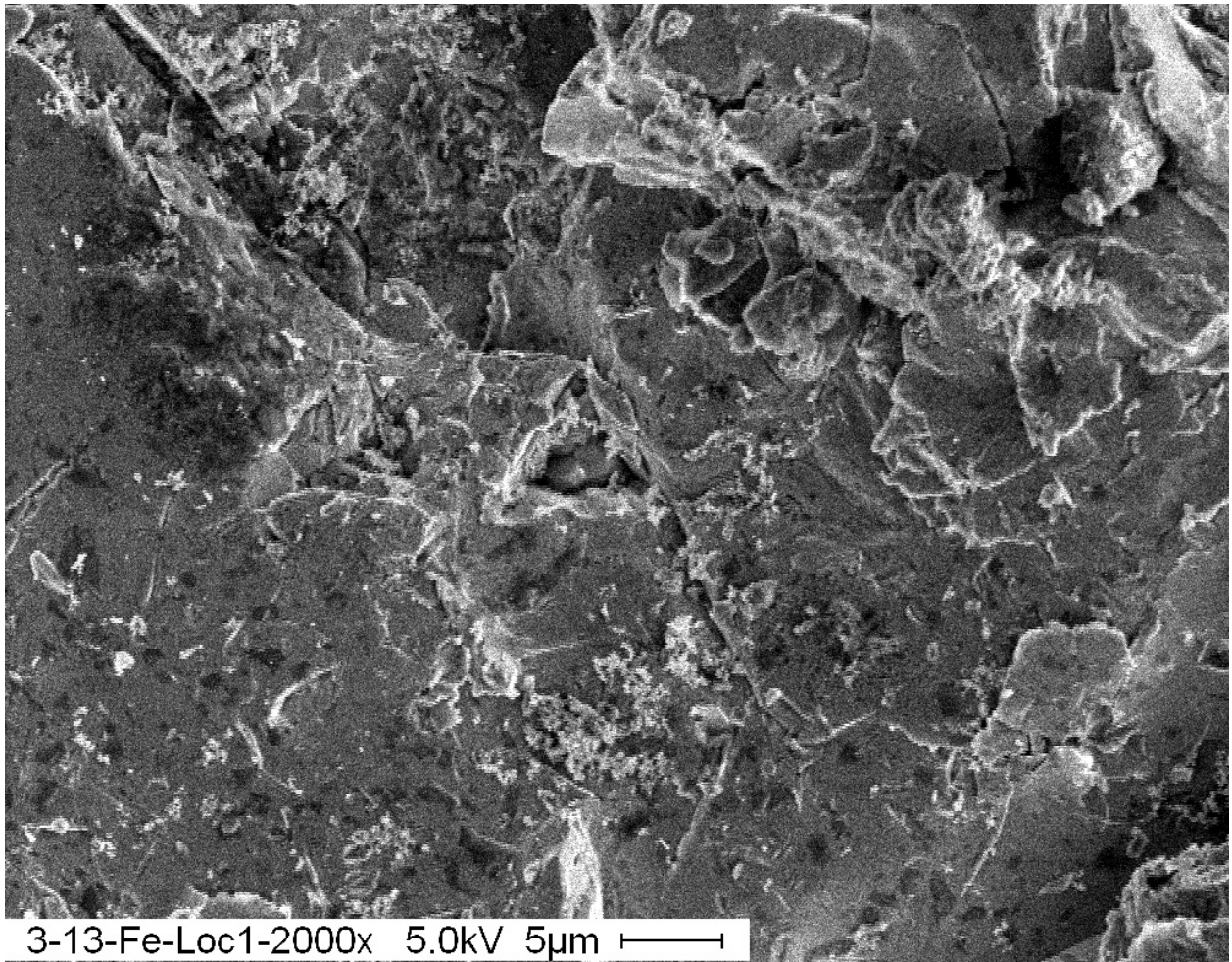


Figure 8.15 Copper surface receiving no inhibitor for three months

## Conclusions

Elevated orthophosphate, alkalinity, and temperature were all factors associated with increased copper surface roughness. The greatest increases in surface roughness were observed with copper coupons receiving phosphate inhibitors. Smaller increases were observed with copper coupons receiving silicate inhibitor or no inhibitor.

With phosphate inhibitors, elevated temperature and alkalinity were associated with larger increases in surface roughness due to precipitation of blue-green copper (II) scales.. Otherwise a compact, dull red copper (I) scale was observed. Phosphate inhibitor addition corresponded with changes in surface morphology, and surface composition, including the oxidation state of copper solids.

Examination of surface deposits by scanning electron microscopy showed that copper surfaces receiving phosphate and silicate inhibitors formed visible deposits that varied in thickness and particle shape. With phosphate inhibitor addition, the deposits were thicker; whereas with silicate inhibitor addition the particles were more round in appearance. In contrast to both inhibitor types, the no inhibitor treatment showed a disintegrating copper surface with mottled appearance indicating general corrosion.

## REFERENCES

- Arevalo, J. 2003. Modeling the Effect of Pipe Material, Water Quality and Time on Chlorine Dissipation. Master's thesis. University of Central Florida, Orlando, Fla.
- Barceloux, D.G. and D. Barceloux. 1999. "Copper." *Clinical Toxicology*. Vol 37. No. 2. 217-230.
- Bendetti-Pichler, A.A. 1964. Identification of Materials via Physical Properties, Chemical Tests, and Microscopy. Springer Wien. Vienna, Austria.
- Clement, J.A., M.R. Schock, and D.A. Lytle. "Controlling lead and copper corrosion and sequestering of iron and manganese." In *Critical Issues in Water and Wastewater Treatment*, Boulder, CO, 1994.
- Colebrook, C.F. 1939. "Turbulent Flow in Pipes, with Particular Reference to the Transition Region between the Smooth and Rough Pipe Laws. *J. Inst. Civil Engrs.* Vol 11. Feb. London.
- Doshi, B., W.M., Grayman, and D. Guastella. 2003. Field Testing the Chlorine Wall Demand in Distribution Mains. Presented at the AWWA Annual Conference, Anaheim, Calif., June 15-19, 2003.
- Edwards, M., L. Hidmi, and D. Gladwell. 2003. Phosphate Inhibition of Soluble Copper Corrosion By-product Release. *Corrosion Science*, 44:1057-1071.
- Edwards, M., L.S. McNeill, and T.R. Holm. 2001. Role of Phosphate Inhibitors in Mitigating Lead and Copper Corrosion. In *Distribution Systems*. Denver, Colo.: AWWARF.

- Eldredge, G.G., and J.C. Warner. 1948. "Inhibitors and Passivators." *The Corrosion Handbook*. pp. 905-916. J. Wiley and Sons. New York.
- Fletcher, M. and K.C. Marshall. 1982. Are Solid Surfaces of Ecological Significance to Aquatic Bacteria? In *Advances in Microbial Ecology*. Edited by K.C. Marshall. New York: Plenum Press.
- Frateur I., C. Deslouis, L. Kiéné, Y. Lévi, and B. Tribollet. 1999. Free Chlorine Consumption Induced by Cast Iron Corrosion in Drinking Water Distribution Systems. *Water Res.*, 33(8):1781-1790.
- Hahn, R.B., and F.J. Welcher. 1968. 2<sup>nd</sup> ed. *Inorganic Qualitative Analysis; A Short Course for Introductory Chemistry*. Princeton: Van Nostrand.
- Hallam, N.B., J.R. West, C.F. Forster, J.C. Powell, and I. Spencer. 2002. The Decay of Chlorine Associated With the Pipe Wall in Water Distribution Systems. *Water Res.*, 36(14):3479-3488.
- He, Q.H., G.G. Leppard, C.R. Paige, and W.J. Snodgrass. "Transmission electron microscopy of a phosphate effect on the colloid structure of iron hydroxide." *Water Res.*, 30(6), 1996: 1345-1352.
- Hem, J.D. 1971. *Study and Interpretation of the Chemical Characteristics of Natural Water*. Geological Survey Water Supply, Paper 1743, U.S. Government Printing Office, Washington, DC.
- Hidmi, L., and M. Edwards. 1999. Role of Temperature and pH in Cu(OH)<sub>2</sub> Solubility. *Environ. Sci. Technol.*, 33(15):2607-2610.

- Hogness, T.R., and W.C. Johnson. 1957. *An Introduction to Qualitative Analysis*. New York: Holt.
- Hudson, W.D. 1966. Studies of Distribution System Capacity in Seven Cities. *Jour. AWWA*, 58(2):157-164.
- Hudson, W.D. 1966. Studies of Distribution System Capacity in Seven Cities. *Jour. AWWA*, 58(2):157-164.
- Kiéne L., W. Lu, and Y. Lévi. 1998. Relative Importance of the Phenomena Responsible for Chlorine Decay in Drinking Water Distribution Systems. *Water Sci. and Technol.*, 38(6):219-237.
- King, E.J. 1959. *Qualitative Analysis and Electrolytic Solutions*. New York: Harcourt Brace.
- Kruger, J. 1959. "The Oxide Films Formed on Copper Single Crystal Surfaces in Pure Water." *J. Electrochem. Soc.* 106, 847.
- LaRosa-Thompson, J., et al. "Sodium silicate corrosion inhibitors: Issues of effectiveness and mechanism." In *Proc. AWWA Water Quality Technology Conference*, Denver, CO, 1997.
- Larson, T.E., and F.W. Sollo. 1967. Loss in Water Main Carrying Capacity. *Jour. AWWA*, 59(12):1565-1572.
- Laurent, P. and P. Servais. 1995. Fixed Bacterial Biomass Estimated by Potential Exoproteolytic Activity. *Canad. Jour. of Microbiol.*, 41(8):749-752.

- Le Puil M., Y.C. Chang, A.A. Randall, and J.S. Taylor. 2005. Effect of Distribution System Materials and Water Quality on HPC and Biofilm Proliferation. In *Water Quality in the Distribution System*. Edited by W.C. Lauer. Denver, Colo.: AWWA.
- Lippold, S. and J. Podlesny. 1998. Wyko Surface Profilers Technical Reference Manual. Tuscon, Ariz: Veeco Instruments.
- Lytle, D.A., and M.R. Schock. "Impact of stagnation time on the dissolution of metal from plumbing materials." In Proc. AWWA Annual Conference, Atlanta, GA, 1997.
- Lytle, D.A., M.R. Schock, and T.J. Sorg. "Controlling lead corrosion in the drinking water of a building by orthophosphate and silicate treatment." Jour. NEWWA, 110(3), 1996:202-216.
- Lytle, D.A. M.R. Schock, and T.J. Sorg. "A systematic study on the control of lead in a new building." In Proc. AWWA Annual Conference, New York, NY, 1994.
- MacNevin, D.E., J.S. Taylor, and Coauthors TBD. 2007a. "Surface characterization and solubility modeling of copper release in the presence of phosphate inhibitors." Draft manuscript.
- MacNevin, D.E., J.S. Taylor, and Coauthors TBD. 2007b. "Surface characterization and solubility modeling of copper release in the presence of silicate inhibitor." Draft manuscript.
- MacNevin, D.E., J.S. Taylor, and Coauthors TBD. 2007c. "Investigating the effect of phosphate and silicate corrosion inhibitors on surface roughness of iron pipe." Draft Manuscript.

Merkel, T.H., H.J. Gross, W. Werner, T. Dahlke, S. Reicherter, G. Beuchle, and S.H. Eberle. 2002. Copper Corrosion By-product Release in Long-term Stagnation Experiments. *Water Research*, 36(6):1547-1555.

Merkel, T.H., and S.O. Pehkonen. 2006. "General corrosion of copper in domestic drinking water installations: scientific background and mechanistic understanding." *Corrosion Engineering Science and Technology*. 41(1):21-37.

Moody, L.F. 1944 "Friction Factors for Pipe Flows." *ASME Trans*. Vol. 66.

Nikuradse, J. 1950. Laws of Flow in Rough Pipes. Translated from "Strömungsgesetze in rauhen Röhren" *Forsch. Arb. Ing.-Wes.* No. 361 (1933).

PQ Bulletin 37-3. 2001. PQ Soluble Silicates: For Protection of Water Systems from Corrosion. Valley Forge, Pa.: The PQ Corporation.

Richardson, H.W. 1997. *Handbook of Copper Compounds and Applications*. CRC Press. Boca Raton, FL.

Rossmann, L.A., R.M. Clark, and W.M. Grayman. 1994. Modeling Chlorine Residual in Drinking Water Distribution Systems. *Jour. of Envir. Eng.*, 120(4):803-820.

Ryder, I, and I. Wagner. "Corrosion Inhibitors." *Internal Corrosion of Water Distribution Systems.*

Schenk, G.H. 1996. 3<sup>rd</sup> ed. *Qualitative Analysis and Ionic Equilibrium*. Boston: Houghton Mifflin Company.

- Schenk, J.E., and W.J. Weber, Jr. 1968. "Chemical interactions of dissolved silica with iron (II) and iron (II)." *Jour. AWWA*, 76(2): 199-212.
- Schindler, P., H. Althaus, F. Hofer, and W. Minder. 1965. Solubility Products of Zinc Oxide, Copper Hydroxide, and Copper Oxide as a Function of Particle Size and Molecular Surface Area: A Contribution to the Thermodynamics of Liquid Surface Boundaries. *Helvetica Chim. Acta*, 48(5):1204-1215.
- Schindler, P.W. 1967. Heterogeneous Equilibria Involving Oxides, Hydroxides, Carbonates and Hydroxide Carbonates. In *Equilibrium Concepts in Natural Water Systems*. Washington, D.C.: American Chemical Society.
- Schock, M.R. 1999. Internal Corrosion and Deposition Control. In *Water Quality and Treatment*. New York: McGraw Hill Inc.
- Schock, M.R., D.A. Lytle, and J.A. Clement. 1995a. "Effects of pH, carbonate, orthophosphate and redox potential on cuprosolvency." In *NACE Corrosion/95*, Orlando, FL, 1995.
- Schock, M.R., D.A. Lytle, and J.A. Clement. 1995b. *Effect of pH, DIC, Orthophosphate and Sulfate on Drinking Water Cuprosolvency*. Risk Management Research Report EPA/600/R-95/085. Cincinnati, Ohio: U.S. EPA.
- Schock, M.R. and J. C. Fox. 2001. Solving Copper Corrosion Problems while Maintaining Lead Control in a High Alkalinity Water Using Orthophosphate. Presented at the AWWA Annual Conference, Cleveland, Ohio, August 30, 2001.
- Seal, S. and T.L. Barr. 2001. Application of Photoelectron Spectroscopy in Inorganic and Organic Material System. In *Advances in Surface Science*. Edited by H.S. Nalwa. San Diego, Calif. :Academic Press.

Shanley, C., R. Hummel, and E. Verink. 1980. *Corros. Sci.*, 20, 481.

Sharp, W.W., and T. Walski. 1988. Predicting Internal Roughness in Water Mains. *Jour. AWWA*, 80(11):34-40.

Shull, K.E. 1980. "An experimental approach to corrosion control." *Jour. AWWA*, 72(5):280-285.

Snoeyink, V; and D. Jenkins. 1980. *Water Chemistry*. John Wiley & Sons. New York, NY.

Swayze, J. 1983. "Corrosion study at Carbondale, Ill." *Jour. AWWA*, 75(2). 101.

Taylor, J.S., J.D. Dietz, A.A. Randall, S.K. Hong, C.D. Norris, L.A. Mulford, J.M. Arevalo, S. Imran, M. Le Puil, S. Liu, I. Mutoti, J. Tang, W. Xiao, C. Cullen, R. Heaviside, A. Mehta, M. Patel, F. Vasquez, and D. Webb. 2005. "Effects of Blending on Distribution System Water Quality." Denver, Colo.: AwwaRF and Tampa Bay Water.

Taylor, J.S., J. D. Dietz, A. A. Randall, C. D. Norris, A. Alshehri, J. Arevalo, X. Guan, P. Lintereur, D. MacNevin, E. Stone, R. Vaidya, B. Zhao, S. Glatthorn, A. Shekhar. 2007 "Control of Distribution System Water Quality in a Changing Water Quality Environment Using Inhibitors." Draft Report. American Water Works Association Research Foundation and Tampa Bay Water. Denver, Colo, USA.

Uhlig H.H. 1985. *Corrosion and Corrosion Control*. J. Wiley and Sons. New York.

Vasconcelos J.J., L.A. Rossman, W. M. Grayman, P. F. Boulous and R. M. Clark. 1997. Kinetics of Chlorine Decay. *Jour. AWWA.*, 89(7):54-65.

- Vic E., Ryder, R., Wagner, I. and Ferguson, J. 1996. "Mitigation of Corrosion Effects." in V. Snoeyink and I. Wagner (9 eds.) *Internal of Corrosion of Water Distribution Systems*. 2nd ed. AWWARF. FVGW-Technologiezentrum Wasser & American Water Works Association Research Foundation, Denver, Colo.
- Vikesland, P.J., K. Ozekin, and R.L. Valentine. 2001. Monochloramine Decay in Model and Distribution System Waters. *Water Res.*, 35(7): 1766-1776.
- Vikesland, P.J., and R.L. Valentine. 2002. Modeling the Kinetics of Ferrous Iron Oxidation by Monochloramine. *Envir. Sci. and Technol.*, 36(4):662-668.
- Wagner, C.D. A. V. Naumkin, A. Kraut-Vass, J. W. Allison, C. J. Powell, and J. R. Rumble, Jr. (Eds.). 2003. NIST Standard Reference Database 20, Version 3.4 available from <http://srdata.nist.gov/xps/>.
- Walski, T.M., D.V. Chase, D.A. Savic, W. Grayman, S. Beckwith, and E. Koelle. 2003. *Advanced Water Distribution Modeling and Management*. Waterbury, Conn.: Haestad Press.
- Xiao, W., 2004. Effect of Source Water Blending on Copper Release in Pipe Distribution System: Thermodynamic and Empirical Models. Ph.D. diss., University of Central Florida, Orlando, Fla.
- Xiao, W., S. Hong, Z. Tang, S. Seal, J.S. Taylor. 2007. "Effects of blending on surface characteristics of copper corrosion products in drinking water." *Corrosion Science*.49(2):449-468.